International Scientific-Technical and Production Journal

The Paton WELDING JOURNAL

March 2004 # 3

English translation of the monthly «Avtomaticheskaya Svarka» (Automatic Welding) journal published in Russian since 1948

Founders: *E.O. Paton Electric Welding Institute of the NAS of Ukraine*
International Association «Welding»

Publisher: *International Association «Welding»*

Address:
E.O. Paton Electric Welding Institute,
International Association «Welding»,
11, Bozhenko str., 03680, Kyiv, Ukraine
Tel.: (38044) 227 67 57
Fax: (38044) 268 04 86
E-mail: journal@paton.kiev.ua
http://www.nas.gov.ua/pwj

State Registration Certificate
KV 4790 of 09.01.2001

Subscriptions:
$460, 12 issues per year,
postage and packaging included.
Back issues available.

CONTENTS

PROBLEMS OF SELECTION OF WELDABLE STEEL FOR HIGH-TEMPERATURE COMPONENTS OF TPS POWER UNITS (REVIEW)

V.Yu. SKULSKY and **A.K. TSARYUK**
E.O. Paton Electric Welding Institute, NASU, Kiev, Ukraine

The paper deals with the features of technical «re-equipment» of power units of thermal power stations over the last 20 years. Advances in this field were made possible by development and application of new complex-alloyed heat-resistant steels with a higher chromium content. Alloying influence on phase composition, corrosion resistance, ageing processes, long-term strength and weldability of new high-chromium heat-resistant steels has been analyzed.

Keywords: *thermal power engineering, efficiency, supercritical steam parameters, heat-resistant steels, alloying, long-term strength, austenitic steels, steel with 9 % Cr*

Thermal power stations (TPS) are currently producing a large fraction of the total volume of power generated by all the types of power generation enterprises [1–3]. To minimize the damage to the environment from operating TPS (as well as heat-electric generation plants), it is envisaged to switch them into modes, providing lower atmospheric emissions of gaseous compounds of carbon and nitrogen (CO, CO_2 and NO_x) during fuel combustion. In addition, reduction of the use of natural gas as fuel and transition to application of cheaper and more readily available solid fuel, namely black and brown coal, are taking place.

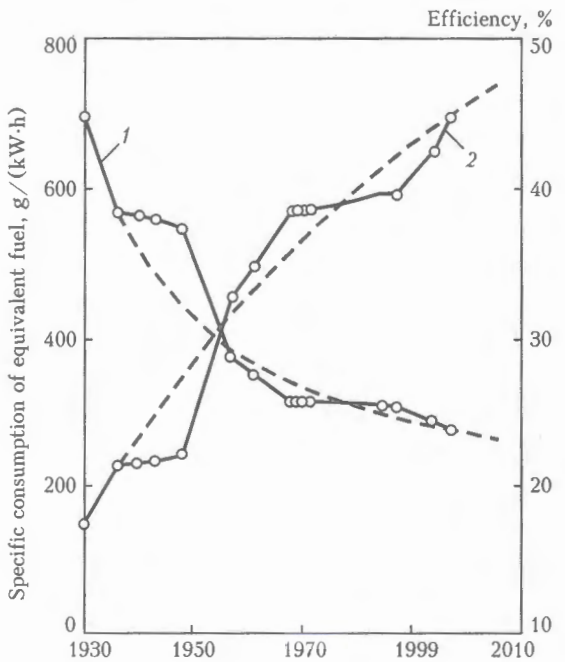

Figure 1. Dynamics of increase of efficiency and reduction of consumption of coal fuel in the case of power stations designed by VKR Company, Germany [6, 12]: *1* — fuel consumption; *2* — efficiency

World resources of these coals will ensure their supply for a term, which is 4 times longer than that of oil and gas consumption [1, 3].

One of the effective directions in solving the ecology problem is reduction of the amount of consumed fuel per a unit of generated power. For this purpose special technologies of coal preparation and equipment, ensuring the most complete combustion of the fuel fractions, are developed, namely furnaces, using pulverized-coal, those with a circulating fluidized bed, those with a higher pressure fluidized bed; combined plants with coal gasification, where part of the coal is processed through pyrolysis into fuel gas, saturated with air or oxygen and burnt in a special chamber, and the thus formed coke and the remaining part of the coal are burnt by the higher pressure fluidized bed technology [1, 3].

Under these conditions the least damage strategy envisages increasing the temperature in the furnaces and operating elements of boiler units, which, in addition to reducing the harmful oxide emissions, is also accompanied by increase of their efficiency (Figure 1) [1, 3–15]. This is related to achievement of supercritical parameters of steam ($T \leq 600$–610 °C, $P \leq 30$–31 MPa) relative to limit parameters, admissible in earlier used units ($T \leq 560$ °C and $P = 16$–25 MPa). Such a transition allows increasing the efficiency of TPS power plants from 36 to 37 % (designed for the following conditions: $T \sim 535$ °C, $P \leq 2$ MPa) up to ~ 45 % [6–8].

Practical implementation of the proposed engineering solutions required a new weldable structural material, providing a rather efficient performance under the new operating conditions. After development of the first heat-resistant steels with Fe–Mo alloying system (15M, 20M type), which had the disadvantage of being susceptible to graphitization at temperatures above 480 °C (such steels are not used now for welded components of power units), a number of different grades of low- and medium-alloyed steels were developed based on Fe–Cr, Fe–Cr–Mo systems with additives of vanadium, niobium, nickel and other elements

Most widely accepted grades of heat-resistant pipe steels and critical conditions of their operation [12, 13, 19, 20]

Steel grade	*Steel standard*	*Manufacturing country*	*Maximum temperature, °C*	*Maximum pressure, MPa*
13CrMo44	DIN 17175	Germany	520	–
10CrMo9 10 P22/T22	DIN 17175 ASTM, A-335/A-199 A-213	Germany USA	540–545	20–28
12Kh1MF 14MoV63 Steel 15128 (CrMoV)	TU 14-3-460–75 DIN 17175 N415128	CIS Germany Czechia/Slovakia	545–550	21–25.5
15Kh1M1F 15CrMoV510	TU 14-346–75 VdTÜV-Wb506	CIS Germany	550	25.5
X20CrMoV121	DIN 17175	Germany	550–560	20

[16–18]. This more complex alloying results in an increase of long-term strength of the steels and raises the upper temperature limit of their operation. So, parts of carbon steels of the type of steel 10, and steel 20 may operate at the temperature of up to 450 °C, those of steel 15KhM – up to 530 °C, 20KhMFL – up to 540 °C [17]. However, the strengthening elements, particularly carbon, impair the weldability of heat-resistant steels. Therefore, it is recommended to apply steels with a relatively low content of carbon of up to 0.2–0.3 % for welded structures (to ensure a satisfactory weldability) [17].

The Table shows the grades of local and foreign heat-resistant steels, which have become the most widely known and applied. It is seen that these materials ensure approximately the same admissible modes of operation of the high-temperature components of boiler units, which is what determines the level of critical parameters of steam. Cr–Mo–V pearlitic steels of 15Kh1M1F, 12Kh1MF type are widely used in boiler units in CIS countries and have foreign analogs of the type of steels 15128 (CrMoV), 14MoV63 and 15CrMoV510 [9, 19, 20]. Starting from 1950s, bainitic steel 2.25Cr–1Mo became the most widely accepted in the world. It was included into the international (EN) and national standards of a number of countries [13] with the following designations: 10CrMo9 10 (EN, Western Europe), 622 (BS, Great Britain), TU10CD9-10 (AFNOR, France), 12CrMo910 (UNI, Italy), STRA 22 (JIS, Japan); USA and German standards are shown in the Table. In Western Europe (primarily in Germany) highly-alloyed steel of martensitic class from a group of materials with 12 % Cr – X20CrMoV121 (X20) began to be applied instead of steel P22. Despite a somewhat higher level of long-term strength of X20 steel, compared to steel P22, the maximum temperature of its operation, similar to other steel grades, is limited by ~ 560 °C.

It is believed that the functional capabilities of steel with a ferrite α-lattice, strengthened by additional alloying, are exhausted at $T > 600$ °C (Figure 2). Above this temperature high-alloyed austenitic steels and alloys are more effective [17, 21]. However, manufacturing of components of heat-and-power generation equipment of austenitic steels involves a number of problems, related to their physical properties and weldability [11, 17]. Study [11] gives analysis of experience of long-term application of austenitic steels of TP304 (06C–18Cr–10Ni), TP316H (06C–16Cr–12Ni–2Mo), TP316LN (03C–16Cr–12Ni–2Mo–N), TP321H (08C–18Cr–10Ni–Ti), TP347 (10C–18Cr–10Ni–Nb), Esshete 1250 (10C–15Cr–10Ni–6Mn–Mo–Nb–V) type, etc. at $T > 565$ °C as part of the structures of power units, developed at the start of 1950s in Great Britain, Germany and the USA. It is noted that one of the features of austenitic steels, compared to steels with a ferrite lattice, is their higher deformability at lower stresses, because of a greater number of atom sliding systems in γ-lattice (12 directions of sliding) [11, 22, 23]. Therefore, to provide a high long-term strength of austenitic materials of Fe–Cr–Ni system, they should be alloyed with molybdenum and effective carbide-forming elements

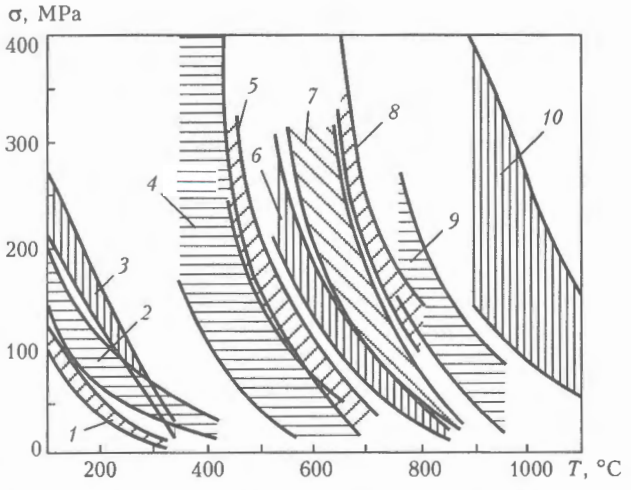

Figure 2. Connection between the temperature and long-term strength over 1000 h for different metallic materials [21]: *1–4* – alloys of magnesium, aluminium, copper, titanium, respectively; *5* – pearlitic heat-resistant steels; *6* – austenitic Cr–Ni steels; *7* – Fe–Cr–Ni–Co alloys; *8* – Ni-based alloys; *9* – cobalt alloys; *10* – molybdenum alloys

(niobium, titanium, vanadium), and also nitrogen should be added to them [11].

Carbide-forming elements of the type of titanium and niobium (steels with niobium are used more often) at cooling from high temperatures bind carbon into stable MX carbides and prevent formation of undesirable enriched in alloying elements intergranular $M_{23}C_6$ and M_6C carbides, which are associated with the possibility of development of intercrystalline fracture due to intercrystalline corrosion. It is logical to assume that local depletion of the solid solution with alloying elements at formation of such carbides may promote its softening, increase of the degree of local deformation under the impact of stresses, as well as initiation of fracture sites. Restraining of precipitation of carbides of $M_{23}C_6$ type is promoted by lowering of carbon content and adding nitrogen, which provides additional strengthening of steel. Moreover, the mechanism of dispersion hardening is further implemented in such steels at ageing temperatures in the presence of strong carbide-forming elements of the type of vanadium.

In operation of stabilized austenitic steels, where carbon is tied up into high-temperature MX carbides, precipitation of carbon-free needle-shaped intermetallic Laves phases, which strengthen the solid solution, proceeds during their ageing (at $T \geq 600$ °C). Longer-term ageing may cause precipitation of σ-phase. Although [11] does not note any adverse consequences of σ-phase formation, it is believed that such intermetallic phases promote embrittlement of the material, lowering of high-temperature ductility, and, therefore, they should be avoided [17, 21, 24]. With this purpose, it is recommended to apply stable austenitic steels without δ-ferrite (for operating temperatures above 650 °C), or limit its amount to the range of 2–5 % (for $T < 650$ °C), as it is exactly in the high-chromium molybdenum-containing two-phase materials that favourable conditions are created for precipitation of σ-phase from ferrite in the temperature range of 650–950 °C [17, 21, 24–26].

The above limits of δ-ferrite content are determined from the condition of providing a satisfactory resistance of welded joints in austenitic steels (weld and HAZ metal) to hot cracking [17]. In its turn, prevention of δ-ferrite formation leads to a considerable lowering of technological strength. The problem of formation of hot cracks, namely solidification cracks and reheat cracks in multipass welds and in the HAZ metal, is the most acute in welding of Nb-stabilized austenitic steels and joints of steels of greater thicknesses [11, 17]. Hot cracking in welding of Nb-containing steels is associated with formation of low-melting interlayers, enriched in niobium and nickel [11]. In addition, overheating of the HAZ metal up to the temperatures of dissolution of secondary phases (up to ~ 1300 °C), in particular niobium carbides, and their repeated precipitation in a finer form leads to strengthening of intergranular regions, lowering of their ductility and initiation of cracks in operation or at heat treatment, performed to relieve inner stresses, particularly in thick-walled components.

Some of the significant drawbacks of materials with γ-lattice are their low heat conductivity, high heat capacity, high thermal expansion, unfitness for welded joint control by the magnetic method and unreliability of their ultrasonic testing (particularly at greater thicknesses) [8, 11]. This makes them less adaptable to fabrication and more complex in manufacture and operation of high temperature components of boiler units, compared to steels with a ferrite lattice. High heat capacity of austenitic steels significantly delays reaching the required operating mode and slows down the processes of heat cycling, high coefficient of thermal expansion (50 % higher than that of the ferritic steel) causes reactive stresses and deformations both in the piping and high temperature components, and in the joints with the supporting structures, which may lead to development of fracture sites in individual zones of boiler equipment and in thick-walled welded sections [17]. Relieving the longitudinal thermal deformations in the piping requires making compensation bends (loops), which increases the labour consumption and cost of welded structures.

Despite the above problems related to use of austenitic steels, their application is justified in many cases, particularly at $T > 600$–650 °C and presence of the factor of aggressiveness of the high-temperature medium. For instance, austenitic materials are sufficiently effective in the structures of modern combined-cycle plants [11]. These plants use both the energy of overheated steam, rotating the steam turbine, and the energy of gases formed at combustion of gaseous products of the process of coal gasification and used for rotation of the gas turbine, located sequentially with the steam turbine. Efficiency of the combined cycle-plant reaches 57–58.8 % [1, 11]. Heat-resistant steels and high-temperature austenitic materials are applied simultaneously in manufacturing of such plants. The latter (for instance, nickel alloys of the type of Alloy 800 (X8NiCrAlTi3120), AC66 (X5NiCrCeNb3227, DIN N1.4877) are used in the structures of equipment for coal gasification and in the systems of gas transportation to the gas turbine [11].

Thus, the technical, ecological and economic reasons necessitated development of a new material with α-lattice, having a sufficient adaptability to fabrication and fit for operation at T ~ 560–600 °C, i.e. in the temperature range limited, on one side, by the admissible (critical) temperature of operation of the existing heat-resistant steels and, on the other hand, by temperatures, at which application of austenitic steels is more rational [7, 9].

Investigations on development of heat-resistant steels with a higher level of long-term strength were conducted for several decades in different countries. Developments were aimed at increasing chromium content from ~ 2 up to 9–12 % at alloying with mo-

lybdenum of up to 1–1.25 % and adding nickel, vanadium, titanium, niobium, cobalt and boron both separately and in certain combinations [7, 27]. However, not all the materials had the required adaptability to fabrication or satisfactory weldability. As a result the level of critical steam parameters in power units remained practically unchanged for quite a long time (about 30 years) [6, 8, 12].

By mid-70s specialists of the Oakridge National Laboratory (ORNL) and Noxville University, Tennessee, USA, based on 9Cr-1Mo steel, known since 1936, developed a modified steel of 9Cr–1Mo–NiVNbN type (designated by ASTM standard as T91 (SA-213) and P91 (SA-335)), and initially designed for making components of an experimental breeder reactor instead of a high-alloyed steel of 316 type [6, 27–29]. The target working temperature was up to 600 °C. Later on this steel was studied by metallurgists in Europe and Japan and recognized to be fit for operation in coal power units of TPS with supercritical parameters of steam, namely at T = 590–620 °C [6, 9]. It was exactly the introduction of the new steel of P91 type, that made possible raising the working parameters of steam in TPS power units in different countries of the world (Figures 1 and 3) [6, 12, 30].

At present the main manufacturers of seamless pipes of steel P91/T91 are Valourec&Mannesmann Tubes in Europe and Sumimoto Pipe&Tube Co., Ltd. in Japan [28]. According to the German standard TRD (material No.1.4903) P91/T91 steel is designated as X10CrMoVNb91 [8, 13].

By its physical properties, determining the adaptability to fabrication at operation in components of power generation equipment, P91 steel compares favourably with austenitic materials [11, 12]. As is seen from Figure 4, steel P91, compared to steel TP316LN,

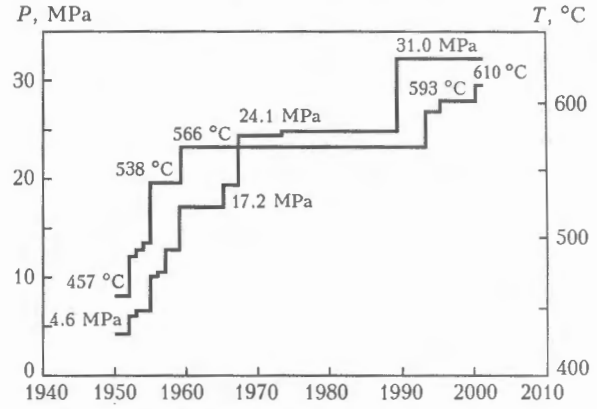

Figure 3. Nature of variation of steam parameters in Japanese TPS [30]

has more than 4 times smaller coefficient of thermal elongation and approximately 1.5 times greater coefficient of heat conductivity at heating up to working range of temperatures (550–600 °C). This means that the piping and thick-walled sections made of steel of P91 type will develop much smaller internal thermal stresses and strains. This is particularly important for thermal cycling conditions, under which thermal fatigue damage may develop in the weldments [31].

Compared to low-alloyed steels of pearlitic and bainitic class, P91 steel has higher scale resistance and long-term strength [27]. As to long-term strength it exceeds even X20CrMoV121 steel (X20) with 12 % Cr, although it has close thermophysical properties [12]. Based on extrapolation of the results of long-term testing of steel P91 at operating temperatures, its long-term strength over 10^5 h period at T = = 600 °C is estimated at 90 MPa [6, 27, 32]. This value is superior to long-term strength of X20 steel by 53 % and that of P22 steel (2.25Cr–12Mo) by 155 %, and it is approximately equal to long-term

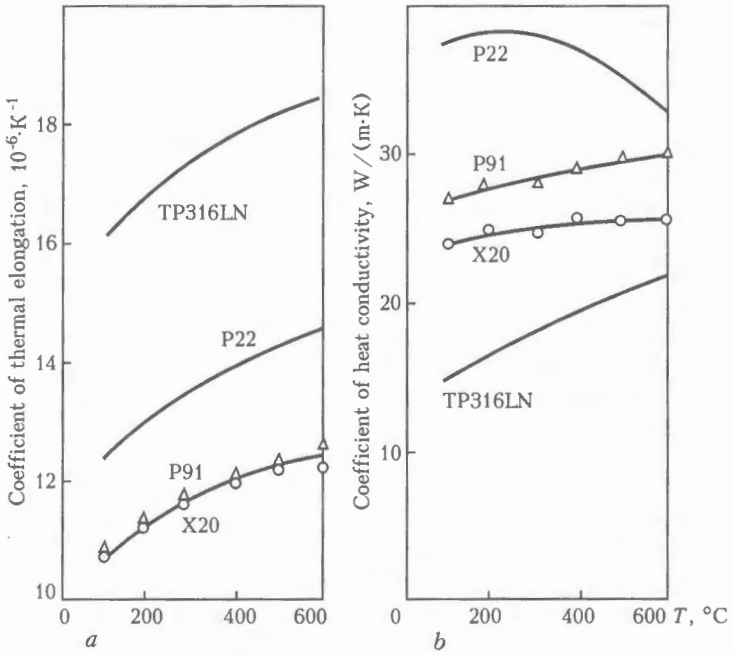

Figure 4. Comparison of physical properties of steels P91, X20 (with 12 % Cr), P22 (2.25 Cr–1Mo) with a ferritic lattice and austenitic steel TP316LN [11, 12, 19]

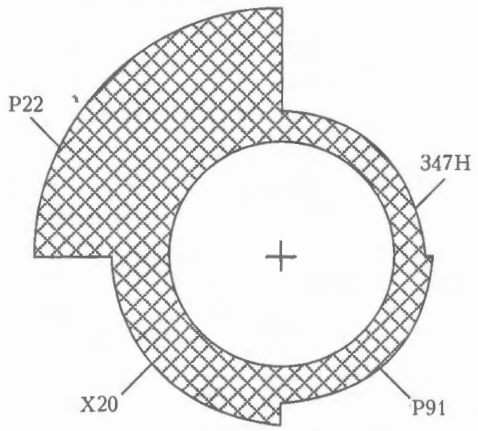

Figure 5. Thicknesses of steam piping walls of different steel grades designed for steam with the following parameters: T = 600 °C, P = = 25 MPa [33]

strength of austenitic unstabilized steel of 06CrNi1811 type [6, 11].

Owing to a higher level of long-term strength, application of steel of P91 type instead of the earlier used low-alloyed steels and steel X20 allows reducing the wall thicknesses of boiler unit components (Figure 5), thus providing a significant reduction of metal content, weight of structures and saving of funds in their manufacture [6, 13, 19, 31]. So, for instance, at replacement of bainitic steel P22 by steel P91 in fabrication of a T-joint, designed for operation at a temperature of 550 °C and pressure of 28 MPa, its weight was reduced by 65 %, and in the case of a similar replacement in manufacture of piping (for the same steam parameters) for a 600 MW power station, the design saving of funds was 34 % [13]. Replacement of steel X20 by P91 allowed reducing the weight of a fitting by 20 % [12].

Thus, development of steel P91 opens a new stage in development of modern highly efficient power generation equipment. Its physical and functional properties are characterized by a quite low heat capacity, coefficients of heat conductivity and thermal expansion, satisfactory (under the manufacturing and operating conditions) long-term strength, corrosion resistance, ductility, weldability, workability and fitness for control of welded joints using the most common ultrasonic and magnetic-powder methods, as well as a lower cost, compared to high-alloyed materials [12, 14, 31]. Steel P91, being the first material of the new generation in the group of steels with 9–12 % Cr, is becoming a rather widely accepted heat-resistant steel in the world. Several modifications have now been developed on its basis, having a higher level of long-term strength (steels of E911, NF616 type), which will be the subject of the next publication.

1. Olkhovsky, G. (1999) Technology for thermal power stations. *Gazoturbinnye Tekhnologii*, **2**, 4–7.
2. Nakicenivic, N., Raihi, K. (2002) An assessment of technological change report across selected energy scenarios. In: *Report of Int. Inst. for applied systems analysis*, May.
3. Gastajger, G., Stamatelopoulos, G.-N. (2002) Coal power stations – current level of engineering and prospects for development in the future. *Chyorn. Metally*, **10**, 26–35.
4. Shvets, I.T., Tolubansky, V.I., Bukshpun, I.D. et al. (1971) *Power engineering*. Kiev: Vyshcha Shkola.
5. Etkins, P. (1987) *Order and disorder in nature*. Moscow: Mir.
6. The success of new material. *Mannesmann Rohr. Report*. Issue S28/29.
7. Adam, W., Mischok, W., Wellnitz, G. et al. (1994) Welding of new types of steel for power plant construction. In: *Proc. of Conf. on Welding and Cutting*, Bremen, Sept. 28–30, 1994.
8. Arnswald, W., Kempkes, B., Wellmitz, G. et al. (1994) Current and future use of the 9 % Cr steel Kh10CrMoVNb91 for power plant applications. *VGB Kraftwerkstechnik*, 73(**3**), 203–208.
9. Hennhoffer, K., Jakobova, A. (1999) Properties of welded joints in 9 % Cr creep resistant steel. *Zvaranie-Svarovani*, 48(**11**), 106–108.
10. Zeman, M., Brozda, J., Pasternak, J. (1999) Ocena spawalnosci stali HSM12A przeznaczenej na elementy kotlow energetycznych pracujace przy parametrach nadkrytychnych. *Przeglad Spawalnictwa*, 71(**6**), 1–7.
11. Bendick, W., Haarmann, K., Richter, H. (1993) Die Anwendung austenitischer Rohrwerkstoffe im Kraftwerksbau. *VGB Kraftwerkstechnick*, 73(**12**), 1062–1069.
12. Bendick, W., Ullmann, K., Harmann, K. et al. (1994) Use of P91 in Europe and overseas. In: *Proc. of ASME Joint Int. Power Generation Conf.*, Phoenix, Az., Oct. 2–6, 1994. ASME.
13. Haarmann, K. (1995) New material grades for tubing and piping as replacement of T22 and P22. In: *Power-Gen'95*. Asia: Mannesmann Workshop, Singapore, Sept. 29, 1995.
14. Chepkin, V.M., Marchukov, E.Yu., Kuprik, V.V. et al. (1999) Organisation of combustion in low-emission combustion chamber GTU AL-13ST. *Gazoturbinnye Tekhnologii*, **2**, 14–17.
15. Schubert, J., Ulrichs, K., Scholler, H. (1997) Weldability of heterogeneous joints between the cast steel GX12CrMoWVNb10-11 and low-alloyed steels. *Schweissen&Schneiden*, **9**, 688–690.
16. German, S.I. (1963) *Electric arc welding of pearlitic heat-resistant steels*. Moscow: Mashgiz.
17. Zemzin, V.N., Frenkel, L.D. (1962) *Welded structures of vapor and gas turbines*. Moscow: Mashgiz.
18. (1993) *ASME Boiler and Pressure Vessel Code*. Section IX.
19. Hahn, B., Baumhoff, V., Peters, K. et al. (1997) Einsatz des Stahles X10CrMoVNb91 im Rahmen von Anlagenertuechtigungen. *VGB Kraftwerkstechnik*, 77(**3**), 214–220.
20. (1967) *Manual on electric arc welding of tubes from carbon and low-alloy steels*. Moscow: Orgenergostroj.
21. Petrov, G.L., Zemzin, V.N., Gonserovsky, F.G. (1963) *Welding of refractory stainless steels*. Moscow: Mashgiz.
22. Smit, M.K. (1962) *Principles of physics of metals*. Moscow: Metallurgizdat.
23. Honeycomb, P. (1972) *Plastic deformation of metals*. Moscow: Mir.
24. Josefsson, B., Nilsson, J.-O., Wilson, A. (1991) Phase transformation in duplex stainless steels and relation between continuous cooling and isothermal treatment. In: *Proc. of Int. Conf. on Duplex Stainless Steels'91*, Baunne, Bourgogne, Oct. 28–30, 1991.
25. Guttmann, M. (1991) Intermediate temperature aging of duplex stainless steels. *Ibid*.
26. Rejaimia, A., Metauer, G., Guantois, M. (1991) Decomposition of delta-ferrite in a Fe–22Cr–5Ni–3Mo–0.03C duplex stainless steel. A morphological and structural study. *Ibid*.
27. Koukal, J., Schwarz, D. (1998) Welding of steels for power engineering. *Zvaranie*, **6**, 2–5.
28. Irving, B. (2001) Welding offers utilities answer about new chrome-moly steel. *Welding J.*, 80(**9**), 40–44.
29. Irving, B. (1991) A promising Cr–Mo steel returns to American shores. *Welding J.*, 70(**12**), 35–40.
30. Kawasaki, H., Toyooka, T., Kimura, M. (2001) High performance tube and pipe contributing to preservation of the global environment. *Kawasaki Steel Tech. Rep.*, **44**, 92–101.
31. Bellanca, Ch., Infield, J., Zschau, M. et al. (1992) Experience with installation of new P91 secondary superheater outlet headers. In: *Reprint from PVP*. Vol. 230. Stress classification, robust methods and elevated temperature design. Book G00665. Ed. by C. Bechtiv, et al. ASTM.
32. Zschau, M., Niederhoff, K. (1994) Construction of piping systems in the new steel P91 including hot induction bends. *VGB Kraftwerkstechnik*, 74(**2**), 142–149.
33. Bergquist, E.-L. (1999) Consumables and welding modified 9Cr–1Mo steel. *Svetsaren*, 54(**1/2**), 22–25.

EFFECT OF METALLURGICAL CHARACTERISTICS OF FLUX ON STRUCTURE AND PHASE COMPOSITION OF HIGH-STRENGTH WELD METAL

G.M. GRIGORENKO, V.V. GOLOVKO, V.F. GRABIN and V.A. KOSTIN
E.O. Paton Electric Welding Institute, NASU, Kiev, Ukraine

It was established that reduction in oxygen potential of a welding flux promotes a change in the content of alloying elements in acicular ferrite and decrease in size of inclusions forming in low-alloy high-strength weld metal. In use of fluxes with a low oxygen potential the integrated deoxidation by aluminium and titanium leads to the decrease in molybdenum content in the acicular ferrite and increase in the brittle fracture resistance of the weld metal.

Keywords: *arc welding, fluxes, oxygen potential, weld metal, microstructure, acicular ferrite, non-metallic inclusions, activity of elements*

The required physical-chemical properties of metal of welds made from low-alloy steels are attained mainly owing to the presence of carbon in them and additional introducing additions of alloying elements. In welds of this type the above-mentioned properties are provided due to formation of ferrite-cementite structures and structures of austenite decay (and in some cases of martensite decay) in the intermediate region. The increase in the level of alloying to provide high strength properties decreases the resistance of this metal to cracking.

Over the recent years the tendency of application of high-strength low-alloy steels with an ultralow content of carbon (less than 0.04 wt.%) has appeared to improve the weldability and to increase the resistance against cracking. As is known, the carbon is the basic hardening element of steel, therefore the decrease in its mass share is accompanied by the decrease in strength characteristics. To provide the required level of strength in these steels, the content of alloying elements is increased to harden the structure constituents of the solid solution.

The process of metal alloying in a general form can be presented by the reaction

$$x[\mathrm{Me}] + y[\mathrm{O}] \leftrightarrow [\mathrm{Me}_x\mathrm{O}_y], \qquad (1)$$

in accordance with which the reaction can proceed both from the right to the left and also in the opposite direction depending on the content of alloying elements in metal and oxygen potential of the flux. This results either in alloying of the solid solution or in the formation of non-metallic inclusions (NMI).

In works [1–4], devoted to investigation of effect of alloying processes on the conditions of formation of structure of low-alloy steels, the authors noted a special role of such highly-active deoxidizers as aluminium and titanium, being simultaneously alloying elements. In study of effect of these elements on structure of weld metal the main attention was paid to Al- and Ti-containing NMI, namely their amount, composition, sizes and density of distribution. The problems of effect of solid solution alloying by aluminium and titanium on the formation of separate structure constituents were remained until now as those of the secondary importance.

The study of peculiarities of alloying the solid solution of weld metal is actual, but a little-investigated problem. Investigations in this field will make it possible to widen the application of such advanced type of structural materials as high-strength low-alloy steels, including those with an ultralow content of carbon.

The aim of the present work is to study the effect of deoxidation of weld pool by aluminium and titanium depending on oxygen potential of flux on the level of alloying and content of separate structure constituents of weld metal and also on the mechanical properties of the deposited metal.

Procedure of experiment. As was mentioned earlier, in arc processes of welding the alloying elements, transferring from welding consumables into a weld metal, are located either in the composition of NMI or in the solid solution depending on oxygen potential of the gas phase. Consequently, by changing the oxygen potential of the flux and its alloying ability it is possible to control the content of definite structure constituents in weld metal produced in submerged arc welding (SAW).

Specimens of deposited metal of multipass welds made by welding using agglomerated fluxes were selected for investigations that gave an opportunity to control both the oxygen potential of gas and slag phases and also the weld metal alloying. To study the effect of solid solution alloying on content of structure constituents in weld metal, aluminium and/or ferrotitanium of 25 % mass share of titanium were added to the composition of fluxes.

Butt joints, prepared in accordance with requirements of European standard EN 1597-1 [5], were produced on 20 mm thick low-alloy steel 10KhSND (GOST 19282–73) in welding with 5 mm diameter

Table 1. Marking of welds and characteristics of welding fluxes

Type of welding flux (BI)	No. of weld	Mass share of alloying elements, %		Oxygen potential π_O, kJ/mol
		Al	Ti	
BMS 166 AC Acid (0.67)	13/1	0.5	–	–307
	13/4	–	0.4	
	13/7	0.5	0.2	
BAB 156 DC Neutral (1.25)	9/1	0.5	–	–337
	9/4	–	0.4	
	9/7	0.5	0.2	
BFB 156 DC Basic (2.53)	19/1	0.5	–	–369
	19/4	–	0.4	
	19/7	0.5	0.2	

wire Sv-04N3GTA. Welding was performed at direct current of reverse polarity using the following conditions: $I_w = (620 \pm 5)$ A; $U_a = (30 \pm 1)$ V; $v_w = (20 \pm \pm 0.5)$ m/h; $q_w = 48$ kJ/cm.

Welding was performed under fluxes of three types, differing by an index of basicity BI, which was calculated by IIW formula [6]. Oxygen potential of flux was determined by formula from [7]:

$$\pi_O = RT \ln P_{O_2} \text{ [kJ/mol } O_2\text{]},$$

where R is the universal gas constant equal to 8.31 J/(mol·K); T is the temperature of melt, K; P_{O_2} is the partial pressure of oxygen over the slag melt, measured by procedure suggested in [8].

Type of welding fluxes (in accordance with EN 756), their oxygen potential, and also content of aluminium and titanium in fluxes are given in Table 1.

Specimens for metallographic examinations were cut from the deposited metal. Chemical composition of metal was determined by a spectral analysis in Baird unit, equipped with IBM computer. From three to five determinations were made for each specimen. Averaged results of analysis and composition of welding wire are given in Table 2.

During metallographic examinations the share of separate constituents of microstructure of metal of welded joints, content of alloying elements in solid solution, element composition and NMI distribution were determined. Microstructure of metal of welded joints was examined by the methods of optical and electron metallography using a light microscope «Neophot-32» and JEOL scanning electron microscope JSM-840, furnished with a board of capture of images MicroCapture for their subsequent recording on the monitor screen. Quantitative determination of microstructural constituents was performed in accordance with procedure of IIW [9]. Content of alloying elements in solid solution and element composition of NMI was determined by X-ray diffraction microanalysis using a Link System energy-dispersion spectrometer Link 860/500 and Ortec wave-dispersion spectrometer.

Microstructures of metal of examined specimens are given in Figure 1.

Data about NMI distribution by sizes and content of alloying elements in NMI are given in Tables 3 and 4.

Results of examinations. It was established during the metallographic examinations that the following main structure constituents are present in the specimens of weld metal: acicular ferrite (AF), polygonal (allotriomorphic) ferrite (PF), Widmannstatten ferrite (WF), ferrite with ordered (FOSP) and non-ordered (FNOSP) second phase, and also martensite-austenite-carbide (MAC) phase. Data about content of these structure constituents in the specimens examined (Table 5) prove that the most remarkable effect on content of separate constituents is exerted by the aluminium alloying of weld metal. As is seen from Figure 2, the deoxidation of the weld pool by aluminium, not depending on the oxygen potential of the flux, leads to the limitation of the volumetric share of PF in weld metal, while in case of deoxidation by titanium the content of this structure constituent is determined only by the level of π_O.

As the results of examinations (see Table 2) showed, the content of aluminium in weld metal is

Table 2. Chemical composition of metal of welds and welding wire (wt.%) in the specimens examined

Object of analysis	C	Al	Si	Ti	Ni	Mn	Mo	Cr	Cu	S	P
Welding wire	0.020	0.002	0.16	0.004	2.29	0.62	0.17	0.17	0.20	0.010	0.011
Weld metal											
13/1	0.032	0.007	0.84	0.001	2.40	0.84	0.19	0.12	0.15	0.009	0.004
13/4	0.031	0.010	0.89	0.003	2.48	0.82	0.20	0.11	0.15	0.019	0.005
13/7	0.035	0.007	0.81	0.001	2.39	0.82	0.19	0.13	0.16	0.009	0.005
9/1	0.036	0.011	0.35	0.003	2.32	0.84	0.18	0.18	0.18	0.009	0.007
9/4	0.036	0.014	0.32	0.003	2.36	0.84	0.17	0.18	0.19	0.008	0.007
9/7	0.039	0.014	0.41	0.003	2.46	0.89	0.19	0.17	0.19	0.009	0.008
19/1	0.037	0.023	0.13	0.005	2.43	0.55	0.17	0.17	0.14	0.009	0.005
19/4	0.036	0.028	0.13	0.003	2.46	0.52	0.16	0.17	0.13	0.007	0.009
19/7	0.038	0.034	0.12	0.002	2.53	0.52	0.19	0.15	0.15	0.008	0.007

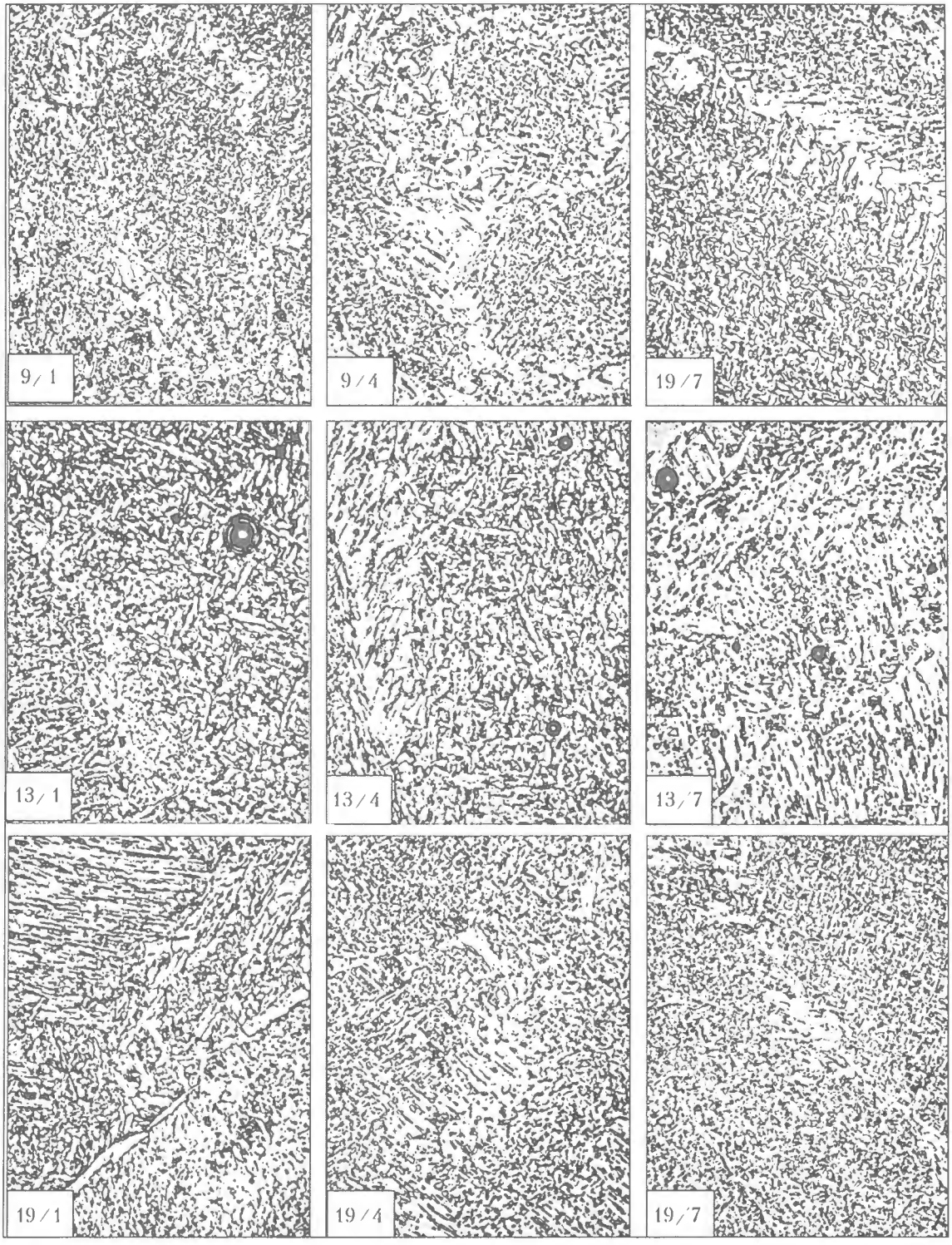

Figure 1. Microstructures of low-alloy high-strength steel metal of welds (×400)

changed negligibly in case of alloying through fluxes of acid and neutral types. In case of use of flux of the basic type (π_O = −369 kJ/mol) the mass share of aluminium in the deposited metal is increased from 0.023 up to 0.034 %. Content of titanium in metal, deposited under flux of all types, is almost similar (0.001–0.005 %).

In accordance with the scheduled program of examinations, the content of alloying elements in separate structure constituents and element composition of NMI were also determined, except the general chemical composition of metal of the specimens. It can be concluded on the basis of data about V_{NMI} in specimens of deposited metal and distribution of NMI by sizes (see Table 3) that NMI of 0.5–1.5 μm size were observed mainly in the specimens examined. Composition of NMI, given in Table 4, proves that they are based mainly on manganese silicates. With decrease in oxygen potential of fluxes the total content of aluminium is increased in the composition of NMI, while that of titanium is increased negligibly. The increase in aluminium content in the deposited metal

Table 3. Distribution of NMI (wt.%) by sizes in metal of welds examined

π_O, kJ/mol	Deoxidizer	Size of NMI, μm									V_{NMI}, vol.%
		≤ 0.5	0.5–1.0	1.1–1.5	1.6–2.0	2.1–2.5	2.6–3.0	3.1–3.5	3.6–4.5	4.6–6.0	
–307	Al	18.6	37.0	21.2	10.5	5.4	2.0	1.7	1.4	0.2	1.18
	Ti	25.1	37.5	18.7	9.0	4.6	1.9	1.4	0.7	0.1	1.36
	Al + Ti	18.1	34.3	17.9	14.2	5.5	4.5	1.2	1.5	0.4	1.09
–337	Al	19.5	50.8	20.5	5.6	2.2	0.7	0.6	0.3	0	0.36
	Ti	21.9	50.8	19.3	4.6	2.2	1.0	0	0	0	0.38
	Al + Ti	19.2	46.9	19.1	7.9	3.27	1.5	1.5	0.6	0	0.33
–369	Al	22.9	50.0	17.2	7.5	2.2	0.2	0	0	0	0.27
	Ti	22.1	44.3	19.9	6.2	1.7	1.0	0.2	0.2	0	0.26
	Al + Ti	20.1	51.2	19.8	5.5	1.7	1.1	0.3	0	0	0.22

*V_{NMI} – volumetric share of NMI.

Table 4. Mass share of alloying elements in NMI, %

π_O, kJ/mol	Al	Ti	Si	Mn	Mo
–307	2.6	1.0	51.0	43.2	0.1
–337	11.5	3.6	21.4	62.9	0.5
–369	27.2	2.0	20.5	49.7	0.5

Note. Nickel in NMI composition is absent.

leads to the increase in its mass share in NMI (Figure 3).

The effect of changes in NMI composition on structure of the deposited metal is shown in Figure 4. In all cases the increase in aluminium content in NMI composition leads to the reduction in amount of PF and growth of AF in weld metal. For metal of welds, produced in SAW at the higher values of the oxygen potential (π_O = –307 and –337 kJ/mol), these changes are more noticeable than in case of SAW at the lower oxygen potential (π_O = –369 kJ/mol) (see Figure 4, Table 5).

Data about content of alloying elements in separate structure constituents of metal of welds examined are given in Table 6.

With reduction in value of the oxygen potential of fluxes the deoxidation of metal of welds by aluminium leads to the decrease in silicon content in PF, AF, MAC-phase and increase in aluminium content in PF and AF. This reduction in content of nickel and manganese in the above-mentioned structure constituents, typical of specimens of weld metal, produced in SAW at a low oxygen potential (π_O = –369 kJ/mol), should be noted.

In weld metal deoxidation by titanium the decrease in oxygen potential of fluxes causes the reduction in a mass share of silicon at almost complete absence of aluminium in PF, AF and MAC-phase, and also a mass share of nickel in AF and MAC-phase. The increase in manganese content in examined structure constituents in specimens of metal, produced in SAW using fluxes of a neutral type (π_O = –337 kJ/mol), and also the increase in molybdenum content in MAC-phase in welding using an acid flux (π_O = –307 kJ/mol) are observed.

Deoxidation of weld pool simultaneously by aluminium and titanium is accompanied by the reduction in a mass share of silicon and increase of aluminium in PF and AF at the decrease in oxygen potential of fluxes. Specimens produced in SAW using neutral fluxes are characterized by an increased content of manganese in PF, AF and MAC-phase, while an abrupt increase in a share mass of molybdenum in MAC-phase and its decrease in AF are characteristic in case of SAW using a basic type of fluxes.

Table 5. Volumetric share of main structure constituents (%) in metal of welds examined

No. of weld	PF	WF	AF	FOSP	FNOSP	MAC-phase
13/1	16–20	10	31–37	14–15	24–27	5.4
13/4	18–20	9–12	25–34	16–27	20–23	5.0
13/7	15–20	6–7	44–48	24–25	20–27	3.4
9/1	13–19	3–5	40–45	17–20	23–25	4.0
9/4	13–17	3–9	46–49	13–19	16–18	5.0
9/7	13–22	7	43–46	13–18	6–14	2.3
19/1	10–15	3	50–55	16–27	17–21	2.5
19/4	10–13	4	48–50	12–25	32–37	3.5
19/7	6–12	2	48–51	11–15	36–38	2.4

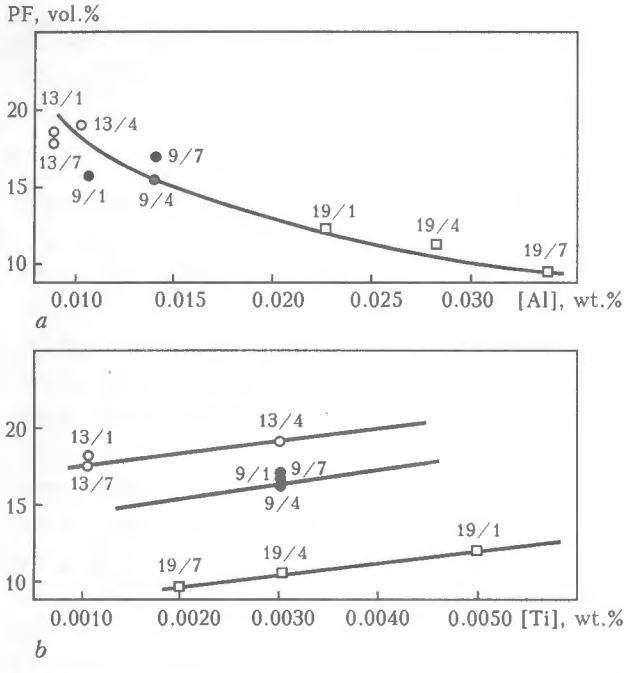

Figure 2. Effect of content of aluminium (*a*) and titanium (*b*) in weld metal on a volumetric share of PF in its structure in SAW at different oxygen potential: ○ – π_O = –307; ● – –337; □ – –369 kJ/mol (figures at signs are the number of welds)

Table 6. Mass share of alloying elements (%) in structure constituents of weld metal

No. of weld	*Object of analysis*	*Al*	*Si*	*Ti*	*Ni*	*Mn*	*Mo*
13/1	PF	0	0.436	0.005	1.978	0.646	0
	AF	0	0.531	0.012	2.261	0.712	0.327
	MAC	0	0.776	0.028	2.202	0.769	0.507
13/4	PF	0	0.504	0.021	2.071	0.627	0.288
	AF	0	0.640	0.030	2.426	0.713	0.427
	MAC	0	0.495	0.056	2.826	0.689	1.130
13/7	PF	0	0.621	0	2.330	0.669	0.626
	AF	0	0.632	0	2.370	0.754	0.618
	MAC	0	0.455	0.034	2.890	0.553	0.256
9/1	PF	0	0.327	0.008	1.836	0.824	0.287
	AF	0.002	0.325	0.020	2.080	0.889	0.167
	MAC	0	0.363	0.026	2.171	0.895	0.822
9/4	PF	0	0.261	0.024	2.159	0.884	0.298
	AF	0	0.338	0.032	2.140	0.901	0.245
	MAC	0	0.411	0.040	2.145	0.867	0.340
9/7	PF	0.030	0.424	0	2.116	0.920	0.477
	AF	0.001	0.329	0.001	2.441	0.963	0.395
	MAC	0	0.585	0.054	3.088	1.144	0
19/1	PF	0.006	0.155	0	1.778	0.436	0.155
	AF	0.008	0.208	0.002	1.979	0.496	0.353
	MAC	0.001	0.249	0.040	2.117	0.544	0.001
19/4	PF	0.002	0.189	0.025	1.609	0.450	0.149
	AF	0	0.233	0.033	1.960	0.541	0.357
	MAC	0	0.215	0.044	1.968	0.567	0.624
19/7	PF	0.010	0.209	0	1.922	0.474	0.282
	AF	0.014	0.200	0.007	2.073	0.579	0.181
	MAC	0.002	0.332	0.040	2.505	0.484	0.726

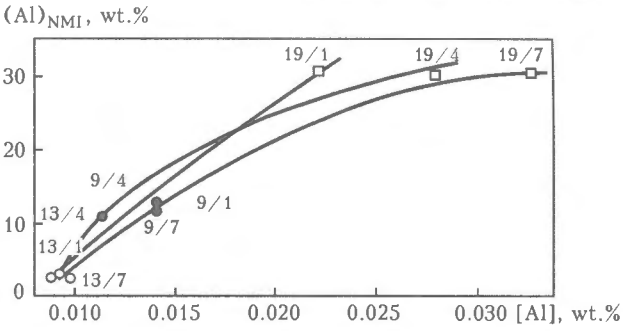

Figure 3. Effect of aluminium content in weld metal on its content in NMI (see designations in Figure 2)

The results obtained make it possible to conclude that with a decrease in oxygen potential of welding fluxes the content of alloying elements (except silicon) in structure constituents of solid solution of the deposited metal is mainly increased. Selection of system of weld pool deoxidation has also a remarkable influence on this process.

Analysis of results of examinations and their discussion. AF structure of metal of low-alloy welds is characterized by the most optimum combination of characteristics of strength and toughness. To have a better understanding of the processes occurring in weld metal, it is rational to study separately the results of investigation of effect of several factors, referred to NMI, and those of analysis of content of alloying elements in main structure constituents.

Numerous works were devoted to the problem of effect of NMI on AF content in structure of weld metal, some fundamental studies among them will be distinguished [10–12]. Authors of these works came to the following conclusion. With increase in a volumetric share of NMI in weld metal the AF content in its structure is decreased. To form this structure constituent in weld metal, the fine-dispersed inclusions

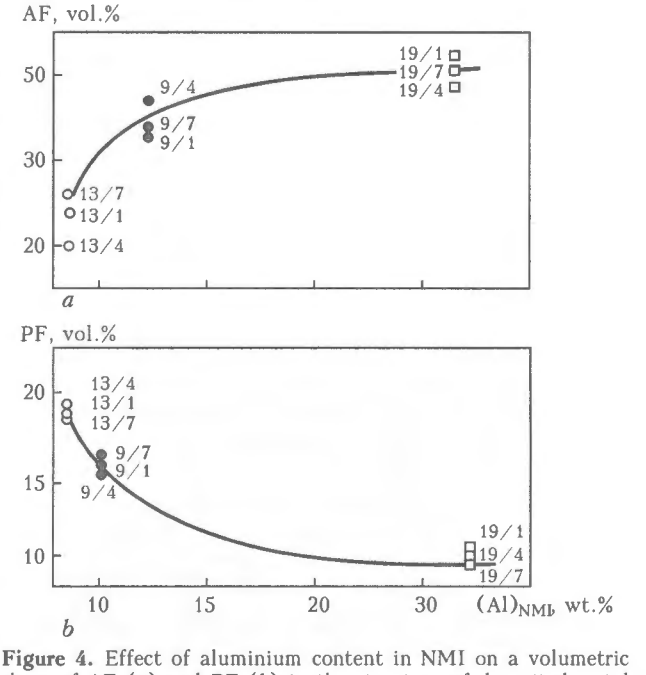

Figure 4. Effect of aluminium content in NMI on a volumetric share of AF (*a*) and PF (*b*) in the structure of deposited metal (see designations in Figure 2)

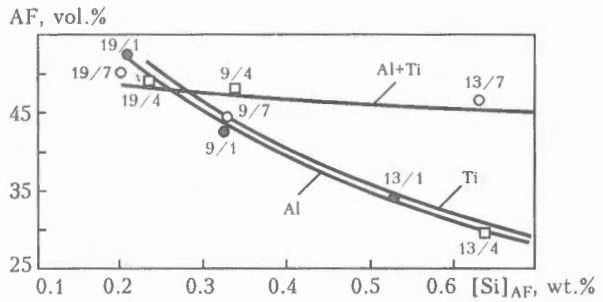

Figure 5. Effect of silicon content in AF on a volumetric share of AF in weld metal at different systems of deoxidation (see designations in Figure 2)

of the manganese alumosilicates type and also NMI with an increased content of titanium are most preferable. As the results of investigation showed, some other dependence is observed in case of weld metal with an ultralow content of carbon. Increase in oxygen potential of fluxes leads to the growth in a volumetric share of NMI in weld metal (see Table 3). Here, the AF content in their composition is though decreased, but remains at a sufficiently high level (see Table 5). It is quite evident that such phenomenon is associated with a level of AF alloying in weld metal of this type. As is seen from Figure 5, in weld metal, produced in SAW using fluxes with a system of alloying by aluminium or titanium, the decrease of silicon content in AF is accompanied by the increase in a mass share of the latter, and in case of using the fluxes of Al + Ti system of alloying the volumetric share of AF is remained almost at the same level independently of the degree of AF alloying by silicon.

This ambiguous effect of level of structure constituent alloying on its content in weld metal is usually due to the change in coordinates of characteristic points of the temperature interval of $\gamma \rightarrow \alpha$ transformation.

It is known [13] that the shifting of characteristic points of temperature interval of $\gamma \rightarrow \alpha$ transformation can be observed by study of changing the sizes of a primary austenitic grain. For this purpose we have made experiments for the determination of a mean size of primary austenitic grains. Results, presented in Figure 6, prove that with decrease in oxygen potential of fluxes the increase in size of the primary austenitic grain in the deposited metal is occurred.

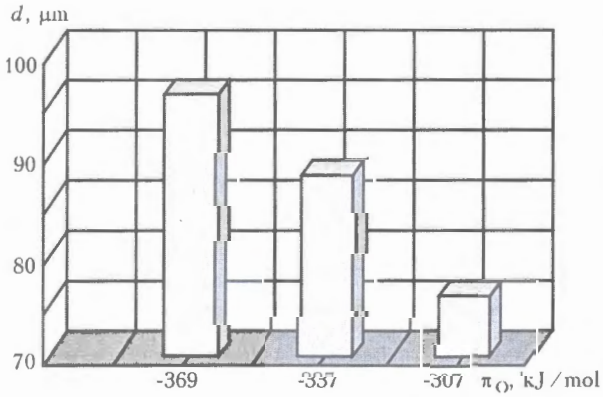

Figure 6. Effect of oxygen potential of fluxes π_O on size of primary austenitic grain d

Table 7. Amount of NMI and their averaged size in weld metal

π_O, kJ/mol	Deoxidizer	Volumetric share of NMI in austenitic grain, %		F	Average value of NMI in austenitic grain, μm	
		Along boundaries	Inside		Inside	Along boundaries
−307	Al	1.398	0.971	0.590	0.590	0.382
	Ti	1.127	0.895	0.557	0.557	0.395
	Al + Ti	1.381	1.023	0.574	0.574	0.323
−337	Al	0.401	0.155	0.529	0.529	0.289
	Ti	0.372	0.172	0.683	0.683	0.249
	Al + Ti	0.341	0.192	0.639	0.639	0.295
−369	Al	0.385	0.124	0.754	0.754	0.253
	Ti	0.330	0.103	0.762	0.762	0.279
	Al + Ti	0.304	0.136	0.691	0.723	0.288

This circumstance, in our opinion, is due to the change in a volumetric share of NMI (see Table 3) and their distribution within the ranges of the primary austenitic grain.

In this connection, a volumetric share of NMI inside and along the boundary of the primary austenitic grain was determined. The results obtained are given in Table 7. It is seen from its data that the fine-dispersed inclusions, located along the primary austenite boundaries, are retarding most effectively its growth. The study of inclusions of the mean size showed that the finer inclusions (0.2–0.4 μm) are located at their boundaries as compared with those inside the grain body (0.5–0.8 μm).

Besides, it was found that the volumetric share of NMI at the boundary of the primary austenitic grain is higher than the volumetric share inside the grain. It was suggested to evaluate the non-uniformity of NMI distribution [12] using coefficient F, representing the relation

$$F = V_{\text{bound}}/(V_{\text{bound}} + V_{\text{inside}}),$$

where V_{bound} and V_{inside} is the volumetric share of NMI, respectively, along the boundaries and inside the primary austenitic grain, as regards to unity of the area.

Coefficient F, connected with their non-uniform distribution, was 0.6–0.7 for the most examined welds. Values F, obtained by us, occurred to be somewhat lower than those presented in [12], i.e. 0.7–0.8. Difference in distribution of NMI between the boundary and inner regions of the primary austenitic grain is due, probably, both to a higher heat input (4.2 kJ/mm in our work against 2.5 kJ/mm in work [12]), and also to the difference in the basicity of the fluxes used.

As was expected, the volumetric share of NMI along the boundary and inside the primary austenitic grain is higher in use of an acid flux as compared with neutral and basic fluxes (see Table 3). From compari-

Table 8. Mechanical properties of weld metal

No. of weld	Ultimate rupture strength σ_t, MPa	Yield strength σ_y, MPa	Elongation δ_5, %	Reduction in area ψ, %	Actual stress of fracture S_k, MPa	Impact strength a_n, J/cm^2, at temperature, °C	
						-40	-60
13/1	662–666	558–565	21–24	56	1505–1514	69–85	10–22
9/1	678–682	560–567	22–24	64–66	1883–2006	68–93	38–49
19/1	759–768	652–673	19–22	49–56	1488–1745	10–22	6–12
13/4	669–680	541–555	20–23	56–58	1545–1593	15–21	9
9/4	680–680	566–562	22–25	62	1789	49–61	10–37
19/4	740	591–601	18	49–51	1451–1510	19–33	7–19
13/7	633–637	548–555	22	53	1347–1355	28–35	9–12
9/7	623	514–529	25–29	71–73	2148–2307	37–44	17–18
19/7	682–700	624–650	21–24	70–71	2333–2352	120–150	56–118

son of data, given in Table 7 and Figure 6, it can be concluded that the increase in NMI content at the boundary of the primary austenitic grain as compared with their content inside the grain body leads, as a whole, to the decrease in the austenitic grain size. When the combined deoxidation of the weld pool by aluminium and titanium is used, the content of inclusions inside the austenitic grain is higher than that in case of use of these deoxidizers separately, that is explained by the effect of an integrated deoxidation of the metal. This phenomenon is well studied and widely used in the ferrous metallurgy. The thermodynamic calculations showed that the reaction of deoxidation (1) is proceeding from the left to the right until finishing of one of reagents in the left part of equation or beginning of saturation of solution with products of interaction. Constant of equilibrium of this reaction is determined from expression

$$K = \frac{a_{Me_xO_y}}{a^x_{Me} a^y_O}, \qquad (3)$$

where $a_{Me_xO_y}$, a^x_{Me}, a^y_O is the activity, respectively, of oxide, deoxidizer and oxygen in metal.

Reduction in activity of oxide in metal for reactions of deoxidation (at the condition K = const) leads to the decrease in content of oxygen in the solution. In case of an integrated deoxidation the oxides of a complex composition, having a lower activity in the molten metal as compared with «pure» oxides of aluminium or titanium, are formed in the weld pool. As a result, the total content of NMI is decreased (see Table 3) and the volumetric share of NMI inside the austenitic grain is increased (see Table 7) in weld metal alloyed by aluminium and titanium as compared with that alloyed only by aluminium or only by titanium. Participation of silicon in the process of deoxidation, which enters the pool from welding consumables, promotes the formation of complex alumosilicates having a relatively high temperature of melting. Refining of weld pool by NMI is defined by interfacial tension at the NMI–slag interface. The interfacial tension at the NMI–slag interface of aluminium oxide type with steel is about 1300 mN/m, while that of manganese-alumosilicate type is 600 mN/m [13]. Therefore, the assimilation of silicate inclusions is increased and their relative content is decreased at an integrated deoxidation in metal of welds. As a result, the role of more refractory NMI of type of alumosilicates and oxides of titanium is increased in the formation of the secondary structure of the weld metal.

It is seen from Figure 5 that in use of an integrated deoxidation of weld pool the AF content in weld metal structure is higher than in two other variants. These changes should be, undoubtedly, at the level of mechanical properties of the weld metal. To check this assumption the specimens were manufactured and tests were conducted, the results of which are given in Table 8.

It is seen in comparison of data, given in Tables 6 and 8, that in case of a separate deoxidation by aluminium or titanium at a low oxygen potential of fluxes (π_O = –369 kJ/mol) the increase in level of AF alloying with molybdenum is occurred, thus deteriorating the toughness and ductility of specimens from deposited metal. At a combined deoxidation by aluminium and titanium the level of AF alloying by molybdenum is reduced with increase in basicity of the welding flux, that is accompanied by the increase in actual fracture stress S_k of specimens (Figure 7) that characterizes the metal resistance against the brittle fracture. This can be explained by the fact that with decrease in oxygen potential of fluxes the value a^x_{Me} is increased in equation (2) which describes a constant of equilibrium of deoxidation reaction and the content of alloying elements in solid solution is increased, respectively, and also the amount and dispersity of NMI in the crystallizing metal is increased. In welding with high-basicity fluxes using a separate deoxidation by aluminium and titanium the increase in level of solid solution alloying leads to extremely high hardening of structure constituents and, due to this, to the reduction in toughness and ductility of metal of welds. In case of an integrated deoxidation of the

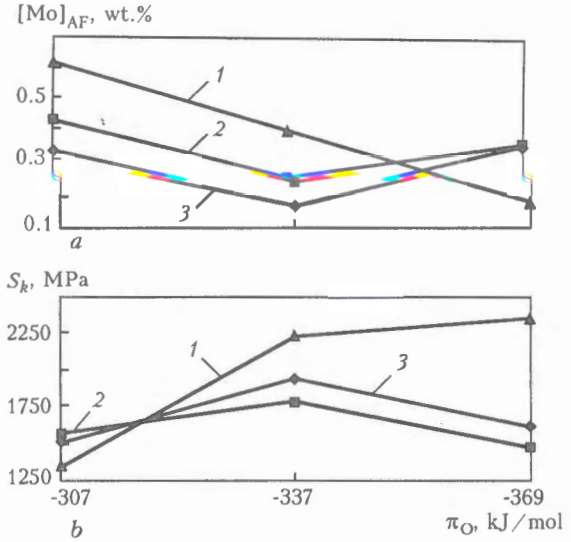

Figure 7. Effect of oxygen potential of fluxes π_O and system of weld pool deoxidation on molybdenum content in AF (*a*) and actual fracture stress of weld metal S_k (*b*): *1* — Al + Ti; *2* — Ti; *3* — Al

weld pool the values a_O^y are decreased and NMI of a complex composition are formed in the metal.

It is known that the elements-net formers (silicon, vanadium, molybdenum, tungsten) are dissolved intensively in oxide melts [14]. As is seen from Table 4, when the integrated deoxidation is used the alumosilicates are mainly formed in weld metal, the melting temperature of which is about 1700 °C, while at separate deoxidation the NMI represent manganese silicates of 1200 °C melting temperature. If the refractory inclusions can be removed into a slag phase as a result of an intensive hydrodynamic stirring of the weld pool, then NMI of silicates type are formed in that temperature zone of the pool which is characterized by a minimum stirring of the melt. Some of these inclusions are precipitated in the form of a condensed phase at the temperature being lower than that of the metal crystallization. Owing to this and also to the fact that the solubility of molybdenum in alumosilicates is higher than in silicates (see Table 4 and Figure 8), the level of molybdenum alloying the structure constituents of the solid solution is decreased at an integrated deoxidation. This results in providing the high level of brittle fracture resistance of metal deposited under the high-basicity flux.

CONCLUSIONS

1. Oxygen potential of welding consumables and also the selection of weld pool deoxidation system influence greatly the conditions of formation of the weld metal structure.

2. Reduction in oxygen potential of welding fluxes from −307 up to −369 kJ/mol promotes the change in content of molybdenum in AF and reduction in size of NMI forming in weld metal from 1.20 to 0.24 %.

3. Content of NMI located along the boundaries of the austenitic grain is higher and their sizes are

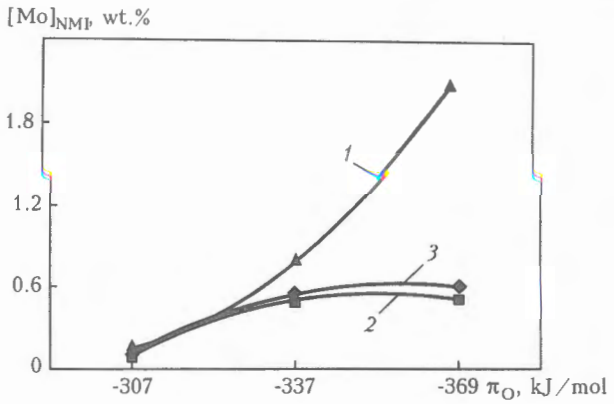

Figure 8. Effect of oxygen potential of flux π_O on molybdenum content in NMI (see designations in Figure 7)

smaller than that of those NMI located in its inner volume.

4. Increase in content of fine-dispersed inclusions along the boundaries of the primary austenitic grain retards their development in the process of metal cooling.

5. When fluxes with a low oxygen potential are used, the integrated deoxidation by aluminium and titanium leads to the decrease in content of molybdenum in AF and to the increase in brittle fracture resistance of weld metal.

6. By changing the system of deoxidation and flux basicity, it is possible to control the processes of formation of optimum structure to obtain the highest characteristics of strength and ductility of welds, made from low-alloy steels with an ultralow content of carbon, resistant to brittle fracture.

1. Povolotsky, D.Ya. (1970) *Aluminium in structural steel.* Moscow: Metallurgiya.
2. Lyakishev, N.P., Pliner, Yu.L., Lapko, S.I. (1985) *Doping alloys and steels with titanium.* Moscow: Metallurgiya.
3. Liao, F.-C., Liu, S. (1992) Effect of deoxidation sequence on carbon manganese steel weld metal microstructures. *Welding J.*, **3**, 94–103.
4. Gutovsky, I.B., Bondarchuk, V.I., Kochkin, V.G. et al. (1991) About influence of oxide inclusions on mechanical properties of steel with low hydrogen content. *Metallovedenie i Term. Obrab. Metallov*, **9**, 13–16.
5. *EN 1597-1.* Schweisszusaetze-Pruefung zur Einteilung. Teil 1: Pruefstueck zur Entname von Schweissgutproben an Stahl, Nickel und Nickellegierungen. Austria.
6. (1978) Guide to the use of wires and fluxes classified in IIW Doc. XII-666–77. *IIW Doc. XII-A-164–78.*
7. Kazachkov, E.A. (1988) *Calculations on theory of metallurgical processes.* Moscow: Metallurgiya.
8. Pokhodnya, I.K., Golovko, V.V., Kushneryov, D.M. et al. (1990) Evaluation of oxidizing ability of ceramic fluxes. *Avtomatich. Svarka*, **2**, 45–48.
9. (1986) Guidelines for the classification of ferritic steel weld metal microstructural constituents using the light microscope. *Welding in the World*, 24(7/8), 144–148.
10. Abson, L.D. (1987) Non-metallic inclusions in ferritic steel weld metal: A review. *IIW Doc. IX-1486–87.*
11. Devillers, L., Kaplan, D., Ribes, A. et al. (1986) Metallurgie et proprietes mecaniques du metal fondu en soudage multipasse sous flux d'acier au C–Mn microallie/ Memoires et etudes scientifiques. *Revue de Metallurgie*, 83(1), 43–62.
12. Liu, S., Olson, D.L. (1986) The role of inclusions in controlling HSLA steel weld microstructures. *Welding J.*, **6**, 139–149.
13. (1985) *Atlas of slags.* Ed. by I.S. Kulikov. Moscow: Metallurgiya.
14. Boronenkov, V.N., Esin, O.A., Shurigin, G.Ya. (1970) *Physical chemistry of molten slags.* Kiev: Naukova Dumka.

FEATURES OF ARGON-ARC TREATMENT WITH INSIPIENT MELTING OF WELDED JOINT ON QUENCHING STEEL

V.M. KULIK, M.M. SAVITSKY, D.P. NOVIKOVA and V.A. KRASNOSHCHEKOVA
E.O. Paton Electric Welding Institute, NASU, Kiev, Ukraine

It is shown that treatment of welded joints on 30KhGSA steel improves weld metal formation, refines its structure, produces higher impact toughness of the HAZ metal of welded joint. It is established that in argon-arc treatment of a welded joint on medium-carbon alloyed steel MAC-phase precipitates can form in the HAZ overheated region.

Keywords: *argon-arc treatment, high-strength steel, welded joint, heating, insipient melting, cooling, quenching, structure, impact toughness*

Thin high-strength steel is used for manufacturing high-performance welded products with a lower metal content. TIG welding with activating fluxes (A-TIG welding) is widely used in their manufacture. This allows eliminating edge preparation, reducing the consumption of power and welding consumables and heat input [1]. However, reduction of the heat input results in higher rate of cooling of the welded joints and greater quenching effect, this leading to lower values of toughness, ductility and crack resistance [2]. Therefore, they are subjected to furnace tempering right after welding or with a minimum interval after it. This makes the technology more complicated, increases the labour and power costs, lowers the productivity, and requires using expensive furnace equipment. In addition, furnace tempering cannot always be implemented, particularly in fabrication of large-sized structures.

Power consumption can be reduced and the effectiveness of the technology can be increased by applying local argon-arc treatment of the welded joints [3, 4]. It further increases the ductility, toughness and delayed cracking resistance of the joint, and, this being important, it can be performed with the same equipment and fixtures and without fastening supports, thus allowing product distortion to be eliminated.

Depending on the mode, argon-arc treatment without insipient melting of the metal leads to quenching or tempering of the welded joint. It may be conducted at a speed many times higher than that of welding. At insipient melting metal heating is enhanced, welded joint quality can be improved, however, it is difficult to perform processing at a high speed because of poorer weld formation. The purpose of this work is investigation and determination of the possibility of changing and improving the structure and properties of a welded joint on high-strength steel, depending on the mode of argon-arc treatment with insipient melting, to simplify the technological process of product manufacturing.

Experiments were conducted in a welding machine ARK-1 with VSVU-315 rectifier. High-strength medium-alloyed 30KhGSA steel 3, as well as 6 mm thick, manufactured and rather widely applied for fabrication of welded structures in Ukraine and abroad, was welded by A-TIG process, and welded joints were subjected to argon-arc treatment with insipient melting. For this purpose the butts were assembled without edge preparation with 50 mm distance between the heat-removing clamps, edges were coated by activating flux VS-2e, and gravity welding was performed with through penetration in modes regular for these thicknesses: I_w = 130 A, U = 9 V, v_w = 12 m/h, and I_w = 180 A, U = 11 V, v_w = 6 m/h. After cooling down and removal of slag from remelted activating flux the butt joints were treated by TIG process in argon with longitudinal displacement and transverse oscillations with an amplitude of 5–7 mm and frequency of 2–3 s^{-1}. Modes of argon-arc treatment were varied in the following range: I_{tr} = 70–140 A, U_{tr} = 11–12 V, v_{tr} = 4.5–12.0 m/h. Thermal cycles of welding and treatment were recorded with WRe–WRe thermocouple VR 20/5 of 0.35 mm diameter and N105 oscillograph.

Macro- and microstructure was studied, using microscope «Neophot-32» at 25-, 50-, 200-, 320-, 400- and 1000-fold magnification after section etching in water solutions of ammonium persulphate, sodium picrate and picric acid. Cross-sectional microhardness of the welded joint was determined by LECO hardness meter at 50 and 10 g load. Detection and determination of the size of grain was performed to GOST 5639–82 (ST SMEA 1959–79), mechanical testing of welded joints was conducted to GOST 6996–66 on flat samples for rupture testing without back reinforcement and samples with a round notch for impact toughness testing. HAZ resistance to cold cracking was evaluated by the time of delayed fracture of a flat sample [5] of 3×14 mm cross-section after appli-

Table 1. Parameters of argon-arc treatment (welding), structure and properties of welded joints on 30KhGSA steel 3 mm thick

Treatment No.	Treatment (welding) mode			Size of IMR		Structure			
						Weld		HAZ overheated zone	
	Current I, A	Speed v, m/h	Heat input q/v, W·h/m	Depth h	Width b	IMR	Beyond IMR	In treatment	In welding
1	(130)	(12)	(97)	–	–	(UB>, LB, M)	(UB>, LB, M)	(UB>, LB, M)	(UB>, LB, M)
2	130	12	119	2.2	7.0	UB>, LB, M	UB>, LB, M	UB>, LB, MACP	UB>, LB, MACP
3	105	12	96	0.5	7.0	UB>, LB, M	UB, LB>, M	UB, LB>, MACP	UB>, LB, MACP
4	105	10	110	1.0	6.0	UB>, LB, M	UB, LB>, M	UB, LB>, MACP	UB>, LB, MACP
5	70	7	110	1.0	6.0	UB>, M	UB>, M	UB>, MACP	UB>, MACP
6	105	7	165	2.6	7.0	UB>, LB, M	UB>, LB, M	UB>, LB	UB>, LB

Table 1 (cont.)

Treatment No.	HV microhardness, GPa				Grain index in HAZ overheated zone		Impact toughness a_n, J/cm^2	
	Weld		HAZ overheated zone					
	IMR	Beyond IMR	In treatment	In welding	In treatment	In welding	Weld	HAZ
1	(2.98–4.05)	(2.60–3.09)	(4.05–4.40)	(4.05)	(4–5)	(4–5)	(71)	(83)
2	2.03–3.73	2.86–4.60	2.68–4.23	2.68–3.56	4–5	4–5	78	62
3	3.21–3.45	2.21–3.66	2.21–2.68	4.60–4.80	4–5	5–6	115	80
4	1.92–2.78	2.10–3.21	2.43–3.21	1.92–3.21	6–7	6–7	122	124
5	2.86–5.05	3.04–3.21	3.45–3.75	2.36–2.78	5–6	5–6	67	134
6	1.96–2.86	2.68–2.98	2.10–4.23	2.36–4.08	4	4–5	67	60

Note. UB, LB are upper and lower bainite, respectively; M – matensite; MACP – MAC-phase; IMR – insipient melting region; > – sign of prevailing constituent.

cation of a tensile load of the magnitude of $\sigma = 0.9\sigma_{0.2}$ of that of the base metal*.

Table 1 summarizes the main data on welding and argon-arc treatment with insipient melting,

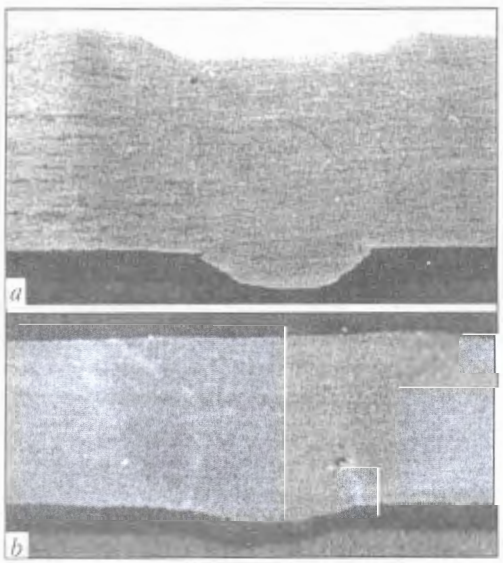

Figure 1. Transverse macrosection of an A-TIG joint before (*a*) and after (*b*) argon-arc treatment with insipient melting

structure and properties of joints of steel 30KhGSA 3 mm thick.

Single-pass A-TIG joints 3 and 6 mm thick are characterized by narrow welds (3.5–4.5 and 4.8–7.2 mm) with form factors of 1.2–1.5 and 0.8–1.2, respectively, which may have a concavity from the face and convexity from the reverse side (Figure 1, *a*). Initial structure of weld metal in the cross-section is represented predominantly by columnar dendrites oriented from the periphery to the center and almost equiaxed at the fusion zone, which are disoriented in the center (Figure 2, *a*). Bainite-martensite structure of the joint metal is coarse-crystalline (Figure 3), *HV* microhardness of the weld and the overheated zone of the HAZ on 3 mm thick steel is 2.60–4.05 and 4.05–4.40 GPa, on 6 mm steel – 2.50–3.40 and 1.96–2.70 GPa, respectively. Joint strength exceeds that of the base metal. However, coarse grains of the HAZ metal may cause cold cracking.

Argon-arc treatment of welded joints 3 and 6 mm thick is conducted with insipient melting of a region 6–7 and 8–9 mm wide, respectively, which is determined by the amplitude of transverse oscillations of the electrode. This region completely covers the initial weld (Figure 4). Its depth decreases with increase of speed, lowering of current and heat input of treatment (see Table 1). Insipient melting reduces (down to

*Cracking resistance was evaluated together with G.V. Bursky.

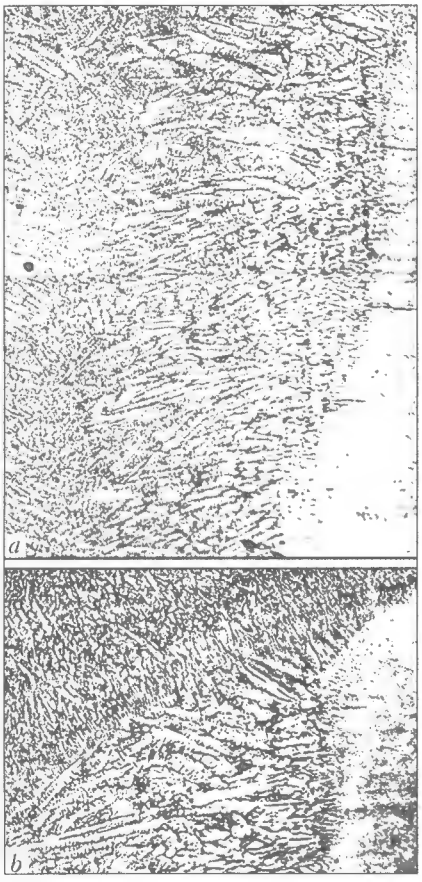

Figure 2. Initial microstructure of weld metal before (*a*) and after (*b*) argon-arc treatment with insipient melting (×50)

elimination) the concavity and creates a two-layer weld structure (see Figure 1, *b*), and also improves joint formation from the face side. Initial structure of weld metal in the region of insipient melting is refined, while remaining unchanged beyond this region (Figure 2, *b*). Refinement of dendritic crystallites is accompanied by a change of their shape, reduction of the number and dimensions of second order nuclei, and more pronounced orientation towards the face surface. Vertical component of crystallite direction becomes greater with decrease of insipient melting depth and increase of penetration form factor $\varphi = b/h$ from 2.7 up to 14, which depends on the treatment modes.

Content of carbon, silicon, manganese and chromium in the metal after two-times melting during welding and treatment is not decreased on the whole (Table 2). In addition, higher concentration of these elements at the surface of a partially melted weld is noted. As they do not penetrate into the metal pool from the outside, this is attributable to their redistribution on the solidification front and accumulation at the surface, where the metal is the last to solidify (in the weld cross-section), i.e. segregation of the type of zone segregation. Such an interpretation is confirmed by that the maximum factor of increasing of the weight fraction of the above elements at the weld surface, compared to the base metal, was observed for carbon (up to 1.25) with the largest segregation coefficient (0.64), and the minimum factor

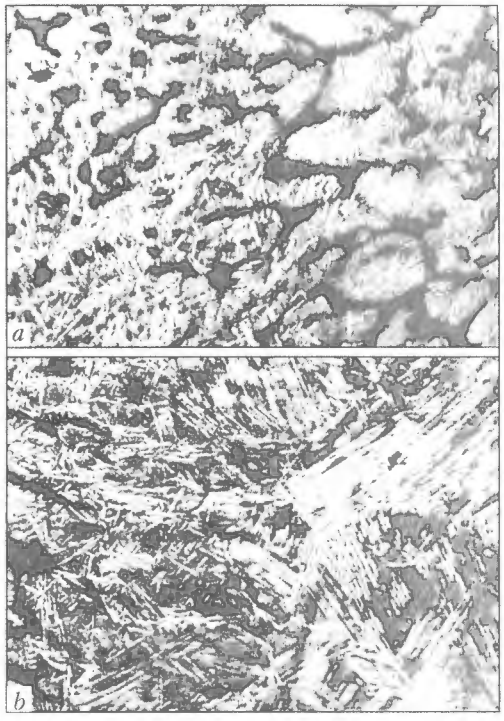

Figure 3. Microstructure of weld metal (*a*) and HAZ (*b*) of a 3 mm joint before treatment (×320)

(1.06) — for manganese with the smallest segregation coefficient (0.05) [6].

In argon-arc treatment with insipient melting in different modes short-term heating of weld metal and overheated zone of the HAZ proceeds up to temperatures certainly higher than those of steel transformation (Figure 5), which in combination with impacts of the arc, pulsing due to transverse oscillations of the electrode, creates the prerequisites for structural change. Rates of cooling of 6–12 °C/s, close to cooling rates in welding in the temperature range of minimum stability of cooling austenite of 600–500 °C, are the quenching rates for steel 30KhGSA [7, 8]. Evolution of the latent heat of melting and dispersed heating by an elongated transversely oscillating arc lead to that the face side of the joint is cooled slower than the reverse side [9]. Thermal conditions in the insipient melting region, less favourable for metal hardening, are to a certain extent compensated by a higher stability of austenite formed at its solidification, which reduces the structural heterogeneity and nonuniformity of metal hardness distribution by the joint height.

Microstructure of the joints 3 mm thick, treated by the arc in different modes, remains to be similar to post-weld microstructure, but is refined in most

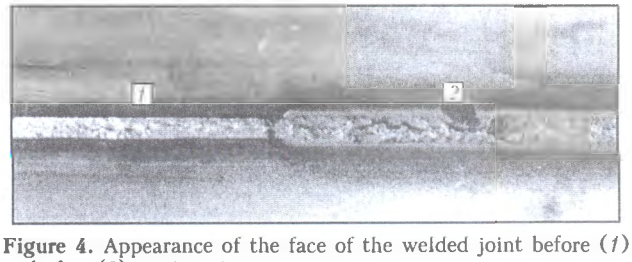

Figure 4. Appearance of the face of the welded joint before (*1*) and after (*2*) treatment

Table 2. Composition of weld metal in insipient melting region in argon-arc treatment and of base metal

Distance from weld surface, mm	Treatment mode		Weight fraction of elements, %			
	I, A	*v, m/h*	*C*	*Si*	*Mn*	*Cr*
0.02–0.03	105	7	0.31	1.23	1.06	1.03
0.30–0.40	105	7	0.29; 0.24	1.23	1.10	0.88
0.02–0.03	130	12	0.35	1.28	1.10	1.03
Base metal			0.28–0.29	1.11	1.00	0.89

cases. Proportion of the structural components is changed in the welds, and round-shaped precipitates of the martensitic-austentic-carbide (MAC) phase can form in the bainite-martensite structure in the HAZ overheated zone. (Presence of MAC-phase is noted in welded joints of low-alloyed steels, but interpretation of its influence on the properties is unambiguous [10–15].) Depending on the treatment mode, the joint hardness, on the whole, is reduced, impact toughness changes according to the produced metal structure, and strength remains on the level of base metal values.

At $I_{tr} = I_w$ and $v_{tr} = v_w$ treatment heat input rises by approximately 23 %, compared to that of welding, due to a higher voltage across an elongated arc. Despite that, the intragranular structure of the joint in the overheated zone is refined with the austenite grain index remaining unchanged on the whole. Impact toughness of the weld increases slightly, but in the HAZ with a bainite-martensite structure and considerable amount of MAC-phase precipitates in the overheated zone it decreases.

Lowering of I_{tr} down to $0.8I_w$ at unchanged or 1.2 times lower speed of longitudinal displacement of the arc, when treatment heat input is equal to 1.0–1.2 of that of welding, causes a greater refinement of the joint structure, smaller ratio of upper and lower bainite and a significant increase of weld metal impact toughness (Figure 6 and Table 1, treatment No.3, 4). Higher impact toughness in the HAZ is observed at treatment speed 1.2–1.7 times lower than that of welding and 13 % increase of the heat input, when a large number of round-shaped precipitates of MAC-phase are found in the bainite structure (Figure 6 and Table 1, treatment No.4, 5). At lowering of treatment speed with a greater (by 70 %) increase of the heat input, both the coarse structure similar to as-welded structure without MAC-phase in the HAZ and a low impact toughness of the joint (Table 1, treatment No.6) are preserved. It should be noted that the high impact toughness of the joint in the HAZ is associated with the presence of MAC-phase precipitates in the overheated zone, and the low impact toughness is found both in the presence and absence of MAC-phase in the structure. More precise determination of the influence of this phase constituent on the joint properties required special studies.

Conducted investigations indicate that in terms of the structure and impact toughness of 3 mm thick joints the optimum mode of argon-arc treatment with insipient melting is the mode, which includes a pro-

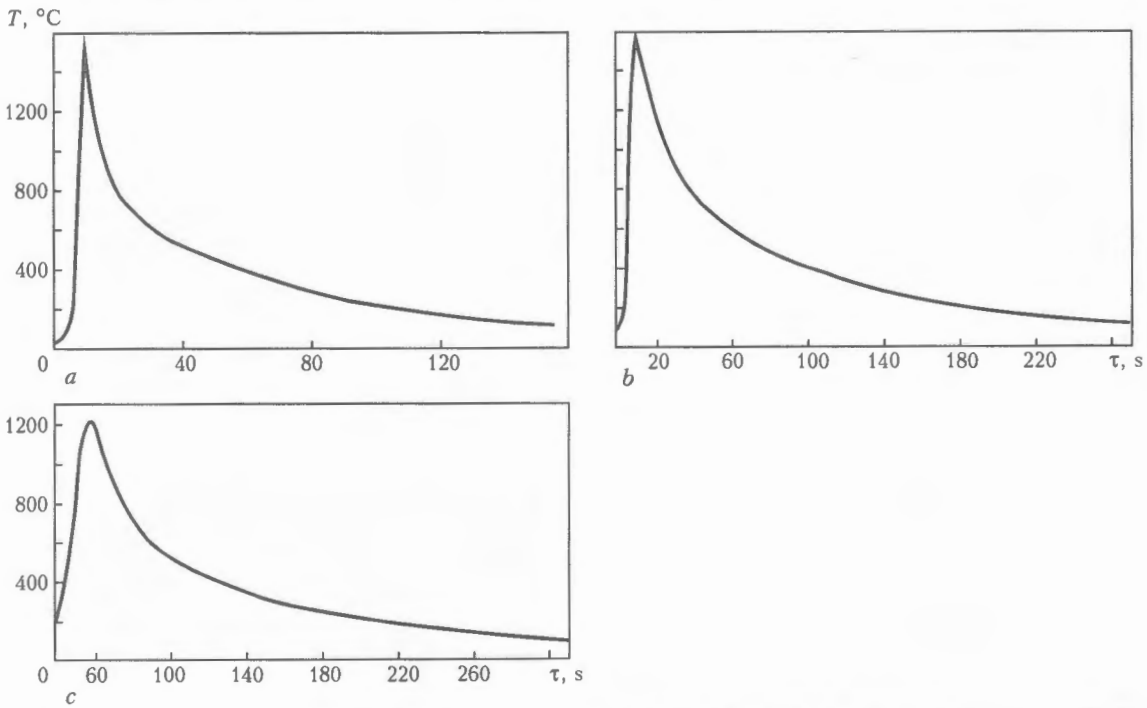

Figure 5. Thermograms of argon-arc treatment with insipient melting of joints 3 (*a*) and 6 (*b*, *c*) mm thick at I_{tr} = 105 (*a*, *b*) and 140 (*c*) A, v_{tr} = 12 (*a*), 6 (*b*) and 4.5 (*c*) m/h

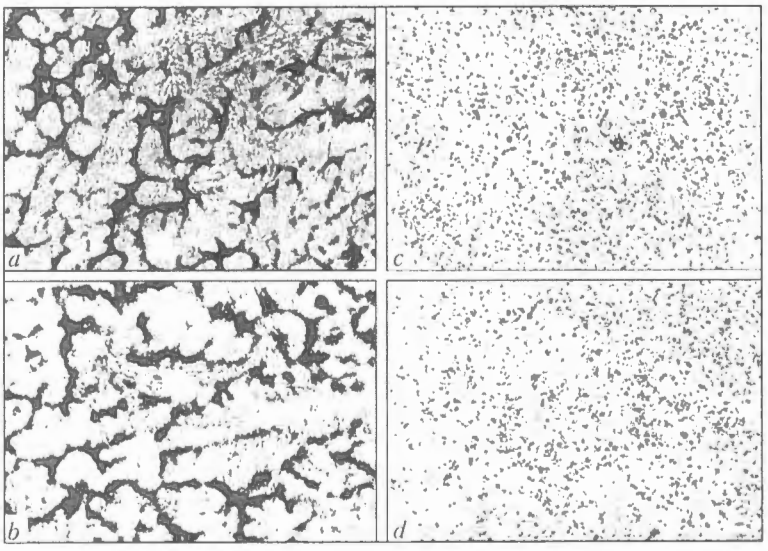

Figure 6. Microstructure of metal in insipient melting region (*a*), beyond the region of insipient melting of the weld (*b*) and in the adjacent overheated zones of the HAZ (*c*, *d*) after treatment of 3 mm thick joint at I_{tr} = 105 A and v_{tr} = 10 m/h (*a*, *c* — ×320; *b*, *d* — ×500)

portional lowering of treatment current and speed 1.2 times at 10–15 % increase of the heat input, compared to that of welding. I_{tr} lowering at preservation of $v_{tr} = v_w$ or simultaneous lowering of I_{tr} and v_{tr} 1.7 times, compared to the respective welding parameters, can be considered acceptable.

Joints 6 mm thick treated at lower heat input than that of welding, with a simultaneous lowering of I_{tr} and v_{tr} or just I_{tr}, also develop high impact toughness in the HAZ (Table 3). Two-times argon-arc treatment with insipient melting of the joint with reduction of the heat input from the first pass to the second is effective enough.

Local argon-arc treatment with insipient melting is rational, if it is necessary to increase the time of soaking before tempering of welded joints. So, if untreated joints failed in the HAZ within in 2–11 min after application of the tensile load, after treatment in different modes, the delayed fracture duration was up to 45–100 min or no fracture was noted for more than a 24 h hin. Promoting higher resistance of welded joints to cold cracking, such a treatment process allows partially or completely, depending on the mode, eliminating the intermediate or subsequent furnace tempering. Power consumption in arc treatment is 0.2–0.6 kW·h per a meter of weld, i.e. by an order of magnitude smaller than in furnace tempering. Time consumption for preparation and performance of argon-arc treatment without fastening after welding or changing the process equipment or fixtures is not greater than 10 min, which eliminates any increase of metal deformation.

CONCLUSIONS

1. Argon-arc treatment with insipient melting with application of transverse oscillations of the electrode significantly improves joint formation and changes its structure. Depending on the treatment mode, the original structure is refined, melting metal crystallites change their shape and are more strictly re-oriented towards the face surface, the metal composition remaining the same on the whole. Repeated short-term austenitization, in combination with a pulsed impact of a transversely oscillating arc, also causes refinement of the unmelted metal microstructure, which may not proceed at excess increase of treatment heat input. Cooling of the treated joint at a rate, close to the rate of cooling in welding, provides repeated quenching, preservation of high values of hardness in the partially melted and austenitized metals and of joint strength.

2. In treatment of joints on medium-carbon alloyed steel of 30KhGSA type, MAC-phase can form in the overheated zone of the HAZ with a bainitic structure, depending on the mode. Its presence may also be anticipated in multilayer joints of such a steel.

Table 3. Influence of the mode of argon-arc theatment (welding) on impact toughness of the fusion zone in 6 mm thick joints

Treatment number	*Treatment (welding) mode*			a_n, *J/cm²*
	I, A	*v, m/h*	*q/v, W·h/m*	
1	(180)	(6.0)	(300)	(40.8)
2	140	6.0	280	50.5
3	100	4.5	245	43.9
4*	140; 100	6.0; 4.5	280; 245	52.6

*Two-times insipient melting.

3. Argon-arc treatment with insipient melting allows improving the impact toughness of joints in quenching steel. Maximum effectiveness for steel 3 mm thick is achieved at simultaneous lowering of current and treatment speed 1.2 to 1.3 times, compared to welding values. Other ratios of these parameter lowering or their separate lowering by 1.2 to 1.3 times can also be acceptable, as well as two-times treatment. It improves the cold cracking resistance of the HAZ in high-strength steel.

1. Savitsky, M.M., Kushnirenko, B.N., Olejnik, O.I. (1999) Features of tungsten electrode welding of steel with activating fluxes (A-TIG welding). *Avtomatich. Svarka*, **12**, 20–28.
2. (1978) *Welding in mechanical engineering*. Refer. Book. Vol. 2. Ed. by A.I. Akulov. Moscow: Mashinostroenie.
3. Asnis, A.E., Ivashchenko, G.A., Frenkel, I.Kh. et al. (1986) Argon-arc treatment as a reserve of reduction of metal content in welded structures. *Avtomatich. Svarka*, **6**, 69–70.
4. Kulik, V.M., Savitsky, M.M. (2001) Arc treatment of quenching steel welded joints. In: *Equipment and technologies of heat treatment of metals and alloys in mechanical engineering*. Coll. pap. of 2nd Int. Symp. Kharkov: KhFTI.
5. Sterenbogen, Yu.A., Bursky, G.V. (1987) Evaluation method of cold cracking resistance of the HAZ in high-strength steel welded joints. *Avtomatich. Svarka*, **3**, 1–5.
6. Kolosov, M.I., Stroganov, A.I., Smirnov, Yu.D. et al. (1973) *Quality of killed steel ingot*. Moscow: Metallurgiya.
7. Popov, A.A., Popova, L.E. (1965) *Isothermic and thermokinetic diagrams of decomposition of overcooled austenite*. Refer. Book. Moscow: Metallurgiya.
8. Shorshorov, M.Kh., Belov, V.V. (1972) *Phase transformations and changes of steel properties in welding*. Atlas. Moscow: Nauka.
9. Kulik, V.M., Savitsky, M.M., Bursky, G.V. (2000) Peculiarities of arc treatment of quenching steels without melting. *The Paton Welding J.*, **5**, 30–35.
10. Makara, A.M., Grabin, V.F., Denisenko, A.V. et al. (1969) On the structure of high-strength low-alloy welds. *Avtomatich. Svarka*, **6**, 11–15.
11. Hrivnyak, I., Matsuda, F. (1994) Metallographic examination of martensitic-austenitic constituent (MAC) of HAZ metal in high-strength low-alloy steels. *Ibid.*, **3**, 22–30.
12. Grabin, V.F., Golovko, V.V., Novikova, D.P. (1995) Peculiarities of weld metal structure in submerged pulsed-arc welding. *Ibid.*, **8**, 3–10.
13. Pokhodnya, I.K., Grabin, V.F., Golovko, V.V. et al. (1996) Influence of pulsed treatment of metal pool by variable power arc on formation of structure, morphology and distribution of nonmetallic inclusions in solidification of low-alloy steel welds. *Svarochn. Proizvodstvo*, **3**, 9–14.
14. Pokhodnya, I.K., Grabin, V.F., Golovko, V.V. et al. (1997) Mechanism and kinetics of austenite decomposition in low-alloy steel HAZ during submerged pulsed-arc welding. *Avtomatich. Svarka*, **4**, 3–13.
15. Hrivnyak, I. (1998) Weldability of current high-strength steels. In: *Transact. of Int. Conf. on Welding and Related Technologies for the 21st Century*. Kiev: PWI.

EFFECT OF MODIFYING OF WELD METAL ON DELAYED FRACTURE RESISTANCE OF HIGH-STRENGTH STEEL WELDED JOINTS

V.I. KABATSKY and A.V. KABATSKY
Donbass State Machine-Building Academy, Kramatorsk, Ukraine

It is shown that at a complex modifying of 10KhGNM type weld metal with nitrogen and vanadium, in combination with cerium, it is possible to obtain the most stable resistance of welded joints, made from martensitic steel 33KhSN2MA, against the cold cracking. This promotes the favourable change in structure and morphology of non-metallic inclusions in metal of the fusion zone of joints.

Keywords: *high-strength steels, low-alloy welds, cold cracks, fusion zone, modifying, nitrides, surface-active elements, ratio, investigations*

One of the major problems, arising in welding of high-strength steels, is a risk of formation of cold cracks in HAZ metal of welded joints (spallings). The modern conceptions about mechanism of initiation and propagation of spallings allow consider their formation as the manifestation of the process of brittle fracture, connected with the development of intergranular slipping and intragranular shear and controlled by the accumulation of damageability with time along the grain boundaries, proceeding under the conditions of complex stressed state in accordance with a modified model of Siener–Straw [1–3]. The main cause of cold crack formation is the increase in resistance of HAZ zone to plastic deformations [1, 4]. Here, in the place of a slip band stop the so-called zones of prefracture, i.e. clusters of dislocation are formed, in the apex of which a zone of local tensile stresses is occurred, thus creating the conditions for fracture initiation in the head part of the cluster [5].

It is shown in some works [6, 7 and oth.) that one of challenging ways of prevention of these cracks formation can be introducing of elements into a low-alloy deposited metal, which form stable precipitations of a modifying phase (in particular, nitride) in combination with surface-active elements. The aim of the present work was to study the effect of modifying mode on the resistance to spallings.

Welded joints with low-alloy welds of 10KhGNM type, made on heat-hardened steel of a martensitic class 33KhSN2MA, very sensitive to the crack formation in HAZ metal, were investigated. Welding was performed using experimental electrodes with a basic coating. Titanium, aluminium, boron, cerium, calcium, vanadium and nitrogen were added to the deposited metal as modifying additions. The modifying elements were added through the electrode coating, while the main alloying was made using an electrode core. Table 1 gives a number of variants of the modifying used.

Mechanical properties of the deposited metal were determined in accordance with requirements of GOST 6996–66. The tests on static short-time tension were performed on specimens (variant No.1) cut in the longitudinal direction from 15 mm thick weld metal of butt joints with V-shaped edge preparation. The impact strength tests were performed on specimens (variant No.9) cut across the joint. The notch was made in weld metal. Resistance of each variant against cold cracks was evaluated from results of welding of not less than 2–3 Tekken samples. Welding of all the variants of samples was made by 4 mm diameter electrodes at the following condition: I_w = 160–180 A, U_a = 22–24 V. Here, only the cracks in HAZ metal and cracks of a combined type, passing partially in weld, were recorded. In case of obtaining the satisfactory resistance against cracks using any of variants, the stability of results was evaluated at repeated tests of electrodes of this variant. Data on mechanical properties and resistance to cracking are given in Table 2. The work gives data on the most optimum types of modifying obtained on the basis of preliminary experimental investigations.

Analysis of obtained results shows that it is possible to attain the quite satisfactory, but insufficiently stable resistance against cracks (variants Nos.1, 3, 7) at sufficiently high strength of the weld metal by using the optimum combination of surface-active modifying additions. On the contrary, the increase in content of active phase-forming elements (for example, boron – variants Nos.2 and 8, titanium – variant No.6, aluminium – variant No.4) leads to a significant reduction in resistance against the cracks-spallings.

The most stable effect of modifying is observed at a combined alloying of welds with vanadium, nitrogen and REM (variant No.10). Here, the cracks in Tekken samples can be prevented also in case of repeated tests of electrodes. At the same time the positive action of modifying is manifested only at a definite ratio of modifying additions.

To explain the results obtained, the comprehensive investigation of welded joints made by the above variants of experimental electrodes was carried out. At

Table 1. Variants of weld modifying

No. of variant	Type of modifying	Calculated chemical composition of deposited metal, %					
		C	Mn	Si	Cr	Ni	Mo
1	Ti–B–Ce–Ca	0.1	1.5	0.5	0.15	1.5	0.5
2	Ti–Al–B–Ce–Ca	0.1	1.5	0.5	0.15	1.5	0.5
3	Al–Ce–Ca	0.1	1.5	0.5	0.15	1.5	0.6
4		0.1	1.5	0.5	0.15	1.5	0.6
5	V–Al–Ce	0.1	1.5	0.5	–	1.5	0.5
6	V–Ti–Ce	0.1	1.5	0.5	–	1.5	0.5
7	V–Ti–B–Ce–Ca	0.1	1.5	0.5	–	1.5	0.5
8		0.1	1.0	0.5	–	1.5	0.5
9	V–N	0.1	1.5	0.5	0.3	1.5	0.5
10	V–N–Ce	0.1	1.0	0.5	0.3	1.5	0.5

Table 1 (cont.)

No. of variant	Type of modifying	Calculated chemical composition of deposited metal, %						
		Ti	Al	V	N	B	Ce	Ca
1	Ti–B–Ce–Ca	0.1	–	–	–	0.001	0.1	0.05
2	Ti–Al–B–Ce–Ca	0.1	0–0.15	–	–	0.002–0.005	0.1–0.15	0.05
3	Al–Ce–Ca	–	0.1	–	–	–	0.1	0.05
4		–	0.15	–	–	–	0.15	–
5	V–Al–Ce	–	0.05–0.1	0.05–0.1	–	–	0.05–0.1	–
6	V–Ti–Ce	0.05–0.15	–	0.05–0.1	–	–	0.05–0.1	–
7	V–Ti–B–Ce–Ca	0.1	–	0.05	–	0.001	0.05	0.05
8		0.05	–	0.05	–	0.005	0.15	–
9	V–N	–	–	0.12	0.015	–	–	–
10	V–N–Ce	–	–	0.12	0.015	–	0.05–0.1	–

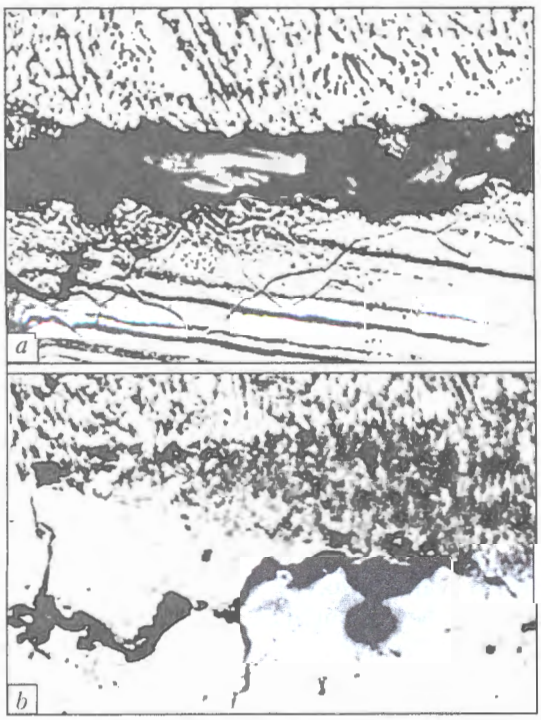

Figure 1. Areas of cold crack along the fusion zone of steel 33KhSN2MA welded joint with a low-alloy weld: *a* — zone of fusion from the weld side; *b* — from the side of a partial fusion area (×125)

the first stage the specimens from single-layer joints of 33KhSN2MA were investigated using the procedure described in [6, 8]. In addition, the change in structure of coarse-grain region of HAZ metal was observed in specimens treated by a thermal cycle close to welding cycle (heating to 1200 °C temperature at 100 °C/s rate, soaking for 15 s, cooling at 7–10 °C/s rate). At cooling down to 200 °C the fracture was initiated by fracture of specimens using their delayed loading with a tension load which creates stresses of about 550–600 MPa in the specimen metal.

As the observations for the austenite decay showed, the bainitic-martensitic transformation (beginning at 340–330 °C) is occurred in the specimens with the formation mainly of a mixture of a lower bainite and tempered martensite (mean value of the primary austenite grain is 5–6). This structure, from some data [2, 9, 10], is preferable for the high-strength metal of welded joints owing to a comparatively high ductility and impact strength.

At the same time the experiments show that the joints can much differ by the resistance against spallings (for example, variants Nos.2 and 10) at very close conformity of parameters of transformation B_l (330–360 °C), M_s (320–350 °C), M_e (200–260 °C). Thus, the study of peculiarities of structure of the

Table 2. Mechanical properties of weld metal and resistance of joints against the cracks

No. of variant	Mechanical properties of weld metal					
	$\sigma_{0.2}$, MPa	σ_t, MPa	δ_5, %	ψ, %	KCU, J/cm^2	
					+20 °C	−40 °C
1	615	758	18.3	48.6	103	70
2	615–636	753–777	19.0–20.0	48.6–50.6	75–106	67–90
3	630	757	15.6	55.6	77	60
4	594	742	20.0	55.6	67	47
5	611–628	806–822	17.3–18.6	51.1–55.6	72–75	60–62
6	658–756	815–876	17.1–18.6	51.0–55.6	70–87	60–64
7	685	862	20.0	56.6	90	75
8	583	742	22.7	55.6	105	60
9	724	862	16.6	55.6	88	60
10	No determined					

Table 2. (cont.)

No. of variant	Presence of cracks in Tekken sample		Time before appearance of a visually-observed crack, its nature
	Visually	In macrosections	
1	Absent	Present	Tear on section; more than 8 h
	Present	–	
2	Same	–	6 h; 1.5 h; 1 h; 20 min; 15 min – combined
3	2 samples were welded without cracks		
	Present*	–	More than 8 h*; 5.5 h*; 5 h*
4	Same	–	1.5 h; 1 h; 1 h
5	»	–	5 h; 45 min; 40 min
6	»	–	6 h; 3 h; 1.5 h; 1 h – combined
7	Absent	Present	Tear on section; 48 h; 7 h*; 1.5 h*
	Present	–	
8	Same	–	3.5 h; 2 h – combined
9	2 samples were welded without cracks		
	Absent*	Present	Tears on section; more than 24 h*
	Present*	–	
10	2 samples were welded without cracks		
	Absent*	Absent	–
	Same*	Present	Tear on section*

*Results of repeated tests of electrodes.

coarse-grain region does not make it possible to explain adequately the causes of different resistance to spallings.

Susceptibility of joints to spallings in the deposited metal, determined by using a glycerin pencil sample, was made by the content of a diffusive hydrogen [1]. Welding conditions are given above. Comparison of measurements show that it little differs and is comparatively low in all the cases (does not exceed 1.2–1.4 ml/100 g of deposited metal). Taking into account the significant differences in the investigated variants by the resistance against cracks (for example, $[H]_{diff}$ ~ 1.2–1.25 (variant No.1) and ~ 1.2–1.3 ml/100 g (variant No.2)) it can be concluded that this factor at observed concentrations of hydrogen is, probably, not determinant as regards to the resistance against cracks-spallings. However, this question can be answered more precisely only after study of the kinetics of hydrogen evolution in the welded joint [6].

There is an opinion [2, 11] that the very favourable conditions for the initiation of cold cracks are created on the fused boundaries of grains of HAZ metal region, adjacent to the parent metal (so-called region of prefusion). Comprehensive analysis of nature of numerous fractures in Tekken samples shows that the trajectory of propagation of cold near-weld cracks inter-

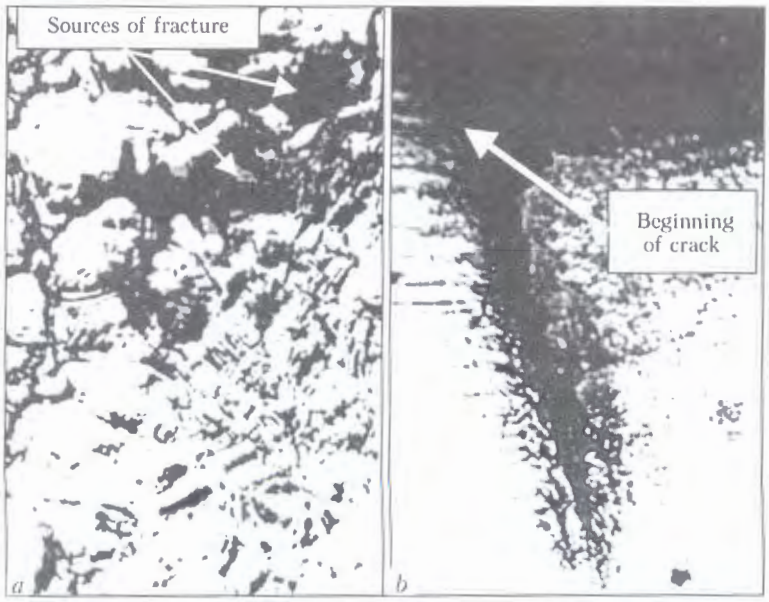

Figure 2. Initiation of fracture in transition zone of loaded specimens: *a* — sources of fracture at the partial fusion area; *b* — crack initiation and propagation at the fusion boundary (×100)

sects in many cases the fusion line, passes along the fusion boundary, or in a direct vicinity from it (Figure 1). This allows suppose with a great confidence that the region of the welded joint, forming in the process of the weld solidification on the fused grains of the parent metal, can serve a place for the initiation of cold near-weld cracks. This is proved also indirectly by observation of the process of a delayed fracture of specimens, treated by a thermal cycle close to the welding cycle. The record of the moment of initiation of cracks in loaded specimens made it possible to reveal the appearance of sources of fracture of the initiation of cracks in the fusion zone region (Figure 2).

The results obtained give grounds to tell about the feasibility of effect of modifying the deposited metal on the resistance of welded joint against the formation of cracks-spallings.

In some works [12, 13] a remarkable role of non-metallic inclusions was revealed in the mechanism of formation of cold cracks in the fusion zone region. Metallographic examinations of the latter showed by using the optical and electron microscopy that the uniformly distributed globular inclusions dominate at optimum modifying (Figure 3). Inclusions are arranged mainly inside the grain body, moreover, the increase in amount of fine inclusions is observed (Figure 4, *a*). The latter follows also from calculation of amount of inclusions with a distribution in sizes, made using the quantitative TV microscope «Quantimet-720». In case of deviation from the optimum modifying the nature of distribution of inclusions is changed, i.e. the noticeable clusters are observed along the boundaries of grains, the inclusions become coarser (Figure 4, *b*). The latter are, evidently, complex compounds of modifying additions with oxygen, nitrogen, carbon and sulphur. As is known, the inclusions at sufficiently high concentration of stresses

Figure 3. Non-metallic inclusions in the zone of 33KhSN2MA welded joint with weld metal of 10KhGNMAFCh type (×1500)

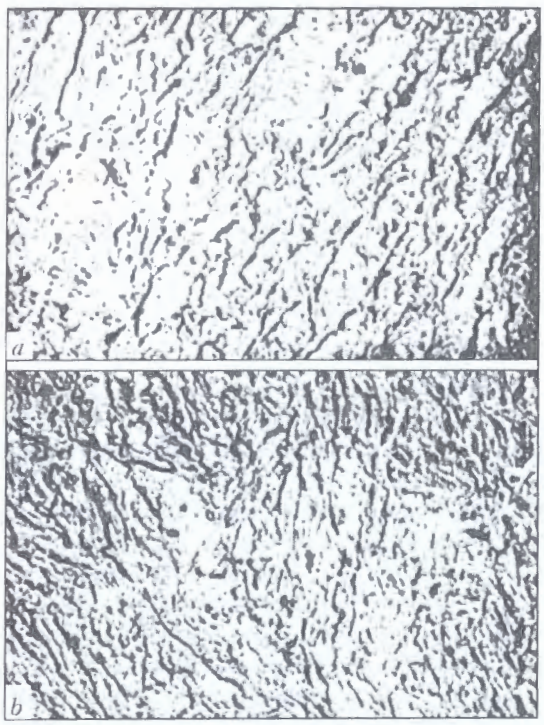

Figure 4. Microstructure of deposited metal adjacent to the fusion zone: *a* — with weld metal 10KhGNMAFCh; *b* — 10GNMTRYuCh (×6000)

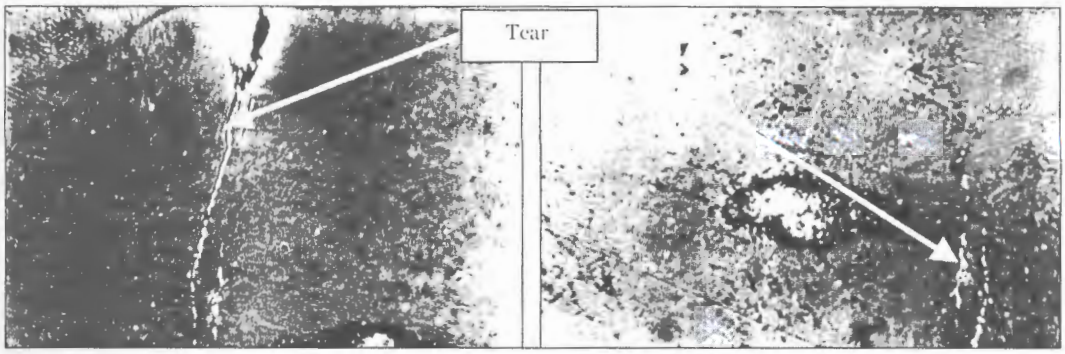

Figure 5. Microstructure of metal in the zone of 33KhSN2MA steel with a low-alloy weld with microcracks (×1500)

can be sources of grain-boundary slipping [2], contributing to the formation of sources of cold cracks under the conditions of welding thermodeformational cycle. Cold cracks can also initiate from hot microtears passing along clusters of inclusions of unfavourable shape (Figure 5), precipitating from a parent solution during solidification in the zone of liquid and solid metal contact.

One of possible explanations of this remarkable effect of optimum modifying on the resistance against the formation of near-weld cracks can serve, probably, a definite action of modifying additions on the metal structure and nature of inclusions of the fusion zone and a pre-fusion area adjacent to it. The latter is, evidently, stipulated by the diffusion, proceeding very intensively in contact of the pool molten metal with the pre-fusion area. Penetration of surface-active elements (for example, cerium) along the boundaries of prefused grains can cause here the decrease in size of grain and degree of etching the grain boundaries (Figure 6). Unfortunately, due to complexity of data of investigations, the authors have no direct experimental confirmation of this fact, however, there are theoretical premises of this effect owing to the peculiarities of cerium behaviour in steels. These peculiarities consist in cerium ability to form a solid solution in iron, and also in a high surface activity and advantageous susceptibility to adsorption of cerium atoms as compared with other elements [13].

Thus, the investigation results obtained prove the significant effect of modifying the deposited metal on the resistance of quenched steel welded joints with low-alloy welds against the formation of cold near-weld cracks. This allows realization of the offered method of increasing the resistance to spallings in the development of welding consumables for welding high-strength steels.

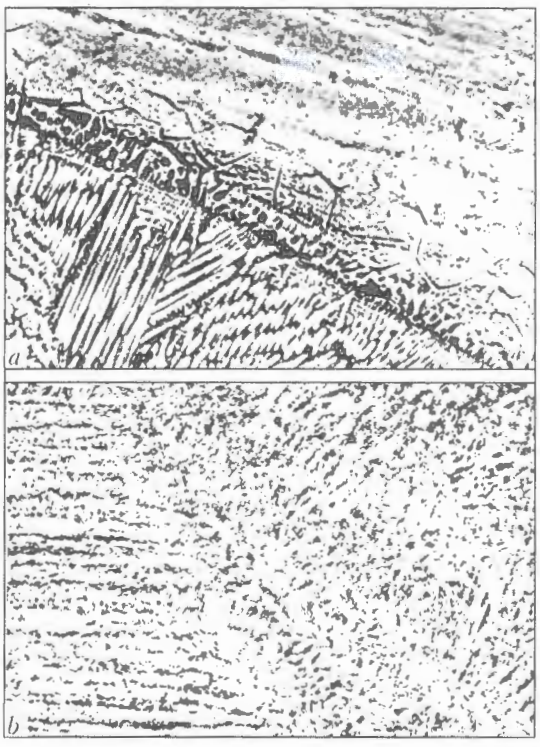

Figure 6. Primary microstructure of metal of fusion zone of welded joints (×200): *a* – weld metal of 10KhGNMTF type; *b* – 10KhGNMAFCh

1. Makarov, E.L. (1981) *Cold cracks in welding of alloy steels*. Moscow: Mashinostroenie.
2. Kasatkin, B.S. (1991) Micromechanism of cold cracking in welding of medium-alloy steels. In: *Proc. of Seminar on Metallurgical Requirements of Manufacturers and Customers on Weldability of Steels*, Kiev, Sept. 16–20, 1991.
3. Zemzin, V.N., Chizhik, A.A., Lanin, A.A. et al. (1983) Conditions of cracking in welding and heat treatment. Part 1. About the role of creep in cracking. *Svarochn. Proizvodstvo*, **11**, 1–4.
4. Sterenbogen, Yu.A. (1986) Some factors determining the HAZ metal resistance of martensitic steels to cold cracking. *Avtomatich. Svarka*, **6**, 5–8.
5. Zolotorevsky, S.M. (1983) *Mechanical properties of metals*. Moscow: Metallurgiya.
6. Kabatsky, V.I., Podgaetsky, V.V., Novikova, D.P. et al. (1988) Structure and properties of heat-affected zone of welded joints from high-strength steel of martensitic class. *Avtomatich. Svarka*, **1**, 16–20.
7. Kabatsky, A.V. (1998) Low-alloy electrode materials for welding of hardening steels. *Vestnik Priazov. GTU*. Issue 6.
8. Novikova, D.P. (1989) *High-temperature metallography of welded joints*. Kiev: Naukova Dumka.
9. Novikova, D.P., Bogachek, Yu.L., Mandelberg, S.L. et al. (1973) Interaction of microstructure with impact strength of weld metal on tube low-alloy steel. *Avtomatich. Svarka*, **8**, 6–9.
10. Grabin, V.F., Denisenko, A.V. (1978) *Physical metallurgy of welding of low- and medium-alloy steels*. Kiev: Naukova Dumka.
11. Kabatsky, V.I., Kiriakov, V.M., Podgaetsky, V.V. et al. (1985) Resistance of welded joints of 25KhGM type steel to cold cracking in fusion zone during calcium alloying of weld metal. *Avtomatich. Svarka*, **1**, 5–7.
12. Kiriakov, V.M., Parfesso, G.I., Podgaetsky, V.V. et al. (1989) Influence of sulfide inclusions in fusion zone of austenitic welds with pearlitic steel on susceptibility of joints to cracks-tears formation. *Ibid.*, **10**, 4–7.
13. Braun, M.P. (1982) *Microalloy steels*. Kiev: Naukova Dumka.

ALLOWANCE FOR EFFECT OF CYCLE ASYMMETRY ON CRACK RESISTANCE OF STEELS AND WELDED JOINTS AT TWO-FREQUENCY LOADING

V.S. KOVALCHUK
E.O. Paton Electric Welding Institute, NASU, Kiev, Ukraine

It was established that increase in a coefficient of cycle asymmetry from $R = 0$ up to $R = 0.5$ at two-frequency loading leads to 3–4 times increase in propagation rate of fatigue cracks in parent metal and up to 2 times increase in weld metal of butt welded joints of high strength ($\sigma_y \approx 1000$ MPa) steel. Calculation method is offered allowing determination of a cyclic crack resistance of structural materials and welded joints under the conditions of a two-frequency loading using the fatigue fracture diagrams corresponding to a single-frequency loading with an appropriate coefficient of a cycle asymmetry.

Keywords: *cyclic crack resistance, two-frequency loading, cycle asymmetry, steels, welded joints, calculation*

The most welded metal structures are characteristic of a complex loading caused by a simultaneous action of two and more alternating loads different in amplitude and frequency. Numerous experimental data show that the superposition of secondary high-frequency stresses from vibrations on alternating stresses caused by main (usually low-frequency) load can reduce significantly a cyclic fatigue life of materials and welded joints at the stages of initiation and propagation of fatigue cracks. This is explained mainly by the increase in a resultant amplitude of stresses due to algebraic summing of both loads and auxiliary damaging action of cyclicity of a high-frequency component. In this case the cyclic life of joints at the stage of fatigue crack propagation depends not only on ratio of amplitudes and frequencies of efficient stresses, but also on a cycle asymmetry of the most low-frequency component of a spectrum. Nevertheless, the existing methods and calculation relationships to estimate a cyclic crack resistance with allowance for the cycle asymmetry are adaptable only to a simple cyclic loading [1–3 and oth.).

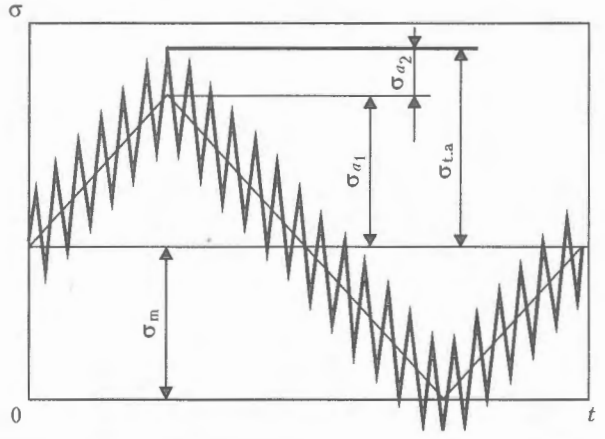

Figure 1. Shape of loading cycle: σ_{a_1}, σ_{a_2} — amplitude of low- and high-frequency stress, respectively; $\sigma_{t.a}$ — total amplitude of stresses; σ_m — mean stress of cycle; t — time

Earlier, the additional correction coefficients were introduced into Paris equation [3] to make allowance for the cycle asymmetry in determination of a propagation rate of fatigue cracks under the conditions of a single-frequency loading. This approach can be applied also at two-frequency loading, however, certain difficulties are encountered, which are caused, first of all, by the fact that it is impossible to determine the range of stresses by the difference in summed values of maximum and minimum stresses of the cycle to determine the coefficient of intensity of stresses at two-frequency and more complex loading. Results of experimental investigations proved that the life value obtained at a single-frequency loading at the level of stresses equal to the sum of amplitudes of two-frequency loading components can greatly differ from the life value corresponding to the two-frequency loading.

When the existing approach for assessment of a cyclic crack resistance of materials and joints at two-frequency loading is used (Figure 1), it should be replaced by the single-frequency loading, equivalent by a damaging action. The solution of this problem can be realized on the basis of earlier dependence [4] for determination of the coefficient of reduction in life using amplitude and frequency ratios of two-frequency loading components up to the moment of initiation of fatigue cracks.

Analysis of results of investigations of steels and welded joints, made at the E.O. Paton Electric Welding Institute, showed that the fatigue curves at two-frequency loading with recorded ratios of frequencies and amplitudes of stresses are arranged equidistantly to the initial fatigue curve, corresponding to a single-frequency loading, and shifted to the region of a lower life (Figure 2). It was established that analytical expression of the coefficient of life reduction æ is determined by the following expression for the additive two-frequency loading with a ratio of frequencies $(f_2/f_1) \geq 10$, when the effect of shifting the phases between the components is very low and it can be neglected:

$$æ = N_1/N_2 = (f_2/f_1)^{\theta\, \sigma_{a_2}/\sigma_{a_1}}, \qquad (1)$$

where N_1 is the fatigue life at a single-frequency loading with a stress amplitude σ_{a_1}; N_2 is the fatigue life at a two-frequency loading determined by a number of cycles of a low-frequency component with amplitude σ_{a_2}; f_1 is the frequency of loading change under the conditions of a single-frequency loading and low-frequency component at an auxiliary superposition of vibrations; f_2, σ_{a_2} are the frequency and amplitude of stresses, respectively, of the high-frequency component of the two-frequency loading; ϑ is the coefficient, allowing for the material effect.

If in a random point A (Figure 2), corresponding to the amplitude of low-frequency stresses $\sigma_{a_1 n_1}$, to superpose additionally a high-frequency stress with amplitude σ_{a_2} on the fatigue curve in a semilogarithmic system of coordinates, then the fatigue life $\lg N_1$ will be decreased to value $\lg N_2$ in point B. This is equivalent to the increase in amplitude of low-frequency stresses $\sigma_{a_1 n_1}$ by $\sigma_{a_1 e}$ up to the level $\sigma_{a_1 n_2}$ in point C. The value of equivalent stress $\sigma_{a_1 e}$ can be determined from a right-angled triangle ABC by expression

$$\sigma_{a_1 e} = \text{tg}\,\alpha(\lg N_1 - \lg N_2), \qquad (2)$$

where $\text{tg}\,\alpha = (\sigma_{a_1 n_2} - \sigma_{a_1 n_1})/(\lg N_1 - \lg N_2)$ is the tangent of angle of inclination of initial fatigue curve to the abscissa axis, having the dimension of stresses.

By denoting $\text{tg}\,\alpha = k$, the relation (2) can be written in the form of $\sigma_{a_1 e} = k \lg (N_1/N_2)$, or

$$\sigma_{a_1 e} = k \lg æ. \qquad (3)$$

After substituting value $\lg æ$ from relationship (1) into expression (3) the amplitude of low-frequency stresses, equivalent by a damaging action to the amplitude of superposed high-frequency stresses, can be determined by formula

$$\sigma_{a_1 e} = k\,\vartheta(\sigma_{a_2}/\sigma_{a_1}) \lg (f_2/f_1). \qquad (4)$$

Amplitude of effective stresses $\sigma_{a_1 \text{eff}}$, equivalent by a damaging action to two-frequency loading with components σ_{a_1} and σ_{a_2}, is determined by expression $\sigma_{a_1 \text{eff}} = \sigma_{a_1 n_1} + \sigma_{a_1 e}$ or after substitution of values from (4) — by expression

$$\sigma_{a_1 \text{eff}} = \sigma_{a_1 n_1} + k\,\vartheta(\sigma_{a_2}/\sigma_{a_1}) \lg (f_2/f_1). \qquad (5)$$

The range of the coefficient of stress intensity at two-frequency loading $\Delta K_{t\text{-}f}$, when the fatigue curve has a form of a straight line in a semilogarithmic system of coordinates, is equal to

$$\Delta K_{t\text{-}f} = 2\sigma_{a_1 \text{eff}} \sqrt{\pi L}\, f_k, \qquad (6)$$

where f_k is the correction function. With allowance for (5), omitting index n_1 at σ_{a_1}:

$$\Delta K_{t\text{-}f} = 2\,[\sigma_{a_1} + k\vartheta(\sigma_{a_2}/\sigma_{a_1}) \lg (f_2/f_1)]\, \sqrt{\pi L}\, f_k. \qquad (7)$$

Amplitude of effective stresses $\sigma_{a_1 \text{eff}}$, equivalent by a damaging action to two-frequency loading with components σ_{a_1} and σ_{a_1}, can be determined also coming from the analytical bond of parameters of the fatigue curve.

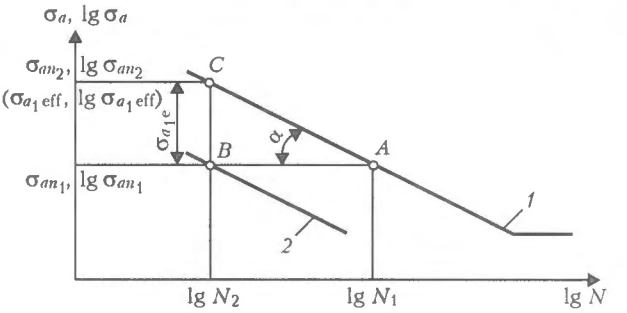

Figure 2. Fatigue curves in semilogarithmic and logarithmic systems of coordinates under conditions of single- (*1*) and two-frequency (*2*) loading

It is known that at a normal temperature and the absence of the corrosion medium a left inclined branch of fatigue curves of carbon steels in semilogarithmic coordinates has a form of a straight line and can be described by the equation [5]

$$\sigma_{a_1 n_2} - \sigma_{a_1 n_1} = k\,(\lg N_1 - \lg N_2), \qquad (8)$$

where k is the parameter characterizing the angle of inclination of a left branch of the fatigue curve to the abscissa axis and determined by formula

$$k = (\sigma_{a_1 n_2} - \sigma_{a_1 n_1})/(\lg N_1 - \lg N_2) = \text{tg}\,\alpha. \qquad (9)$$

From equation (8) we shall find

$$\sigma_{a_1 n_2} = \sigma_{a_1 n_1} + k \lg (N_1/N_2). \qquad (10)$$

As was mentioned, during superposition of secondary, higher-frequency stresses σ_{a_2} on initial stresses $\sigma_{a_1 n_1}$, the cyclic fatigue life is reduced to value $\lg N_2$, that corresponds to the level of effective stresses of a single-frequency loading $\sigma_{a_1 \text{eff}} = \sigma_{a_1 n_2}$. The ratio of lives N_1/N_2 is determined in this case in accordance with expression (1).

Taking into account the above-mentioned the relationship (10) can be presented in the form of

$$\sigma_{a_1 \text{eff}} = \sigma_{a_1 n_1} + k\vartheta(\sigma_{a_2}/\sigma_{a_1}) \lg (f_2/f_1). \qquad (11)$$

Equation (11) coincides completely with equation (5), and, consequently, $\Delta K_{t\text{-}f}$ is determined by equation (7).

In those cases when the left inclined branch of fatigue curves has a form of a straight line in logarithmic coordinates, it can be described by the exponential equation

$$\sigma_a^m N = C, \qquad (12)$$

where σ_a is the amplitude of alternating stresses; N is the number of cycles before fracture; m and C are the parameters of the fatigue curve.

In the region of a limited fatigue life the equation (12) can be presented by two points of the left inclined branch of the fatigue curve with coordinates ($\sigma_{a_1 n_1}$, N_1) and ($\sigma_{a_1 n_2}$, N_2) by the equation in the form of

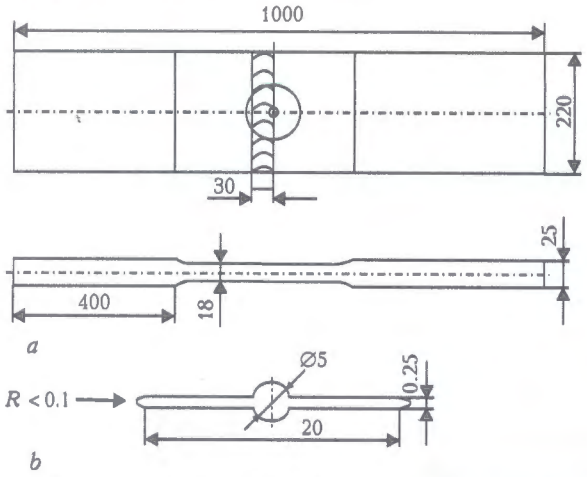

Figure 3. Shape and sizes of welded specimen with removed reinforcements (*a*) and initial notch of a through central crack (*b*)

$$\sigma^m_{a_1 n_1} N_1 = \sigma^m_{a_1 n_2} N_2, \qquad (13)$$

where $\sigma^m_{a_1 n_1}$ and $\sigma^m_{a_1 n_2}$ are the limits of a limited endurance corresponding to number of cycles N_1 and N_2; $m = \lg (N_1/N_2)/\lg (\sigma_{a_1 n_2}/\sigma_{a_1 n_1})$ is the characteristic of the fatigue curve inclination.

If to superpose the high-frequency stress $\lg \sigma_{a_2}$ in a random point A of logarithmic coordinates (Figure 2), corresponding to low-frequency stresses $\lg \sigma_{a_1 n_1}$ on initial fatigue curve *1*, then the fatigue life $\lg N_1$ will decrease to the values $\lg N_2$ in point B. This corresponds to the increase in low-frequency stresses $\lg \sigma_{a_1 n_1}$ up to the level $\lg \sigma_{a_1 n_2}$ in point C.

It follows from equation (13) that

$$\sigma^m_{a_1 n_2} = \sigma^m_{a_1 n_1} N_1/N_2. \qquad (14)$$

Taking into account the accepted designations N_1/N_2 and its values from equation (1) we shall obtain

$$\sigma^m_{a_1 n_2} = \sigma^m_{a_1 n_1} (f_2/f_1)^{\vartheta \sigma_{a_2}/\sigma_{a_1}}. \qquad (15)$$

It follows from the equation that the amplitude of effective stresses $\sigma_{a_1 \text{eff}} = \sigma_{a_1 n_2}$, equivalent by a damaging action to the two-frequency loading with components σ_{a_1} and σ_{a_2}, is determined by expression

$$\sigma_{a_1 \text{eff}} = \sigma_{a_1 n_1} (f_2/f_1)^{\vartheta \sigma_{a_2}/m\sigma_{a_1}}. \qquad (16)$$

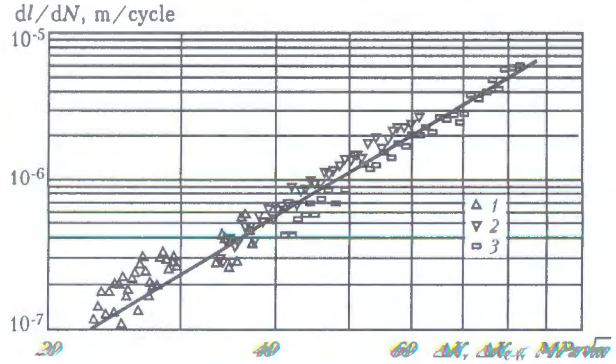

Figure 4. Averaged dependence of growth rate of fatigue cracks along the fusion line of high-strength steel welded joints on the range of stress intensity coefficient at from-zero single- and two-frequency ($f_2/f_1 = 100$) loadings (*solid line*): *1* — single-frequency loading; *2* — two-frequency loading $\sigma_2/\sigma_1 = 0.2$; *3* — two-frequency loading $\sigma_2/\sigma_1 = 0.4$

After substituting values $\sigma_{a_1 \text{eff}}$ from (16) into (6) and omitting index n_1 at σ_{a_1}, the range of coefficient of the stress intensity at two-frequency loading (when the left inclined branch of fatigue curves has a form of a straight line in logarithmic coordinates) can be presented in the form of

$$\Delta K_{t\text{-}f} = 2\sigma_{a_1} (f_2/f_1)^{\vartheta \sigma_{a_2}/m\sigma_{a_1}} \sqrt{\pi L}\, f_k. \qquad (17)$$

The obtained relationships (7) and (17) allow determination of the propagation rate of fatigue cracks in the materials and welded joints at two-frequency loading by kinetic diagrams of the fatigue fracture corresponding to a single-frequency loading. They are designed for use in the construction of diagrams when the left inclined branch of fatigue curves has a form of a straight line in semilogarithmic and logarithmic coordinates, respectively.

The fatigue tests were performed on plane large-sized specimens with a butt weld and removed reinforcements (Figure 3), made from high-strength steel ($\sigma_y \approx 1000$ MPa) to check experimentally the offered method of determination of a range of the stress intensity coefficient $\Delta K_{t\text{-}f}$ as regards to the evaluation of a cyclic crack resistance of welded joints under the conditions of two-frequency loading.

To initiate a fatigue fracture of the specimens in HAZ metal, an initial notch in the form of a central through crack was located along the fusion line of weld with the parent metal. Initial experimental data were obtained at a soft condition of single- and two-frequency loadings. The single-frequency loading and low-frequency component of the two-frequency loading had a triangular shape of a cycle with a coefficient of asymmetry $R = 0$ and varied at the frequency $f_1 = 0.05$ Hz. At the two-frequency loading the ratio of frequencies f_2/f_1 was 100, while the ratio of amplitudes of stresses $\sigma_{a_2}/\sigma_{a_1}$ was 0.2 and 0.4.

Tests were performed in servohydraulic machine «Shenk 1000 kN», equipped additionally with electronic-optical system providing no-contact measurement of linear sizes of cracks at the surface of specimens in the 0.1–200 mm interval at 0.01 mm accuracy.

Range of the stress intensity coefficient at two-frequency loading was determined by expression (7). The values of coefficient $\vartheta = 16.7$ and tangent of angle of inclination of initial fatigue curve $k = 52$ MPa were taken from the results of experimental investigations of the parent material.

Results of investigation of a cyclic crack resistance of the welded joints at single- and two-frequency loadings are presented in the form of points in Figure 4. Median values of these data are located almost at the same straight line that makes it possible to replace them by a single line of regression (a solid line). A good correlation of rates of the fatigue fracture at $\Delta K = \Delta K_{t\text{-}f}$ confirms the capability of this method to determine a cyclic crack resistance of materials and welded joints under the conditions of two-frequency loading by kinetic fatigue fracture diagrams corresponding to a single-frequency loading.

To evaluate the effect of cycle asymmetry on the propagation rate of fatigue cracks under the conditions of two-frequency loading, the investigations were car-

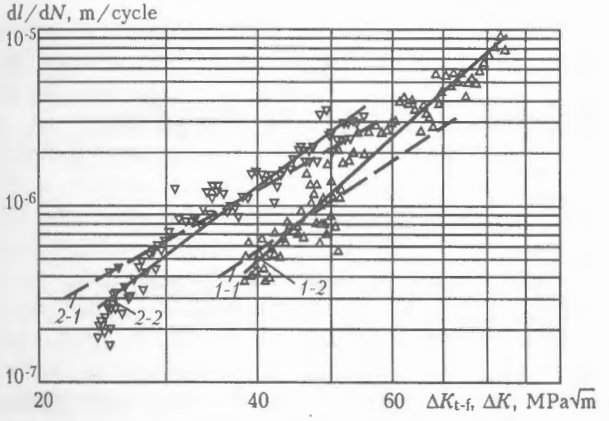

Figure 5. Kinetic diagrams of fatigue fracture of high-strength steel at two-frequency ($f_2/f_1 = 100$ and $\sigma_2/\sigma_1 = 0.2$ — *solid lines*) and single-frequency (*dashed lines*) axial tension: (*1-2*) and (*1-1*) at $R = 0$; (*2-2*) and (*2-1*) at $R = 0.5$

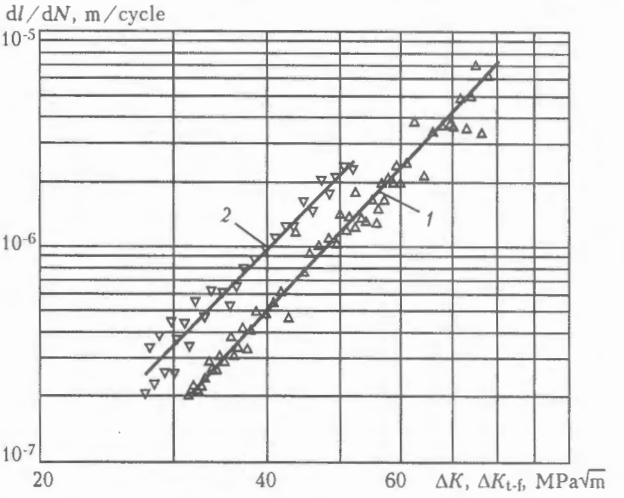

Figure 6. Kinetic diagrams of fatigue fracture of weld metal of welded joints made from high-strength steel at two-frequency axial tension ($f_2/f_1 = 100$, $\sigma_2/\sigma_1 = 0.2$): *1* — $R = 0$; *2* — $R = 0.5$

ried out on specimens, similar in shape and sizes, with a central through crack (see Figure 3), identical to the specimens which were investigated earlier under the conditions of a single-frequency loading [3] and manufactured from the parent metal of the same steel ($\sigma_y = 1000$ MPa).

Specimens were tested under the conditions of axial two-frequency soft cyclic tension at ratio of stress amplitudes $\sigma_{a_2}/\sigma_{a_1} = 0.2$ and ratio of frequencies $f_2/f_1 = 100$ at cycle asymmetry coefficient $R = 0$ and 0.5. Range of stress intensity coefficient $\Delta K_{t\text{-}f}$ was determined by the above-described procedure using expression (7). Relations $dl/dN - \Delta K_{t\text{-}f}$ under the conditions of two-frequency loading at $R = 0$ (*1-2*) and $R = 0.5$ (*2-2*) are given in Figure 5. For comparison, this Figure has also dashed lines (*1-1*) and (*2-1*) of relationships $dl/dN - \Delta K$ obtained earlier [3] at a single-frequency loading on similar specimens and at the same values of the cycle asymmetry. It is seen from the Figure that curves (*1-1*) and (*1-2*), and also (*2-1*) and (*2-2*), obtained, respectively, under conditions of single- and two-frequency loadings at a fixed value of the cycle asymmetry coefficient, have a good coincidence. In transition from $R = 0$ to $R = 0.5$ the rate of propagation of fatigue cracks in the parent metal of the steel investigated is 3–4 times increased at both types of alternating loading.

To evaluate the effect of cycle asymmetry on the rate of propagation of fatigue cracks in weld metal of welded joints, the fatigue tests under the conditions of two-frequency loading were performed also at a soft condition of a cyclic tension at a ratio of stress amplitudes $\sigma_{a_2}/\sigma_{a_1} = 0.2$ and ratio of frequencies $f_2/f_1 = 100$. Cycle asymmetry coefficient was taken equal to $R = 0$ and $R = 0.5$. To initiate the fatigue fracture of welded specimens (see Figure 3) in weld metal, an initial notch was located in its central part. Kinetic diagrams of fatigue fracture of weld metal of high-strength steel welded joints at from-zero and asymmetrical two-frequency axial tension are presented in Figure 6. These data show that the increase in coefficient of cycle asymmetry from $R = 0$ to $R = 0.5$ at two-frequency loading leads to the 2 times increase in rate of propagation of fatigue cracks in weld metal in butt welded joints made from the investigated steel.

It is seen from the comparison of kinetic diagrams (Figures 5 and 6) that at fixed values of the cycle asymmetry coefficient the rates of fatigue fracture in parent metal and weld metal of welded joints are almost comparable and the nature of effect of cycle asymmetry on the rate of fatigue fracture for the mentioned zones of the welded joint is identical.

CONCLUSIONS

1. With a growth in the cycle asymmetry coefficient from $R = 0$ to $R = 0.5$ the rate of fatigue crack propagation in the parent metal of the investigated steel is 3–4 times increased at single- and two-frequency loadings.

2. At two-frequency loading the increase in the cycle asymmetry coefficient from $R = 0$ to $R = 0.5$ leads to about 2 times increase in rate of fatigue crack propagation in weld metal of butt welded joints of investigated steel.

3. At fixed values of the cycle asymmetry coefficient the rates of fatigue fracture along the fusion line, weld metal of welded joints and parent metal are comparable.

4. Nature of effect of cycle asymmetry on the rate of fatigue fracture is almost identical for different zones of the welded joint and parent metal. This allows, using the method offered, determination of a cyclic crack resistance of materials and welded joints at two-frequency loading by kinetic diagrams corresponding to a single-frequency loading with an appropriate value of the cycle asymmetry coefficient.

1. Forman, R., Kerni, V., Angle, R. (1967) Computational investigations of crack propagation in cyclic-loaded structures. *Transact. of ASME*, Series D, **3**, 8–16.
2. Trufyakov, V.I., Knysh, V.V., Mikheev, P.P. et al. (1987) Relationship between fatigue crack propagation rate and cycle asymmetry. *Avtomatich. Svarka*, **3**, 5–7.
3. Kovalchuk, V.S. (2003) Allowance for effect of cycle asymmetry on cyclic crack resistance of materials and welded joints. *The Paton Welding J.*, **9**, 2–4.
4. Trufyakov, V.I., Kovalchuk, V.S. (1982) Determination of service life at two-frequency load. Part 2. Proposed procedure. *Problemy Prochnosti*, **10**, 15–20.
5. Troshchenko, V.T., Sosnovsky, L.A. (1987) *Fatigue resistance of metals and alloys*. Refer. Book. Part 1. Kiev: Naukova Dumka.

TITANIUM: ALLOYS, WELDING, APPLICATION

V.E. BLASHCHUK
E.O. Paton Electric Welding Institute, NASU, Kiev, Ukraine

Advantages of titanium and its alloys compared with currently available traditional materials are shown. Processes for producing commercial titanium and titanium alloys, as well as processes for their welding and welding consumables, are described. The most promising cases of application of titanium and its alloys are noted.

Keywords: *titanium and its alloys, production, welding methods, application, weldments and structures*

Titanium is a new metal. It was re-discovered by M.H. Klaprote* in 1795 and called by him after mythological gods. Today titanium is considered to be the metal of the 21st century. It takes the ninth place among metals found in the earth crust, being exceeded in abundance only by such structural metals as aluminium, iron and magnesium. Studies of properties of titanium performed in the 20th century showed that the name given to this metal is fully justified owing to its remarkable mechanical properties and high corrosion resistance. Before titanium, none of the structural materials had had such a long history of research and such a rapid growth of production. Discovered at the end of the 18th century, its commercial production began in the U.S. only in 1948 and in the USSR — in 1954.

Titanium and its alloys have a number of advantages over the majority of traditional structural materials, the most important of which are as follows [1, 2]:

- high corrosion resistance in many natural, biological and technological environments, where application of traditional steels and alloys is either impossible at all or requires the use of extra shielding means;
- possibility of a substantial increase in corrosion resistance of titanium through microalloying, e.g. surface microalloying, with noble elements (palladium and ruthenium) and cathodic additions (nickel, molybdenum, cobalt, vanadium, tungsten, *etc.*);
- higher or equivalent specific strength and fatigue life, compared with corrosion-resistant steels and alloys;
- environmental cleanness and good biological compatibility with live tissues, which allows titanium and its alloys to be successfully applied to make endoprostheses.

However, wide application of titanium and its alloys is hindered by:

- high cost of the metal;
- more sophisticated and, therefore, more expensive technology for making semi-finished products and parts (especially by welding), compared with the majority of corrosion-resistant structural steels and alloys;
- high sensitivity to hydrogen-induced embrittlement and gas absorption;
- strong adhesive sticking of rubbing surfaces in the case of violation of the surface of a protective film.

High cost of titanium is associated primarily with sophistication of the technology used to produce it. Titanium sponge, i.e. the raw material for production of compact metal, is made today by the Kroll process or the magnesium reduction (sometimes sodium reduction) method [3, 4]. The resulting titanium sponge is pressed together with alloying elements and utilisable materials to make a consumable electrode, which is melted in vacuum arc furnaces [3, 4]. There is a trend today towards increase in volumes of melting in electron beam [5, 6] and plasma [7] furnaces. Of limited utility is melting in electroslag furnaces [8], as well as processing of the sponge by the powder metallurgy methods [9]. Electrolytic, metal reduction and other processes used for production of titanium are at a stage of experimental-industrial tests [10]. Another important problem in metallurgy of titanium is processing of metal scrap and wastes [3].

The demand for titanium has been decreased lately. This tendency is related to its reduced utilisation in the defence industry (which cannot be compensated for by the volume of its utilisation in civil aircraft engineering), as well as to the fact that its high corrosion resistance and corrosion-mechanical properties have led to a relative saturation of the titanium market (in chemical, petrochemical and pulp and paper industries). Therefore, the industrialised countries are looking now for the new application fields for titanium alloys, allowing for the necessity to address the problems of environmental protection and safe operation of equipment and transportation facilities.

The main alloying element in titanium alloys is aluminium. Next in importance are vanadium and molybdenum, which form a continuous series of solid solutions with β-Ti. Chromium, manganese, iron, copper, tin, zirconium and vanadium are used as alloying elements for commercial alloys. Cathodic alloying with small amounts of electropositive metals (rubidium, platinum, rhenium and ruthenium) is employed

*Martin Heinrich Klaprote (1.12.1743, Wernigerode — 1.01.1817, Berlin) — the famous German chemist and naturalist.

to improve resistance of titanium alloys to active environments. Restricted alloying with silicon, boron, carbon and oxygen is used as well [1].

As to the character of interaction with titanium, alloying elements are conditionally subdivided into three groups: α-stabilisers (elements that increase temperature of α→β transformation of titanium), such as aluminium, oxygen, nitrogen and carbon; β-stabilisers (elements that decrease the polymorphic transformation temperature), such as vanadium, molybdenum, niobium, tantalum, chromium, manganese, iron, copper, nickel, cobalt, silicon and tungsten; and elements that exert a negligible effect on the polymorphic transformation temperature, such as tin, zirconium, hafnium and gallium.

Phase composition of titanium alloys can be evaluated from the relative β-stabilisation coefficient $K_\beta = C_\beta/C_k$, where C_β is the β-stabiliser content of an alloy considered, and C_k is the β-stabiliser content of a binary alloy with a critical composition. As to the K_β values, all commercial titanium alloys can be subdivided into α-alloys, pseudo α-alloys ($K_\beta \le 0.25$), (α + β)-alloys ($K_\beta = 0.3–0.9$), transition-type alloys ($K_\beta = 1.0–1.4$), pseudo β-alloys ($K_\beta = 1.4–2.4$), and β-alloys ($K_\beta \ge 2.5$).

Table 1 gives compositions of foreign titanium alloys commercially produced in compliance with ASTM B265 [1, 2]. These alloys can be classified into alloys with low strength – $\sigma_t \le 600$ MPa (e.g. series VT1, grades AT2 and PT-1M), medium strength (PT-3V, series AT and OT4, VT20 and VT5-1), and high strength – $\sigma_t > 1000$ MPa. Alloys VT3-1, VT8, VT18, VT25, VT36, etc. are classed with heat-resistant alloys and used for the manufacture of compressor disks and blades, as well as casing parts of aircraft engines. This applies also to foreign alloys of the type of IMI 318, 550, 685, 829 and 834, as well as alloys Ti-6-4, Ti-6-2-4-2, Ti-2-4-2, etc.

Much consideration has been given lately to development of sparsely alloyed titanium alloys, which contain inexpensive alloying elements. Iron holds promise for titanium alloys in this respect, as it stabilises the β-phase and is one of the most efficient strengthening elements for titanium. At a content of iron in annealed alloys equal to 0.5 wt.%, each tenths of a percent of iron increases σ_t and $\sigma_{0.2}$ by 20 MPa. At an iron content of 2–10 wt.%, an increase of 1 wt.% in the iron content leads to an increase of 45–70 MPa in σ_t. This causes a substantial decrease in ductile properties of these alloys, although at an iron content of 2–6 wt.% they remain at a satisfactory level (for the technology reasons, the iron content of titanium under industrial conditions should not exceed 2 %) [11–16].

Iron in titanium acts as an eutectic-forming β-stabiliser, and as such it is used in high (α + β)- and pseudo β-alloys containing β-isomorphic stabilisers (vanadium and molybdenum). Iron is contained in these alloys primarily in β-solid solution, providing an additional increase in their stability [13–16].

Mechanical properties of titanium alloys depend upon the character of their alloying, as well as upon their phase composition and structure. Structure of metal is determined by conditions of its hot plastic deformation and heat treatment.

Heat treatment used for titanium alloys is of the following types [1, 17–21]: complete, incomplete, stepwise and isothermal annealing. The latter includes heating in the β-region, cooling to the (α + β) temperature, holding at this temperature and subsequent cooling to room temperature. The choice of a type of annealing is based on alloy composition and application of a semi-finished and finished product. The time of annealing depends upon the section of a workpiece. As the (α + β)-alloys of titanium have an increased sensitivity to heat treatment, incomplete annealing is employed to relieve internal stresses formed as a result of processing of workpieces (including welding). The basic mode of heat treatment of these alloys is isothermal annealing leading to formation of a stable

Table 1. Designations of titanium alloys used in different countries

Alloy (ASTM B265, U.S.)	*Composition, wt.%*	*UNS*	*DIN 17850*	*ThyssenKrupp VDM*	*Other*
Grade 1	0.03[N]; 0.10[C]; 0.015[H]; 0.20Fe; 0.18[O]	R50250	Ti I	Titan 995	IMI115; Ti35A
Grade 2	0.03[N]; 0.10[C]; 0.015[H]; 0.30Fe; 0.25[O]	R50400	Ti II	Titan 994	IMI125; Ti50A
Grade 3	0.03[N]; 0.10[C]; 0.015[H]; 0.30Fe; 0.35[O]	R50550	Ti III	Titan 993	IMI130; Ti75A
Grade 4	0.05[N]; 0.10[C]; 0.015[H]; 0.50Fe; 0.40[O]	–	–	–	–
Grade 5	6A1–4V	R56400	–	–	–
Grade 6	5A1–2.5Sn	R54520	–	–	–
Grade 7	0.03[N]; 0.10[C]; 0.015[H]; 0.30Fe; 0.25[O]; 0.20Pd	R52400	Ti IPd	Titan 994Pd	IMI260; TiPd
Grade 9	3A1–2.5V	R56320	–	–	–
Grade 11	0.03[N]; 0.10[C]; 0.015[H]; $O_3$20Fe; 0.18[O]; 0.20Pd	R52250	Ti IIPd	Titan 995Pd	–
Grade 12	0.3Mo–0.8Ni	–	–	–	IMI325; Ti Code 12
Grade 23	6A1–4VELI	R56401	–	–	–
Grade 25	6A1–4V–0.6Pd	–	–	–	–

two-phase ($\alpha + \beta$) structure, which provides $\sigma_t \geq$ $\geq$ 1000 MPa, high ductility and thermal stability during the entire service life. The most efficient type of heat treatment for these alloys is strengthening heat treatment that includes quenching and ageing.

High-temperature and long-time heating can be performed in vacuum, shielding gases or by using special protective coverings.

Deformation leads to a substantial growth of tensile strength of titanium. In the case of a 80 % reduction, tensile strength of commercial titanium is increased by a factor of 3. Strength of titanium alloys can be doubled.

Alloying of the weld metal leads to decrease in sensitivity of welded joints to embrittlement caused by harmful gas impurities, and to hydrogen-induced embrittlement in particular. Alloying elements increase strength of the weld metal to a different degree. Increase in the content of alloying elements leads to growth of hardness and decrease in elongation of the weld metal. At the same time, reduction in area first increases (in addition of 2–3 % of alloying elements) and then decreases. Impact toughness changes in a similar way. Multicomponent alloying of the weld metal allows achievement of a more uniform distribution of atoms of alloying elements and a uniform distortion of crystalline lattice of titanium. In the degree of improvement of mechanical properties of welded joints in titanium alloys provided by alloying with β-stabilising elements, the latter rank as follows: Cr, Fe, Cr + Fe, Mn, V + Fe, Mo, Mo + Fe, Mo + V, Mo + Cr, Mo + V + Cr + Fe. In welding titanium alloys, it is often required that chemical composition of the weld metal be different from that of the base metal to provide optimal properties of welded joints [19, 21].

Different compositions of titanium welding wires have been developed and commercially produced (Table 2). The wires are supplied in etched and degassed condition.

Almost all the methods initially developed for steels and non-ferrous metals are employed for welding titanium alloys (Figures 1–3) [18–28]. Quality of welded joints in titanium is determined in many respects by the thermal-deformation cycle of welding, differing from that used to weld steels. In titanium welding the power losses are lower, and the time during which the HAZ metal dwells in a high-temperature range is longer by a factor of 2–3. Sensitivity to the thermal cycle of welding is related to occurrence of $\alpha \rightarrow \beta$ transformation, rapid growth of grain of the high-temperature β-phase in heating to a temperature above the polymorphic transformation point, overheating and formation of brittle phases in cooling and ageing.

High reactivity of titanium with respect to the atmospheric gases ([O], [N], [H]) leads to an appreciable saturation of metal of welded joints with them. This causes embrittlement and decrease in mechanical properties (ductility, long-time strength and corrosion resistance). The appreciable saturation of metal during welding occurs now at $T \geq 350$ °C. Therefore, the welding zone limited by the isothermal line of 350 °C should be thoroughly shielded from the interaction with air. Pure argon and helium (GOST 10157–79 and EN439) or their mixtures, as well as special no-oxygen fluxes are applied for shielding. Also, welding in vacuum excludes interaction of titanium with gases. The absence of extra shielding is permitted in pressure joining.

Controlling mechanical properties and structure of the weld and HAZ metal through choosing a rational welding technology and parameters to ensure minimal losses of heat input during welding is an indispensable condition for producing sound welded joints. Quality of welded joints depends in many respects upon the weld groove preparation technology.

Choice of methods for welding titanium alloys is based on the requirement to shield the welding zone and welded joint regions that cool down from interaction with the atmospheric gases, allowing for peculiarities of joining metal of small, medium and large thickness [18–24].

Tungsten-electrode arc welding in inert gases (argon or helium) (TIG) is the most extensively applied and versatile method for welding titanium alloys. It allows the joints with high mechanical properties to be produced on metal of a wide range of thicknesses. Welding can be performed in air with a spray shielding or in chambers with a controllable inert atmosphere. Small captive chambers are employed to shield the overheating zone of cooling regions of the joints in welding tubular structures and circumferential roll and position joints. Tungsten electrodes of the EVL ($W-La_2O_3$) and EVI ($W-Y_2O_3$) grades according to GOST 24949–80, and EWTh ($W-ThO_2$) according to ANSI/AWS A5.12–92 are used as the non-consumable electrodes [18, 19, 21, 24].

Shielding means used in plasma welding of plate materials with thickness $\delta \geq 10$ mm and microplasma welding of sheet materials with thickness $\delta \leq 1.5$ mm are similar to those used in TIG welding. Beam welding methods gain an increasingly wide acceptance in different industrial sectors. The most extensively applied welding method among them is electron beam welding (EBW) in vacuum. Laser welding (LW) of titanium alloys is performed in air, argon or helium, this permitting its application for joining members of large-size structures.

Metal-electrode welding in inert gases (MIG) and submerged-arc welding using no-oxygen fluxes are the high-productivity processes for joining titanium alloys, providing welded joints with desirable properties and absence of pores, cracks and lacks of fusion. Electroslag welding (ESW) is used to make joints in heavy sections.

Explosion welding is one of the popular methods for pressure joining of titanium without preheating using an external heat source (Figure 2). It is employed to join high-strength alloys and dissimilar met-

Table 2. Grades and compositions of titanium-base welding wires

USA		*Japan, JIS Z3331*	*Russia, GOST 27265–87*	*Ukraine, TUU 05416923.041–98*	*UNS*	*Chemical composition of wire, wt.%*	*Grade of base metal*
AWS A5.16–90	*SAE, AMS*						
ERTi-1	495	YTB28/YTW28	VT1-00sv	VT1-00sv	R50100	0.03C; 0.1[O]; 0.005[H]; 0.015[N]; 0.1Fe	Commercially pure titanium
ERTi-2		YTB35/YTW35			R50120	0.03C; 0.1[O]; 0.008[H]; 0.02[N]; 0.2Fe	
ERTi-3		YTB45/YTW49			R50125	0.03C; 0.12[O]; 0.008[H]; 0.02[N]; 0.3Fe	
ERTi-4					R50130	0.03C; 0.2[O]; 0.008[H]; 0.02[N]; 0.2Fe	
ERTi-5	4954	YTB640			R56400	6Al; 4V; 0.005Y; 0.18[O]; 0.015[H]; 0.03[N]	Ti6Al4V
ERTi-5ELI	4956	YTB640E			R56402	6Al; 4V; 0.005Y; 0.1[O]; 0.005[H]; 0.012[N]	Ti6Al4VELI
ERTi-6		YTB525			R54522	5Al; 2.5Sn; 0.005Y; 0.18[O]; 0.015[H]; 0.05[N]	Ti5Al2.5Sn
ERTi-6ELI					R54523	5Al; 2.5Sn; 0.005Y; 0.1[O]; 0.005[H]; 0.12[N]	Ti5Al2.5SnELI
ERTi-7		YTB28Pd/YTW28Pd			R52401	0.18Pd	Ti–Pd alloy
ERTi-9		YTAB325			R56320	3Al; 2.5V; 0.12[O]; 0.008[H]; 0.02[N]	Ti3Al2.5V
			VT6sv	VT6sv		4Al; 3V	VT6; VT23
			2V	2V		2Al; 1.5V	PT-3V; AT3; AT6
ERTi-9ELI					R56321	3Al; 2.5V; 0.1[O]; 0.005[H]; 0.012[N]	Ti3Al2.5VELI
ERTi-12					R53400	0.3Mo; 0.7Ni	Grade 12 ASTM/ASME
ERTi-15					R56210	6Al; 2Cb; 1Ta; 1Mo	Ti-6-2-1-1
			PT-7Msv	PT-7Msv		2Al; 2.5Zr	PT-7M
			VT20-1sv	VT20-1sv		2.5Al; 1V; 1.5Zr	VT20
			VT20-2sv			4Al; 1Mo; 1V; 1.5Zr	VT20
			SP15sv	SP15sv		4.2Al; 2.7V; 2.7Mo; 3.5Nb; 1.5Zr	SP15; VT6; VT23
			SPT-2			4Al; 3V; 1.5Zr	VT6; VT14; VT23.1
				SP17		3.7Al; 4Nb; 0.5Zr; 1.5Fe	Ti–Al–Nb–Fe–Zr
			OT4-1sv			2Al; 1.5Mn	OT4-0; OT4-1
			OT4sv			4.2Al; 1.5Mn	OT4; OT4-2
			VT2sv			2.5Al	OT4-1; 3M; PT-3V; AT3; AT6

Note. Diameters of wires manufactured according to GOST 27265–87 and TUU 05416923.041–98 range from 1.4 to 7.0 mm, and those manufactured according to ANSI/AWS A5.16–90 range from 1.6 (1/16") to 4.8 mm (3/16").

als. Among the methods for pressure joining of titanium with preheating of metal (Figure 3), the most widespread method is resistance welding.

The world-largest welded structure of titanium alloys is Project 941, which is the strategic low-noise heavy missile cruiser (SLNHMC) (code «Akula», «Typhoon» according to the NATO classification). Totally 6 ships (a division) were constructed under Project 941. One of them is shown in Figure 4. The first of these cruisers was launched in September 1979, and the last — in July 1988. These are the largest submarine ships all over the world.

The Project 941 cruisers have impressive characteristics: length — 172.8 m, width — 23.3 m, normal displacement — 28,500 m^3, maximum depth of submergence — 500 m, working depth of submergence — 380 m, surface speed — 13 knots, and subsurface speed — 27 knots.

Physically, Project 941 SLNHMC is of the type of catamaran. It consists of two separate high-strength

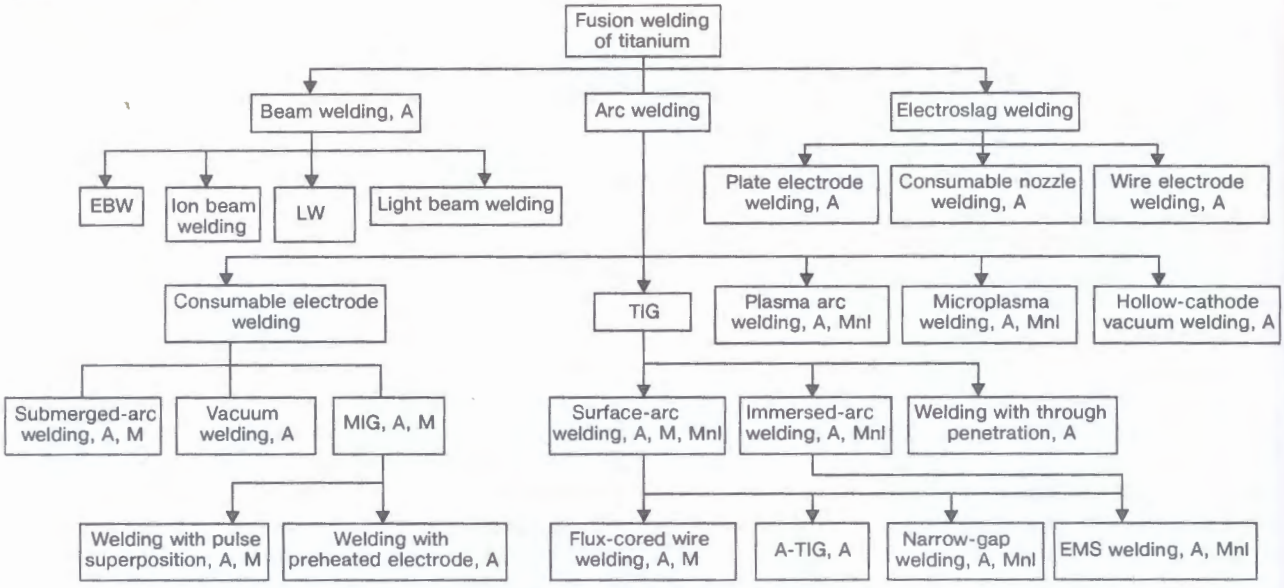

Figure 1. Commercial methods for fusion welding of titanium: A — automatic welding; M — mechanised welding; Mnl — manual welding; EMS — electromagnetic stir welding; the rest of the designations see in the text

hulls (diameter of each is 7.2 m) arranged parallel to each other on a horizontal plane. Additionally, there are two separate waterproof capsules: torpedo compartment and control module located between the main hulls on a centreline plane. The control module houses a central station and a radio equipment compartment located behind it. The missile compartment is placed between the strong hulls in the fore of the ship. Both hulls and capsules of the compartment are connected to each other via passageways. The total number of waterproof compartments is 19. Strong hulls, central station and torpedo compartment are made from titanium alloy, while the light hull is made from steel [29]. The main difficulties in the fabrication of structure of such sizes lay in the development of a technology for welding long welds in a heavy-section metal. This technology had to ensure a reliable shielding of the weld and weld regions cooling during the fabrication process in order to provide the welded joints with desirable properties.

Application of titanium for the fabrication of the ship hulls allows weight of a hull to be reduced, depth of submergence to be increased, and magnetic field to be decreased, which adds to improvement in its

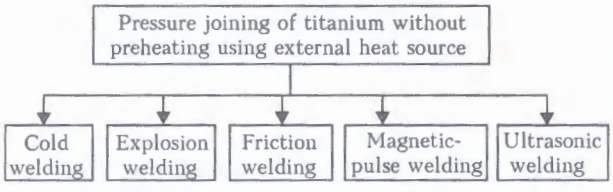

Figure 2. Methods for pressure joining of titanium without preheating using external heat source

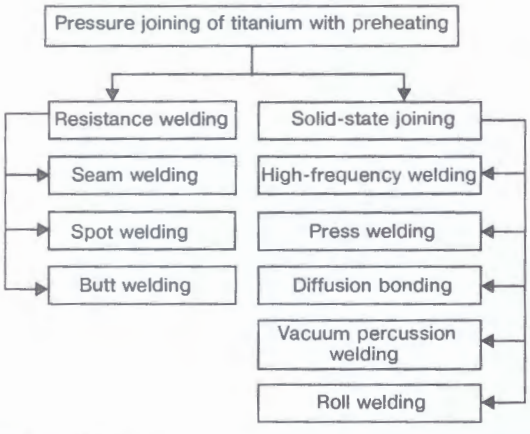

Figure 3. Methods for pressure joining of titanium with preheating of metal

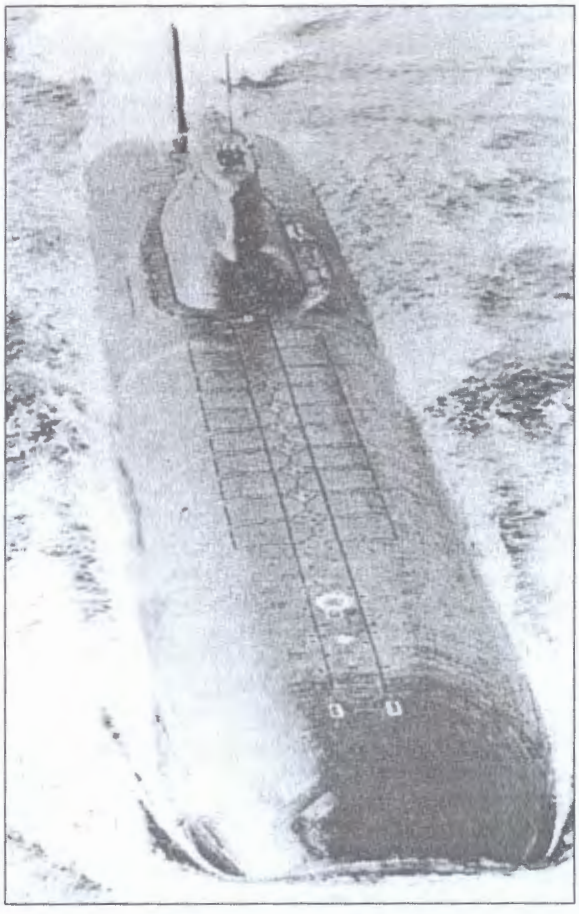

Figure 4. Strategic heavy missile cruiser (USSR)

main tactic advantage — hiding ability. Furthermore, this leads to reduction in maintenance costs for the exterior and interior parts of the hulls. The cost of such submarines is much higher compared with those with a steel hull. Therefore, further on they will be manufactured on a custom-made basis and used to address special problems.

Titanium alloys PT-3 and PT-3V were used as a hull material also for the construction of atomic-powered submarines:

- Project 685 — «Plavnik» («Mike» according to the NATO classification), K-278 «Komsomolets»: working depth of submergence — 1000 m, maximum depth of submergence — 1250 m, full subsurface speed — 30.6 knots, normal displacement — 5680 m^3;
- Projects 705 and 705K — «Lira» («Alfa» according to the NATO classification): working depth of submergence — 350 m, maximum depth of submergence — 400 m, full subsurface speed — 41 knots, normal displacement — 2300 m^3 (6 ships were constructed);
- Project 661 — «Anchar» («Papa» according to the NATO classification): maximum depth of submergence — 400 m, full subsurface speed — 44.7 knots (until now this speed is the absolute world record for submarines), normal displacement — 5197 m^3 (one atomic-powered vessel was constructed);
- Project 10831 — first-class atomic-powered deep-see station AS-12, i.e. research submarine having no arms («Norsus-5» according to the NATO classification): the hull made from titanium alloy and designed for a submergence depth of more than 1000 m, normal displacement — 1600 m^3, full subsurface speed — 30 knots (launched in August 1995).

Strong hulls of the above submarines are all-welded heavy-section spatial structures made from titanium alloys. Because of their large sizes and heavy weight, such structures cannot be subjected to post-weld heat treatment (residual welding stresses amount to 40 % of $\sigma_{0.2}$). However, no delayed fracture and corrosion cracking of the hulls took place, which was ensured by a rational design and proper selection of the welding technology, as well as by high values of ductility of the hull materials and high production standards.

Figure 5 shows appearance of plane SR-71A with the airframe for 95 % made from titanium alloys. Its performance characteristics are as follows: wingspan — 16.95 m, length — 32.74 m, height — 5.64 m, nominal take-off mass — 63,505 kg, maximum take-off mass — 77,110 kg, maximum Mach number — 3, maximum speed at altitude of 24,000 m — 3220 km/h, service ceiling — 24,400 m, operational radius — 1930 km, and flight endurance — 15 h. The use of titanium is related to high aerodynamic heating of the plane in long-time flights at a high speed. 24 planes were constructed. Figure 6 shows appearance of the Sukhoj plane SuT-100 with the airframe 90 % of which was made from titanium

Figure 5. Lockheed two-seater reconnaissance plane SR-71A «Blackbird» (USA)

alloys. The maximum Mach number is 2.8 [30]. Associates of the E.O. Paton Electric Welding Institute participated in the development of the welding technology.

One of the U.S. companies manufactured the world-largest titanium alloy reactor for chemical industry. The head of the reactor was made from commercial-purity titanium of Grade 2 (see Table 1), while its central part was made from alloy of Grade 3. The use of titanium for the manufacture of the reactor body instead of steel clad with titanium allowed decrease in the wall thickness, reduction of 2 times in the scope of work at all the manufacture stages, decrease in weight and reduction in the lifetime maintenance costs. The resulting apparatus is more cost-effective compared with that made from steel. Length

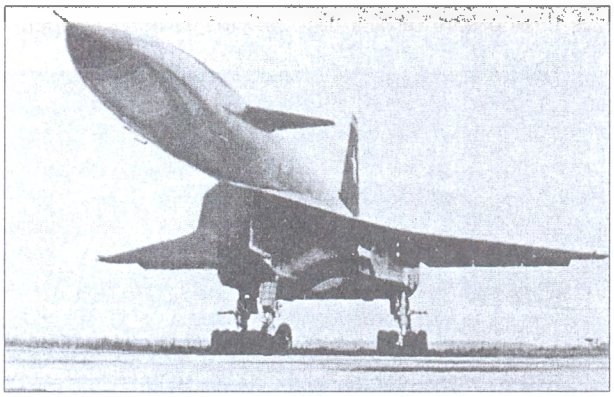

Figure 6. Prototype of the Sukhoj bomber SuT-100 (USSR)

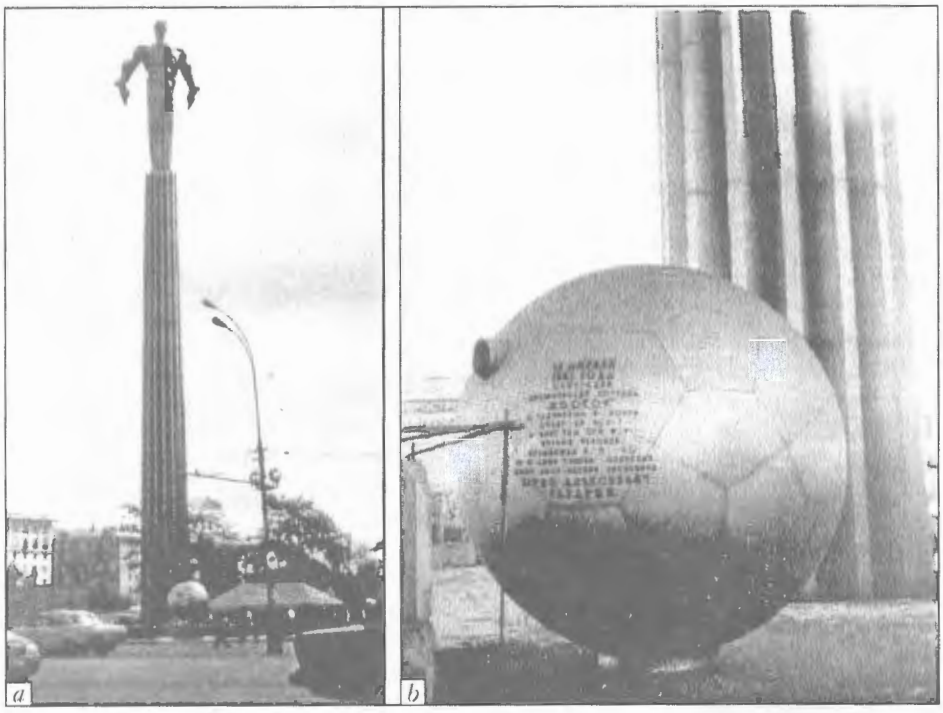

Figure 7. General view (*a*) and fragment (*b*) of the monument to the first cosmonaut of the Earth Yuri Gagarin

of the reactor body is 46 m, diameter is 3 m, volume is 1080 m^3, and total weight is 156,500 kg (including the body — 110,000 kg and internal devices — 46,500 kg).

The largest apparatus of titanium alloy AT3 in the domestic practice was the hydrolysis apparatus with a capacity of 160 m^3. It is a welded vessel with upper elliptical and lower conical bottoms. Casing of the apparatus with a diameter of 3.8 m and 17.07 m high is made from AT3 alloy plates 26 mm thick, and its internal devices are made from plates 3, 6 and 12 mm thick. Different modifications of the TIG welding process were employed for the manufacture of the apparatus.

Owing to its unique properties and high corrosion resistance under atmospheric conditions, titanium has found application in monumental sculpture. For example, two titanium sculptures were installed in Moscow: monument to the space explorers opened on 18 August 1964 in honour of launching of the first man-made satellite, which is covered with polished plates of commercial titanium VT1-0, and monument to the first cosmonaut of the Earth Yuri Gagarin, opened on 4 July 1980 in the Kaluzhskaya Square, which is made from monolithic titanium (sculptor — P. Bondarenko, architects — Ya. Belopolsky and F. Gazhevsky) (Figure 7).

Also, titanium is widely utilised in architecture, despite the fact that it costs much higher than stainless steel. It is applied for the interior decoration in the cases where its mild grey colour is more preferable, compared with bright grey colour of stainless steel. Owing to its high specific strength, high corrosion resistance and low maintenance costs, titanium is used also for the exterior operations. This is economically sound, as it has a long service life and is little sensitive to environmental effects [31, 32]. Thus, building of the Research Centre opened in 2000 in Glasgow (Great Britain) has a roof with a surface area of 6000 m^2, made from titanium sheets 0.3 mm thick. In Oita (Japan) titanium was used to make a roofing for the main sporting arena constructed in a park (1999) (Figure 8). Consumption of titanium for construction of roofing in Japan amounted to 1300 t.

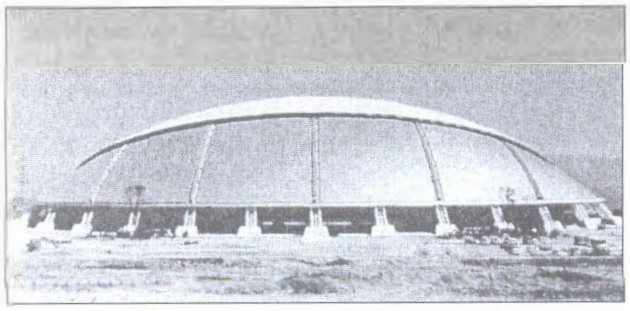

Figure 8. Main sporting arena with a titanium roofing installed in the Oita park

Because of its unique properties, titanium is applied in automotive industry, building of short-haul shipping vessels, masts and yacht hulls, as well as in production of consumer goods [31]. It is used to manufacture heat exchangers for nuclear power stations, hydrofoils, ship propellers, heavy-duty elements of bottom parts of off-shore platforms, drill pipes, etc.

Because of low biological activity of titanium with respect to blood plasma, titanium is a good candidate material for the manufacture of medical equipment and domestic appliances. Low weight, non-allergenic properties and high corrosion resistance in contact with chemicals made it a material for medical implants and wheelchairs [32].

Titanium and especially its highly corrosion-resistant alloys find an increasingly wide application also in chemical and petrochemical industries [33].

1. Gorynin, I.V., Chechulin, B.B. (1990) *Titanium in mechanical engineering*. Moscow: Mashinostroenie.
2. (1994) *Materials properties handbook. Titanium alloys*. ASM Int.
3. Garmata, V.A., Petrunko, A.N., Galitsky, N.V. et al. (1983) *Titanium*. Moscow: Metallurgiya.
4. Kasemura, S., Fukasawa, E., Ampo, S. et al. (2002) Technology trend of titanium sponge and ingot production. *Nippon Steel Techn. Rep.*, 85(**1**), 31–35.
5. Paton, B.E., Trigub, N.P., Kozlitin, D.A. et al. (1997) *Electron-beam melting*. Kiev: Naukova Dumka.
6. Paton, B.E., Trigub, N.P., Zamkov, V.N. et al. (2000) Development of technology for electron beam melting of titanium. *Problemy Spets. Elektrometallurgii*, **2**, 35–40.
7. Zhadkevich, M.L., Likhobaba, A.V. (1998) Selection of parameters for plasma-arc refining remelting of titanium billets. *Ibid.*, **2**, 26–30.
8. Paton, B.E., Medovar, B.I., Benz, M.G. et al. (1999) ESR for titanium: Yesterday, today, tomorrow. In: *Proc. of 9th World Titanium Conf.*, St.-Petersburg, June 7–11, 1999.
9. Fujii, H., Fujisawa, K., Takahashi, K. et al. (2002) Development of low cost powder metallurgy process of titanium alloy products. *Nippon Steel Techn. Rep.*, 85(**1**), 77–81.
10. Reznichenko, V.A., Goncharenko, T.V., Reznichenko, E.A. (2002) Thermic production of titanium metal. *Tekhnologiya Metallov*, **11**, 2–7.
11. Blashchuk, V.E., Gurevich, S.M., Kulikov, F.P. et al. *Electrode wire for welding of titanium alloys*. USSR author's cert. 188278. Int. Cl. B 23 K 36/01. Publ. 20.10.66.
12. Blashchuk, V.E., Gurevich, S.M., Kushnirenko, N.A. *Electrode wire for welding of titanium alloys*. USSR author's cert. 203449. Int. Cl. B 23 K 36/01. Publ. 28.11.67.
13. Kolachev, B.A., Ryndenkov, D.V. (1996) Iron-alloyed titanium alloys. In: *Treatment of light and special alloys*. Moscow: VILS.
14. Radionov, V.L., Ishunkina, T.V., Moiseev, V.N. et al. (1997) Investigations of sparsely-alloyed titanium alloys. *Tekhnologiya Lyog. Splavov*, **1**, 59–61.
15. Zamkov, V.N., Topolsky, V.F., Petrichenko, I.K. et al. (1998) Weldable alloys of Ti–Al–Fe–Nb–Zr system. *Avtomatich. Svarka*, **3**, 23–27.
16. Fujii, H., Takahashi, K. (2002) Development of high performance Ti–Fe–Al alloy series. *Nippon Steel Techn. Rep.*, 85(**1**), 113–117.
17. (1997) *Stamping, welding, brazing and heat treatment of titanium and its alloys in aircraft engineering*. Ed. by A.G. Bratukhin. Moscow: Mashinostroenie.
18. Shelenkov, G.M., Blashchuk, V.E., Melekhov, R.K. et al. (1984) *Manufacture and operation of equipment from titanium*. Kiev: Tekhnika.
19. Gurevich, S.M., Zamkov, V.N., Blashchuk, V.E. et al. (1986) *Metallurgy and technology of welding of titanium and its alloys*. Kiev: Naukova Dumka.
20. Nazarenko, O.K., Kajdalov, A.A., Kovbasenko, S.N. et al. (1987) *Electron beam welding*. Ed. by B.E. Paton. Kiev: Naukova Dumka.
21. Gurevich, S.M. (1990) *Handbook on welding of non-ferrous metals*. Kiev: Naukova Dumka.
22. Zamkov, V.N., Prilutskii, V.P., Shevelev, A.D. (1992) Metallurgy and technology of welding titanium alloys. In: *Welding and Surfacing Rev. Series*, Vol. 2, Part 1. Amsterdam.
23. Blashchuk, V.E., Onoprienko, L.M., Shemlenkov, G.M. et al. (1993) Plasma welding of titanium alloys. *Avtomatich. Svarka*, **3**, 31–33.
24. (1998) *AWS welding handbook*. Miami: AWS.
25. Nerovny, V.M. (2001) Vacuum arc welding of titanium alloys. *Tekhnologiya Mashinostroeniya*, **2**, 27–30.
26. Hitoshi, H.H., Kenichi, F., Konsaku, O. et al. (2002) Nd:YAG laser welding of pure titanium to stainless steel. *Q.J. JWS*, 19(**4**), 716–726.
27. Bondar, A.V., Peshkov, V.V., Kireev, L.S. et al. (1998) *Diffusion bonding of titanium and its alloys*. Voronezh: VGU.
28. Wisbey, A., Wallis, Il., Ubhi, H.S. et al. (1999) Mechanical properties of friction welds in high strength titanium alloys. In: *Proc. of 9th World Titanium Conf.*, St.-Petersburg, June 7–11, 1999.
29. Iliin, V.E., Kolesnikov, A.I. (2002) *Russian submarines: Illustr. Refer. Book*. Moscow: AST.
30. (1992) *Foszination Flugzeuge*. London: Aerospace Publ.
31. Gorin, V.V. (1999) Titanium in the art of the 21st century. In: *Proc. of 9th World Titanium Conf.*, St.-Petersburg, June 7-11, 1999.
32. Kimura, K., Kinoshita, K., Tokuno, K. et al. (2002) Application of titanium to construction, civil engineering and ocean development. *Nippon Steel Techn. Rep.*, 85(**1**), 6–10.
33. Blashchuk, V.E. (1996) Corrosion of titanium alloy welded joints. In: *Welding and Surfacing Rev. Series*, Vol. 6, Part 3.

PWI DEVELOPMENTS IN THE FIELD OF UNDERWATER WELDING AND CUTTING

V.Ya. KONONENKO
SVP «Ekotekhnologiya», Kiev, Ukraine

Generalizing information is given on a number of design developments in the field of underwater welding and cutting, performed at the E.O. Paton Electric Welding Institute since 1966. An attempt has been made to evaluate them from the user's viewpoint.

In memory of A.E. Asnis and I.M. Savich

Keywords: *wet welding, flux-cored wires, semi-automatic machine, coated electrode, oxygen-arc cutting, arc cutting, plasma cutting*

In FSU investigations and development of electrode materials, technologies and equipment for underwater welding and cutting were conducted by various organizations, directly or indirectly related to performance of salvaging and underwater engineering operations. At the end of 1960s–beginning of 1970s the Search-and-Rescue Service of the USSR Navy was supplied with a number of electrode materials and equipment for performance of underwater engineering operations, which allowed solving certain problems, related to providing help to ships and vessels, which had combat and navigation damage [1–4]. They include:

- coated electrodes of EPS-52 grade for manual arc welding of low-carbon and low-alloyed steels (were batch-produced in the amount of 2 to 10 t/year in 28th Munitions Factory);
- coated electrodes of EPS-A grade for manual arc welding of hull steels of AK type. They provided an austenitic structure of weld metal (were produced in small batches in 28th Munitions Factory);
- coated tubular electrodes of EPR-1 grade for oxygen-arc cutting of low-carbon and low-alloyed steels (were batch-produced in the amount of 5 to 20 t/year in 28th Munitions Factory);
- holders for underwater welding and cutting with coated electrodes of EPS-2 grade and holders of EKD-4-60 grade for oxygen-arc underwater cutting (were batch-produced in 28th Munitions Factory);
- self-contained arc power sources of PAS-400-VI grade with a drooping external volt-ampere characteristic and higher open-circuit voltage for underwater welding and cutting with coated and tubular electrodes, as well as deck power source ASUM-400 with a drooping and flat external volt-ampere characteristic;
- PPSR 300-2 semi-automatic machine for wet mechanized underwater welding and cutting with solid wire (passed state testing and is approved for use by Navy Search-and-Rescue Service; 3 semi-automatic machines have been produced).

Diving boats and rescue ships were fitted with all the above equipment, except for PPSR 300-2 semi-automatic machines. Electrode materials, even though they provided a low efficiency and insufficient level of strength and ductility of welded joints, allowed solving the current problems of Navy Search-and-Rescue Service at that time.

In 1966 the USSR Navy leadership decided to transfer part of the subjects related to development of advanced technologies, electrode materials and equipment for performance of underwater welding and cutting at different depths to the E.O. Paton Electric Welding Institute of the NAS of Ukraine. The team of researchers was headed by I.M. Savich. Scientific guidance was provided by Prof. A.E. Asnis.

In 1967 a team of researchers led by I.M. Savich developed a self-shielded flux-cored wire PPS-AN1 [5]. Investigations, which preceded the development, were conducted in the following sequence:

- welding with solid wires of different alloying systems was performed. Welding was conducted both with gas shielding of the arc zone and without it. No positive results were achieved;
- possibility of protection of the reaction zone by fluxes, developed for welding in air, was evaluated. Encouraging results were obtained.

It is known that application of fluxes in welding involves a number of problems. First of all, this is making welds in all the positions other than the downhand position, when it is difficult to protect the reaction zone with flux, particularly under the conditions of underwater welding in the presence of wave impact and currents.

The idea of application of self-shielded flux-cored wire for underwater welding was suggested by Prof. Boris E. Paton. However, application of self-shielded flux-cored wires, developed at that time for welding in air, did not yield any positive results in underwater conditions.

Laboratory investigations conducted at PWI allowed development of an ingenuous composition of

the flux-cored wire charge and technology of its manufacture, ensuring tightness of the lock joint. This enabled placing the flux-cored wire in the water-filled immersible module of the semi-automatic machine, which simplified its design. The need to supply gas to the immersible module was eliminated. The wire of rutile-acid-ore type, called PPS-AN1, provided welding in fresh water at down to 20 m depth of a number of low-carbon and low-alloyed steels [6, 7]. At the time of its development the technology of wet mechanized underwater welding with self-shielded flux-cored wires was unique and did not have any analogs in the world.

For implementation of the technological process, PWI Experimental Design-Technological Bureau (EDTB) developed a number of semi-automatic machines for orbital welding of butt joints, automatic welding of lifting lugs, immersible arc power sources and other unique products. Brief description of part of the developed equipment is given in the Table. Figures 1–5 show for the first time the pilot samples of equipment, individually and batch produced at PWI Pilot Plant of Welding Equipment (PPWE).

Design developments became more sophisticated as experience of operation of individual samples of semi-automatic machines was gained. Most of the designs were developed by PWI EDTB designers under the guidance of Vladimir E. Paton. The main efforts of the designers in development of the semi-automatic machines were aimed at lowering the weight of the immersible module and improvement of the reliability of electric circuit operation. The first semi-automatic machine for mechanized underwater welding, which has passed state testing and was accepted for fitting the Navy Search-and-Rescue Service is A1450 semi-automatic machine («Neptun 4»). The weight of the immersible module under the water with a stock of wire was up to 46 kg in this design. In the recent designs (PSh141, PSh146) it was possible to reduce the weight of the immersible module with a stock of flux-cored wire to 7 kg, and the electric circuit ensured a uniform feed of the electrode wire into the arcing zone, irrespective of the load, at 675 m length of the control cable. PSh141 semi-automatic machine has also passed state testing and in 1991 was accepted for supplying the Navy Search-and-Rescue Service.

As was noted above, flux-cored wire has an important role in the process of wet mechanized underwater welding. The main strength and ductility values of the joints depend on the way the reaction zone is protected, and on the weld metal alloying system. Work on improvement of the composition of PPS-AN1 flux-cored wire to achieve higher mechanical properties of the joints has been conducted since 1974. These efforts resulted in development of a family of flux-cored wires, providing equivalent joints on a number of casing and pipe steels at different depths. PPS-AN5 flux-cored wire was batch-produced under the conditions of PWI Pilot Production.

A research team led by A.A. Ignatushenko developed pilot samples of nickel-base flux-cored wires, which provided a stable austenitic structure of weld metal [8]. These wires were used in the simulation conditions of a deep-water chamber to produce by the wet process the joints of steels at down to 1200 m depths, and in the actual underwater conditions they were used to weld a position butt of a pipe sample, which withstood more than 20 MPa test pressure.

In addition to work on development of technologies and equipment for wet mechanized welding, PWI staff also conducted training of civil and military experts to use this process. Training was conducted both with trips to the facilities to be repaired and in PWI underwater welding laboratory.

Wet mechanized welding with self-shielded flux-cored wires was adapted to the technologies of conducting underwater engineering operations in FSU, as it allowed performance of repair work under the conditions, when it is impossible to use deep-drawing diver vessels. This technology and equipment were applied to perform a large scope of work on repair of underwater river crossings of gas and oil pipelines [9], repair of ships and vessels, which have accident and navigation damage [10–12], waterfront structures and stationary bases of producing offshore platforms. Repair work was conducted both in summer and in winter time from ice. High level of specialist training facilitated successful performance of the work. PWI specialists were usually invited to perform repair work on pipelines.

Coated-electrode welding was the main process of wet underwater welding abroad and till the end of 1980s also in FSU [13–16]. This process has its positive and negative sides. It is popular with the users, as the equipment for its implementation is reliable, mobile and has small weight and dimensions. Widely accepted mobile welding plants with a self-contained drive are used for powering the arc. Low efficiency of the welding process, high requirements to training of divers-welders and considerable scatter of mechanical property values of the joints, dependent on objective and subjective factors, can be regarded as negative aspects of the technology. This process allows performance of repair work in facilities, where a large scope of welding operations is not needed.

A large number of coated electrodes were developed abroad for wet underwater welding of low-carbon and low-alloyed steels at different depths [13–16]. Their application ensures mechanical properties of welded joints on the level of class «C», sometimes «B» by AWS D3.6–99 specification [17].

In connection with the fact that mechanical properties of the joints provided by EPS-52 electrodes were low, and no electrode purchases for the Navy were made abroad, the issue of development of new electrodes with improved welding-technological and mechanical properties was raised. Such work was started at PWI in 1985. Practical experience gained in the underwater welding laboratory in development

Equipment for underwater welding and cutting developed and manufactured by PWI

Year	*Title*	*Brief description*
1967	A1200 «Neptun 1»	Hardware cabinet with starting-adjusting and control devices is located on the surface. Immersible module of organic glass of 54 kg weight is gas-filled (was filled with air). Wire stock of 10 kg, smooth adjustment of feed rate, holder length of 2 m. Hardware cabinet and immersible module are connected by control circuit cable (100 m), welding cables and air hose. Batch-production was not organized
1968	A1242 «Neptun 2»	Hardware cabinet with the same working parameters as in «Neptun 1». Feed mechanism is open (no protective box). This results in high leakage currents from the surface of the wire and feed rollers in welding in salt water (up to 150 A). A compensator of external pressure in the form of a rubber gas-filled tank was used for the first time. Batch-production was not organized
1970	«Neptun 3»	Hardware cabinet similar to «Neptun 2». Immersible module is closed, metal, coated with epoxy with a rubberized inner surface. Motor and reduction gear in a metal sleeve were filled with liquid and have a system of pressure compensation. A pilot sample was made
1972	A1516 «Neptun 5»	Hardware cabinet of splash-proof modification with starting-adjusting devices, with a circuit ensuring smooth regulation of the rate of electrode wire feed and control devices. Immersible module is made of epoxy-foam composition. Reduction gear and motor are located in an inner cavity of the cast immersible module and are filled with PES-1 liquid. Weight of immersible module fitted with wire was 10 kg under the water, and 30 kg in air. Immersible module is convenient in operation. Working depth is 60 m. During operation the liquid penetrated into the pores of epoxy-foam composition, saturating the latter. Gas bubbles formed inside the cavity. This resulted in compensating diaphragm being pressed in by external pressure. 15 semi-automatic machines were manufactured. Later on A1516 immersible module was a prototype of the design of immersible module in PSh141 semi-automatic machine
1974	A1450 «Neptun 4»	Hardware cabinet with starting-adjusting devices, circuit of smooth adjustment of electrode wire feed rate and control devices. Water-filled immersible module is made of rubber with metal reinforcing elements. Weight in ready-for-work condition is 45 kg. Motor and reduction gear are enclosed in a metal case, which has a system of pressure compensation. Welding wire stock is 7 kg, holder length is 3 m. Length of welding and control circuit is 180 m. Test pressure was 4 MPa. The machine passed state testing and was approved for supplying the Navy Search-and-Rescue Service. More than 100 sets of the semi-automatic machines were manufactured
1977	A1660	Hardware cabinet with starting-adjusting devices, circuit of smooth adjustment of electrode wire feed rate and control devices. Immersible module is similar to that of A1450 design. Length of welding circuit and control cable of 60 m, working depth of 60 m. The machine was manufactured with different modifications of electric circuit of motor control. The most recent models are fitted with a module for protection from overloads and short-circuiting in the control circuit. The machine was developed for national economy needs. More than 140 sets of the semi-automatic machines were made
1977	A1715	A unit for welding position butts of pipes in the automatic mode. Incorporates feed unit of A1450 semi-automatic machine. Hardware cabinet with a system of following the butt and electrode position. A pilot sample was made
1977	A1773	A semi-automatic machine for underwater cutting with flux-cored wire of 3 mm diameter at down to 60 m depth with a deck power source. Smooth adjustment of flux-cored wire feed rate. Flux-cored wire stock of 10 kg, holder length of 3 m. A pilot sample was made
1985	A1802	A unit for welding ship-lifting lugs by two-sided multipass welds in the automatic mode. A pilot sample was made and successfully passed full-scale testing in the Black Sea
1986	A1821 «Skat 3»	A unit for underwater plasma-arc cutting. 2 units were made
1989	PSh131 V5	A semi-automatic machine for flux-cored wire mechanized underwater cutting. Hardware with starting-adjustment and control devices. Flux-cored wire feed rate is not controlled. Reduction gear and motor are placed into a metal case with a system of pressure compensation. The case of immersible module of epoxy-foam composition has a weight of 14 kg under the water. Up to 10 kg stock of flux-cored wire, holder length of 3 m, working depth of 60 m. 18 sets were made
1991	PSh141 V5 «Protok»	A semi-automatic machine for wet mechanized welding with self-shielded flux-cored wires. Hardware cabinet of a modular type with starting-adjusting devices, system of smooth adjustment of electrode wire feed and control devices. It is fitted with a system of circuit protection from overloads and short-circuiting in the control cable. Motor of 55 W power together with a planetary reduction gear is placed into a liquid-filled metal case. A pressure compensation system is provided. Immersible module case is made of spheroplast. Weight in the water is 7 kg, wire stock on the reel of up to 5 kg. Gear-type press-down rollers. Length of holder with a plastic guide is 3 m. Test pressure of 6.25 MPa. Length of control cable of 625 m. The machine has passed state testing. 8 sets of the semi-automatic machines were made
1991	PSh146 V5 «Protok»	Analog of PSh141 semi-automatic machine. Working depth of 60 m, length of control circuit of 75 m. The machine was developed for national economy needs. 4 sets of the semi-automatic machine were made

Figure 1. Semi-automatic machine A1200 «Neptun 1»

of self-shielded flux-cored wires enabled creating a novel gas-slag composition of the coating and developing a new electrode for welding in all the positions in space. EPS-AN1 electrode has good welding-technological properties and is designed for underwater welding of a number of carbon and low-alloyed steels

Figure 2. Semi-automatic machine «Neptun 3»

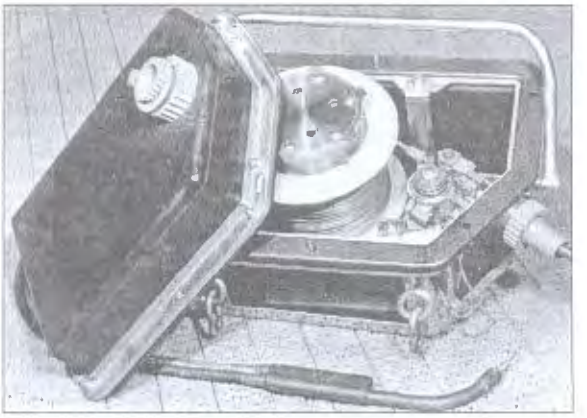

Figure 3. Semi-automatic machine A1450 «Neptun 4»

at down to 20 m depth. Its use ensures mechanical properties of weld metal on the level of joints made in air with electrodes of E42 type. In addition to welding under the water these electrodes are also used in welding in air of metal structures, having a layer of water on the surfaces to be joined. A new holder DPS-AN1was developed at PWI for fastening the electrodes and transfer of welding current.

Coated-electrode arc underwater cutting has its positive and negative aspects. It is applicable in the case, if the metal structures are made of stainless steels, cast iron or non-ferrous metals. Sometimes, through lack of equipment, arc cutting was applied also for severing of metal structures of general-purpose steels. The process is similar to metal-electrode manual arc underwater welding, performed at increased current density. However, it is low-efficient, because of a long time, required for piercing the entire thickness of the metal at the initial moment of cutting, high overheating of the electrode, which causes its higher consumption and frequent replacement during operation [18]. Arc cutting was performed with EPS-52 electrodes.

PWI conducted studies to increase the cuttability of electrodes by changing the composition of electrode coating. This resulted in development of EPR-1 elec-

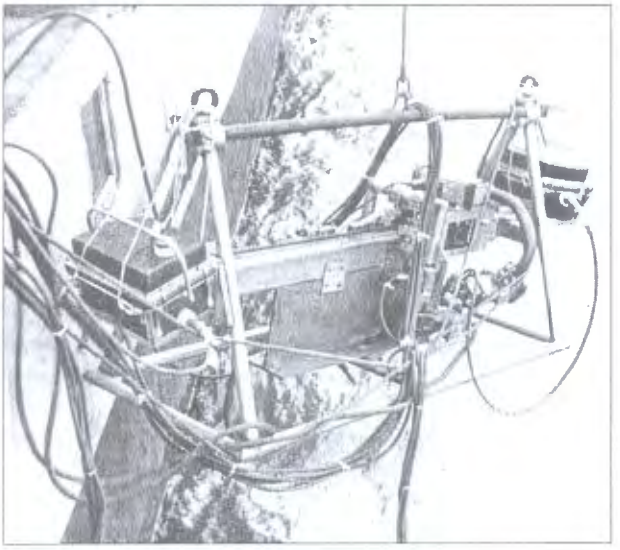

Figure 4. Unit A1802 for welding ship-lifting lugs

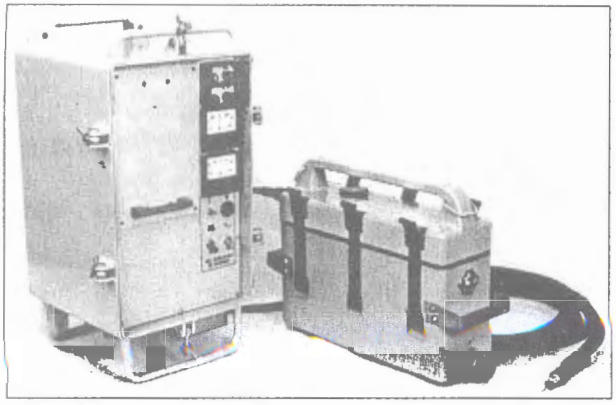

Figure 5. Semi-automatic machine PSh141 for underwater welding

trode, having a higher cuttability in underwater welding. It enables cutting metal up to 16 mm thick at down to 20 m depth in fresh and sea water in all the positions. Electrode cuttability decreases with increase of metal thickness. The greatest effect is achieved in cutting up to 6 mm metal, when oxygen-arc cutting is ineffective. The same holders are used for fastening and transfer of welding currents, as in underwater welding (EPS-2-76 and DPS-AN1).

During development of flux-cored wires for mechanized underwater welding it was established that a number of components, added to the charge, promote increase of base metal penetration depth. Performed research enabled development of the technology and flux-cored wires for mechanized underwater welding of steels, cast iron and non-ferrous metals [19–21]. Flux-cored wires of 2.2–3.0 mm diameter were manufactured.

In terms of energy, the process of underwater severing is quite attractive, as energy equivalent to 10–25 kW power evolves in a small volume. Metal, irrespective of the composition, is melted by an arc, which under the conditions of wet underwater welding has a temperature of 6000–12000 °C. Gas flow formed at the tip of melting electrode and arc pressure ensure removal of molten metal from the cutting zone. Process of arc severing with flux-cored wires can be performed at more than 600 m depth.

From the user viewpoint the process was also attractive, as it eliminated the need to purchase various sets of equipment, it was enough to have a stock of flux-cored wire for cutting at the diver station, which could be placed into the semi-automatic machine for underwater welding. In addition, problems related to supply and storage of a large amount of oxygen were eliminated. At metal thickness ≤ 18 mm, arc power sources and equipment, applied for mechanized welding, could be used for cutting. When standard equipment for mechanized welding was used, the speed of underwater cutting with flux-cored wires was close to these values for oxygen-arc underwater cutting [21].

In view of the positive aspects of the technology of mechanized underwater cutting with flux-cored wires, the work in this area was carried on. By a request from the Navy, a set of equipment was developed, which included a semi-automatic machine A-1773 and specialized arc power source, installed on the deck. Flux-cored wire of 3 mm diameter was used at I_c = 1000 A, U_a = 50 V. Release of such power in a local volume allowed cutting any metals up to 50 mm thick. This technology and equipment were applied for cutting out a process hole in a reactor compartment of a submarine at 40 m depth [22].

Further development of this area followed the path of reducing the weight of the immersible module of the semi-automatic machine, reducing the flux-cored wire diameter and decreasing the takeoff power of the arc power source. A specialized system of equipment was developed for underwater severing. Design of the semi-automatic machine, designated as PSh131 was simplified, immersible module weight was reduced, wire diameter was decreased to 2.4 mm and regulation of its feed rate was eliminated. This allowed using standard power sources of 40–50 kW power. However, in this case the process lost its versatility. Flux-cored wires of PPR-AN1, PPR-AN2, PPR-AN3 and PPR-EK3 grades of 2.2–2.4 mm diameter were manufactured for wet mechanized cutting of steels, non-ferrous metals and cast iron up to 40 mm thick in fresh and sea water.

Oxygen-arc cutting under the water with a tubular electrode has been applied for severing steel metal structures for more than 50 years. It was implemented using thin-coated tubular electrodes of EPR-1 grade. Use of EPR-1 electrodes did not ensure the required labour efficiency of the diver during performance of underwater engineering operations. PWI conducted studies to increase the cuttability of the electrodes by changing the coating composition. This resulted in development of a new tubular electrode of ANR-T8 grade with higher cutting characteristics. Using one such electrode an experienced diver-cutter can perform severing of metal structures 22 mm thick at 400 mm length. Cutting current, when using ANR-T8 electrode, is 30 to 70 A lower than when EPR-1 electrode is used.

For fastening the electrodes, electric current transfer from the power source to the electrode and supplying oxygen, PWI developed an all-purpose electrode holder EKD-AN2 of a higher reliability. It is designed both for electrodes of 8 mm diameter, used in oxygen-arc cutting, and for electrodes of 10 mm diameter, used at exothermal cutting.

At Navy request PWI developed pilot samples of electrodes for exothermal underwater cutting. They passed full-scale testing in the Black and Baltic Seas. Design work was also performed, which allowed designing the main components of equipment for batch-production of these electrodes. As the work on USSR Navy orders was stopped starting from 1992, PWI did not organize any batch production of theses electrodes. At present PWI is manufacturing exothermal electrodes of ANR-E10 grade to order in the laboratory conditions.

Under the guidance of Prof. K.K. Khrenov, PWI conducted since 1972 the work on development of the

technology of severing metal structures under the water, using a constricted plasma arc [23]. Air was used as the working plasma-forming medium in underwater cutting. PWI EDTB developed «Skat-2M» and «Skat-3» units for air-plasma underwater cutting in sea water. When the units were developed, a number of engineering problems were solved, which were related to the need to protect the plasma arc from the impact of sea water, ensuring arc ignition and stable arcing at the depth, and preventing the risk of electric shock for the diver. The unit consisted of a hardware cabinet, water and air supply module, manual plasma cutter with power and water-air supply lines and a reel for lowering and lifting the plasma cutter. The unit was controlled by a remote panel, which was located directly at the point of a diver going down. The main parameters of the process were established and controlled by instruments, located on the front panel of the hardware cabinet.

Pilot sample of «Skat-2M» unit for underwater air-plasma cutting in sea water has been successfully tried out during salvaging of «Ludwig Svoboda» tanker. This unit was used to make 1160 run. m of the cut in metal structures with wall thickness of 15–35 mm. Two such units were manufactured.

The work performed at PWI in the field of wet underwater welding and cutting allowed development of novel technologies and equipment for underwater engineering operations, which have no analogs abroad. Success of this effort was due to continuous guidance, provided by B.E. Paton. This enabled focusing PWI intellectual and material-engineering base, involving high class specialists, knowledgeable in the field of development of electrode materials and welding technologies, and having design skills and experience of performing underwater operations. A significant contribution to scientific advances in this field was made by Prof. A.E. Asnis.

1. Avilov, T.I. (1955) Electrodes for underwater welding and cutting of metal. *Svarochn. Proizvodstvo*, **6**, 9–10.
2. Avilov, T.I. (1958) Investigation of underwater arc welding process. *Ibid.*, **5**, 12–14.
3. Madatov, N.M. (1965) *Underwater repair of ships and water-crafts*. Moscow: Voenizdat.
4. Madatov, N.M. (1967) *Underwater welding and cutting of metals*. Leningrad: Sudostroenie.
5. Savich, I.M. (1969) Flux-cored wire underwater welding. *Avtomatich. Svarka*, **10**, 70.
6. Savich, I.M., Smolyarko, V.B., Kamyshev, M.A. (1976) Technology and equipment for semi-automatic underwater welding of metal structures. *Neftepromyslovoe Stroitelstvo*, **1**, 10–11.
7. Pokhodnya, I.K., Suptel, A.M., Shlepakov, V.N. et al. (1980) *Flux-cored wires for arc welding*. Catalogue-Refer. Book. Kiev: Naukova Dumka.
8. Asnis, A.E., Ignatushenko, A.A., Diachenko, Yu.V. (1983) Measures for decrease of hydrogen content in heat-affected zone during mechanized underwater welding. *Avtomatich. Svarka*, **8**, 1–4.
9. Kononenko, V.Ya., Rybchenkov, A.G. (1994) Experience of wet mechanized self-shielded flux-cored wire welding in underwater repair of gas and oil pipelines. *Ibid.*, **9/10**, 29–32.
10. Kononenko, V.Ya., Gritsaj, P.M. (1994) Wet mechanized welding in repair of hulls. *Mor. Flot*, **11/12**, 21–22.
11. Kononenko, V.Ya., Gritsaj, P.M., Semyonkin, V.I. (1994) Application of wet mechanized welding in repair of ship hulls. *Avtomatich. Svarka*, **12**, 35–38.
12. Kononenko, V.Ya., Lomakin, N.N. (1996) Application of self-shielded flux-cored wire underwater mechanized welding in repair of ships and waterworks. *Ibid.*, **4**, 36–39.
13. Liu, S., Olson, D., Ibarra, S. (1991) Electrode formulation for underwater welding. In: *Proc. of Int. Conf. on Underwater Welding*, New Orleans, March 20–21, 1991. Miami: AWS.
14. Grantham, J. (1990) Development of an underwater SMAW electrode for improved fatigue strength in wet welded joints. In: *Abstr. of pap. of 71st Int. AWS and Solder. Conf.*, Miami, April 22–27, 1990.
15. West, T.C., Mitchell, G. (1988) Evaluation of commercially available wet welding electrodes for potential repair of U.S. Navy ships. *J. Ships Production*, **4**, 228–243.
16. Pett, M. (2000) Wet welding-significant advances in quality. *Welding Met. Fabr.*, **4**, 22–24.
17. (1999) *ANSI/AWS D3.6*. Specification for underwater welding. Miami: AWS.
18. Danchenko, M.E., Lappa, A.V. (1993) Stick electrode underwater cutting (Review). *Avtomatich. Svarka*, **8**, 35–37.
19. Danchenko, M.E., Savich, I.M., Nefyodov, Yu.N. (1988) Flux-cored wire arc underwater cutting. *Ibid.*, **4**, 59–61.
20. Danchenko, M.E., Savich, I.M., Nefyodov, Yu.N. (1989) Influence of hydrostatic pressure on technological parameters of flux-cored wire arc underwater cutting. *Ibid.*, **1**, 48–49.
21. Danchenko, M.E., Nefyodov, Yu.N. (1990) Flux-cored wire underwater cutting using the semi-automatic machine. *Ibid.*, **1**, 70–71.
22. Savich, I.M., Maksimov, S.Yu. (2001) Application of underwater cutting in salvaging operations of submarine. *Ibid.*, **2**, 59–60.
23. Dudko, D.A., Khrenov, K.K., Esibyan, E.M. et al. (1976) Air-plasma underwater cutting of metals. *Ibid.*, **3**, 55–56.

DEVICE FOR FIXATION OF OSCILLATIONS OF THE WELD POOL

G.I. LESKOV and **S.V. PUSTOVOJT**
E.O. Paton Electric Welding Institute, NASU, Kiev, Ukraine

One of the factors that increase penetrating power of the pulsed arc is making the current pulse frequency match the frequency of natural free oscillations of the weld pool. Device that allows fixation of amplitude and period of oscillations of the metal melt during welding has been made to find conditions for «resonance» to be established between the disturbing force and natural oscillations of the weld pool.

Keywords: *arc welding, pulsed arc, weld pool, fixation of oscillations, device*

One of the methods for improving technological properties of the welding arc is to use the pulsed mode of arcing, at which the arc current is superimposed by low-frequency pulses. This allows the penetrating power of the arc to be increased and, therefore, the welded joints with a larger penetration depth to be produced. In this case the maximal effect of using the pulsed arc can be achieved at values of the coefficient of matching of the frequency of superimposed current pulses with that of natural oscillations of the weld pool close to one [1], where the «resonance» phenomenon takes place.

At present the model of a stretched membrane is used to estimate frequency of natural oscillations of the weld pool [2]. Values of frequencies calculated by means of this model, e.g. for submerged-arc welding using the pulsed arc at different values of heat input, range from 5 to 10 Hz [1]. However, this model does not allow the required conditions for «resonance» to be determined at a sufficient accuracy.

It is a known fact that molten metal of the weld pool during welding performs periodic forced oscillations under the effect of a pulsed force, and the pool elements perform free oscillations. A device was made to fix such oscillations of the molten pool metal. This device allows measurement of the amplitude of the forced oscillations and finding, from their maximum value, the required «resonance» conditions. Basic circuit diagram of the device is shown in Figure 1. Principle of its operation is based on conversion of mechanical vibrations performed by the melt into electrical oscillations using the piezoelectric effect.

Signal from a sensing piezoelectric element (*PE*) comes via a coaxial *cable* to one of the channels of the filter block (*FB*) and then to input of an amplifier (*A1*). After amplification, the signal is fed to input

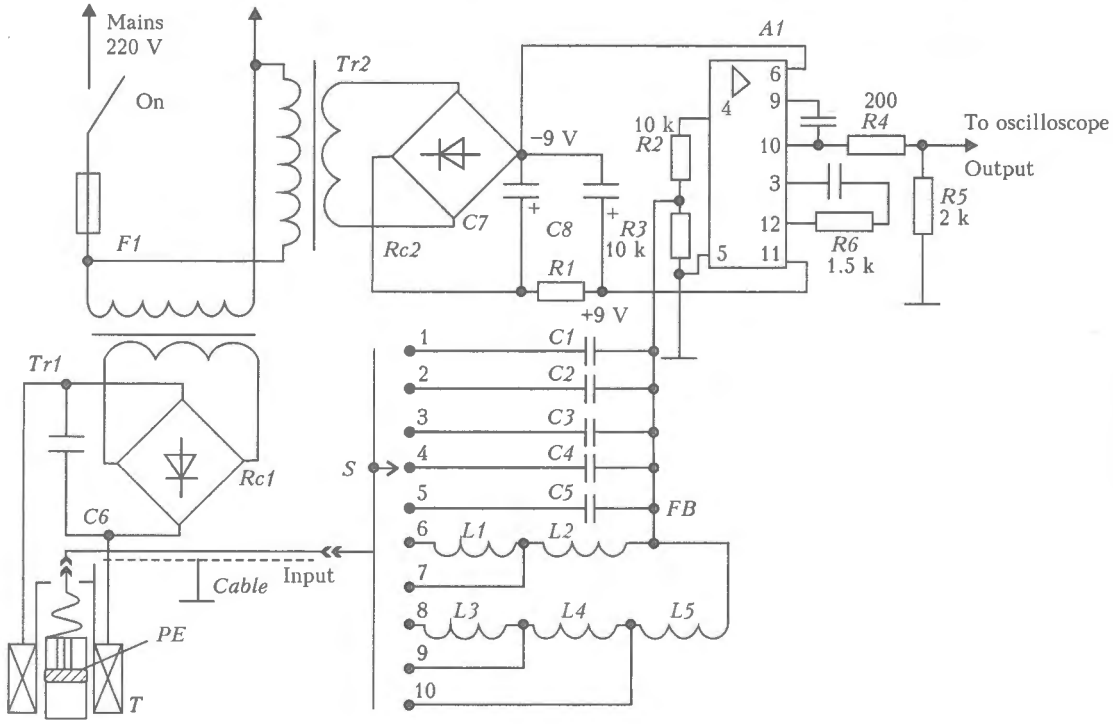

Figure 1. Basic circuit diagram of the device

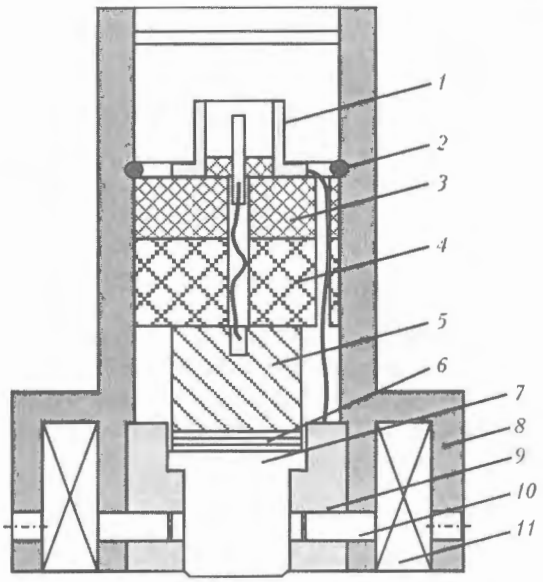

Figure 2. Schematic of a sectional view of the transducer for fixation of oscillations of the weld pool: *1* — connector; *2* — stopper; *3* — cover; *4* — spring; *5* — seismic mass; *6* — piezoelectric element; *7* — wave guide; *8* — casing; *9* — support; *10* — pin; *11* — winding

of the electronic storage oscilloscope and fixed on its screen. If necessary, it can be photographed.

The sensing piezoelectric element is a disk of lead zirconate-titanate located inside the transducer (*T*). To fix oscillations of the weld pool, this element is spaced at 5–10 cm from the pool and secured by magnetic suckers to ferromagnetic workpieces being welded.

Transverse section of the transducer is shown in Figure 2. Winding *11* powered by direct current from the source consisting of transformer *Tr1*, rectifier *Rc1* and filtering capacitor *C6* (see Figure 1) is located in the lower circular part of the transducer ferromagnetic casing. When voltage is on, the magnetic field presses the transducer to a workpiece, thus providing the acoustic contact between it and wave guide *7*, on which piezoelectric element *6* is placed. Seismic mass *5* provides immobility of its upper cover and the electric contact with it. The signal from this cover is fed to connector *1*, to which coaxial *cable* is connected.

Operational amplifier *A1* mounted on microcircuit K553UD1A, at the values of input and output resistance in the feedback circuits as given in the circuit diagram, provides $2 \cdot 10^3$ amplification of the signal fed to its input. Supply voltage to the amplifier is fed from a separate power source (see Figure 1) consisting of transformer *Tr2*, rectifier *Rc2* and filter *C7–R1–C8*.

As found in adjusting the device, the transducer located on a plate, even before welding, generates a signal from different high-intensity noise sources situated outside the test piece, which most often are power sources, transformers or exhaust ventilation motors operating nearby or in neighbouring rooms. The spectrum of frequencies of such noises is intermittent and lies mostly in a range of 20–200 Hz. To attenuate them, the filter block is added to the circuit. This block comprises frequency-sensing elements, i.e. capacitors and induction coils. Each of the elements turned on by a switch (*S*), together with resistor *R3* having a rated resistance of 10 kOhm, forms a divider of voltage of a signal fed from the transducer. Capacitors with a capacitance of 80, 200, 400, 800 and 4000 pF are switched on at stages 1–5, and induction coils with an inductance of 1.0, 0.8, 0.6, 0.4 and 0.2 H, which physically are the windings of transformer TA-1-220-400, are switched on at stages 6–10.

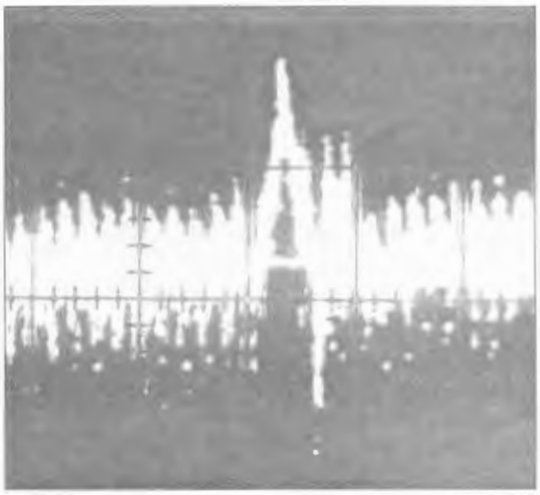

Figure 3. Oscilloscope picture of oscillations of the weld pool under the effect of a single current pulse

All the units of the device, except for the transducer, are assembled in a metal casing, which should be earthed during experiments to eliminate noises induced in it due to external electric and magnetic fields.

Every time before using the device it is necessary to examine parasitic low-frequency oscillations coming to the amplifier input through the filter block. For this, after examination and switching on of all the welding units (power source, ventilation system), it is necessary to find such a position for the device with the help of the switch located in the filter block,

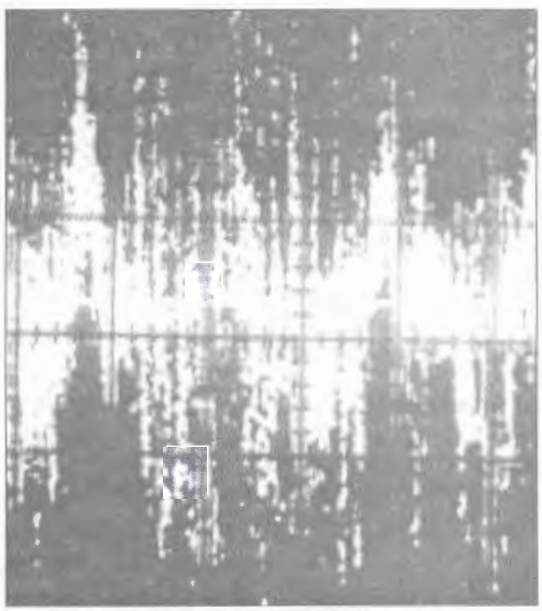

Figure 4. Oscilloscope picture of oscillations of the weld pool in pulsed arc welding

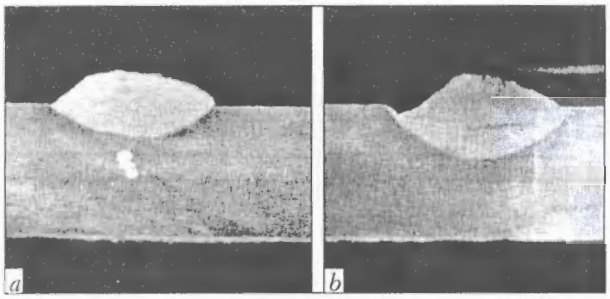

Figure 5. Transverse macrosections of the welds made by welding at a direct current (*a*) and with the pulsed arc (*b*)

at which the amplitudes of the noises seen on the oscilloscope screen are minimal.

Oscillations seen during the welding process are totally different. They differ from noises both in frequency and amplitude. So, here they should be related to the weld pool.

Oscilloscope pictures of oscillations of the weld pool during welding with the pulsed arc were recorded using the new device. Figure 3 shows the oscilloscope picture of the oscillations resulting from the effect on the pool by a single current pulse with a duration of 1 s and maximum value of 350 A. It can be seen that the molten metal affected by the current pulse generates a mechanical impulse with a duration of about 0.1 s. This oscilloscope picture was recorded by using filter No.5 at an oscilloscope sweep of 0.2 s/div and sensitivity of 10 mV/div.

The found period of free oscillations of the pool, $\tau \approx 0.1$ s, was used for penetration of a specimen with the continuous pulsed effect of the arc having the same period. Processes of oscillations of the pool are depicted in the oscilloscope picture (Figure 4). It illustrates variations in amplitude of oscillations of the entire weld pool and in frequency of oscillations of its elements, which in turn causes mechanical vibrations of a specimen welded.

Transverse macrosections of the weld beads deposited at the same mean power of the arc with and without oscillations of the current are shown in Figure 5, *a* and *b*. In the last case the penetration depth was increased by more than 40 %. This effect is attributable to an improved heat transfer from the arc to the specimen welded because of decrease in a liquid interlayer under the arc.

CONCLUSIONS

1. The device developed allows fixation of oscillations of the weld pool under different conditions of welding with the pulsed arc.

2. Affecting the weld pool by a single current pulse enables its dynamic properties to be examined in order to select an optimal frequency of the current pulses to ensure conditions of «resonance» of the disturbing force and natural oscillations of the weld pool.

1. Pokhodnya, I.K., Golovko, V.V., Shejko, P.P. (1996) Influence of submerged pulsed arc welding parameters on base metal penetration depth. *Avtomatich. Svarka*, **5**, 3–7.
2. Kotecki, D.J., Cheever, D.L., Howden, D.G. (1972) Mechanism of ripple formation during weld solidification. *Welding J.*, **8**, 386–391.

UNDERWATER WET WELDING OF 17G1S STEEL WITH PRELIMINARY EXPLOSION TREATMENT OF EDGES

S.Yu. MAKSIMOV
E.O. Paton Electric Welding Institute, NASU, Kiev, Ukraine

The effect of a charge type of explosives and method of their application at preliminary shock-wave treatment of edges welded on the parameters of HAZ of 17G1S steel joints, made under the water, were investigated. The feasibility of significant refining of grains in HAZ area, decrease in its width, localization of lineage non-metallic inclusions was established. Application of preliminary explosion treatment of edges allows reducing the risk of cold cracking in the HAZ metal.

Keywords: *underwater welding, explosion treatment, heat-affected zone, cold cracks*

The accelerated cooling and hydrogen atmosphere of a vapour-gas bubble, characteristic of a wet underwater welding, increase the risk of cold cracking in HAZ metal. This problem is especially acute in welding steels (of 17G1S type), susceptible to the formation of quenched structures and having lineage sulphide inclusions. In this case the formation of cold cracks along the boundaries of coarse grains of martensite or bainite is observed near a fusion line, while the presence of lineage sulphide inclusions, located in the direction of rolling, promotes their propagation inside the HAZ metal. In routine practice, this problem is solved using an appropriate heat treatment that is almost impossible under the conditions of a water medium. At the beginning of the 1980s at PWI the explosion treatment of edges prepared for fusion welding was suggested to improve the properties of welded joints [1]. A pulse of pressure, occurring during explosion of explosives, leads to the exciting of a shock wave in the metal, which causes the refining of grains and violation of continuity of sulphide lines, increase in concentration of crystalline lattice defects. At a subsequent welding heating this creates the favourable condition for the occurrence of a large amount of recrystallization centres. Growth of grains is retarded, thus narrowing the width of a coarse grain zone in HAZ metal. The evaluation of the feasibility to use a preliminary shock-wave loading of edges welded as a means for reducing the risk of cold crack formation in underwater welding represents an interest.

Experiments were carried out on 14×150×200 mm plates, made from 17G1S steel, containing 0.19C, 0.49Si, 1.43Mn, 0.021P and 0.033S (%) and characterized by a high susceptibility to cold cracking. For preliminary treatment the explosives with 1–20 GPa pressure at the front of detonation were used. Explosion loading* was realized using a scheme of skew shock waves excited in metal by a detonation wave sliding along the surface. After treatment in a laboratory pool at 1 m depth, the welding was performed by a flux-cored wire PPS-AN1 at the following conditions: I_w = 180 A; U_a = 32 V; v_w = 6 m/h. Then, the transverse sections were manufactured from specimens and subjected to their metallographic examination. Results were compared with data of examined specimens made without treatment.

The first series of specimens was subjected to treatment using a cord contact charge (DShA-12), laid by a periodic curve. Here, we were trying to provide the zone width covered with the explosive and maximum coincided with a zone of action of residual tensile stresses which could be formed in the given welded joint at the selected conditions of welding.

In the second series of specimens the strip charges of plastic explosives NIL-2 (with a pressure of 1, 2 and 2.5 GPa) and elastite of V84-1994-82 type (with 20 GPa pressure) were used.

In both series the charge was laid on face and reverse surfaces of the plates, the so-called flat method of charge laying.

Results of metallographic analysis (Table) show that the more noticeable narrowing of the coarse grain region of HAZ occurs when the strip charge of ductile explosives is used, NIL-2 in particular, however, to avoid the formation of cold cracks was not managed (Figure *a*), though their amount was decreased remarkably as compared with untreated specimens.

Effect of type of explosive charges and method of their laying on width of coarse grain region in HAZ metal

Specimen No.	*Type of explosive charge*	*Method of charge laying*	*Width of coarse grain region, μm*
1	Without treatment	–	1652–1950
2	DShA-12	Flat	1495–1950
3	Elastite	Same	1755–1820
4	NIL-2	»	1300–1365
5	Elastite	Volume	1300–1365
6	NIL-2	Same	780–1170

*Specimens were prepared by eng. E.Ya. Lokshina.

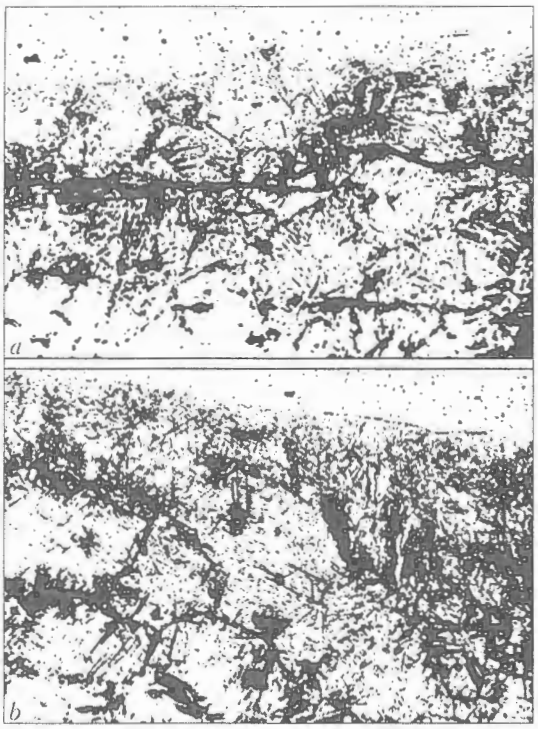

Microstructure of HAZ metal of 17G1S steel welded joint made under the water: *a* — treatment with a strip charge (elastite); *b* — treatment with a volume charge (NIL-2) (×200)

To intensify the effect of treatment by explosives, the charge of NIL-2 in the next series was laid not only on face and reverse, but also on edge surfaces welded [2], so-called a volume method of charge applying. Owing to this arrangement a transverse deformation, occurring under action of opposite waves from the charge of explosives, located on the face and reverse planes, is added with a longitudinal deformation, which is caused by the charge of explosives on the edge plane. During the process of a two-dimensional displacement of the metal a high degree of deformation is attained, thus leading to much higher refining of grains in the region of HAZ metal adjacent to the fusion line (see the Table). Here, the texture in metal is violated, thus leading to fracture and localization of lineage non-metallic inclusions. Besides, the compressive stresses, occurred in the treated metal [3], eliminate the favourable conditions for hydrogen diffusion from weld metal to the HAZ. The combined action of the above-mentioned factors hinders finally the formation of cold cracks in the HAZ metal (Figure *b*).

1. Petushkov, V.G., Lokshina, E.Ya., Novikova, D.P. et al. (1992) Improvement of welded joint properties by preliminary explosion treatment of edges to be welded. *Avtomatich. Svarka*, **9/10**, 48–52.
2. Petushkov, V.G., Savich, I.M., Lokshina, E.Ya. et al. Author's cert. 1487319. Int. Cl. B 23 K 28/00. Issued 15.02.89.
3. Lobanov, L.M., Pivtorak, V.A., Andrushchenko, S.T. et al. (1989) Investigation of stressed state of 17G1S steel welded joints in wet underwater welding. In: *Proc. of Int. Conf.*, Helsinki, Sept. 4–5, 1989. Helsinki.